Atomic force microscopy and spectroscopy analysis of membrane protein stability and conformation in cellular bilayer mimics

Inaugural-Dissertation

zur Erlangung des Doktorgrades
der Mathematisch-Naturwissenschaftlichen Fakultät
der Heinrich-Heine-Universität Düsseldorf

vorgelegt von

Anna Bronder
aus Chorzów

Düsseldorf, Dezember 2015

Aus dem Institut für Physikalische Biologie
der Heinrich-Heine-Universität Düsseldorf

Gedruckt mit der Genehmigung der Mathematisch-Naturwissenschaftlichen Fakultät der
Heinrich-Heine-Universität Düsseldorf.

Referent: Prof. Dr. Dieter Häussinger
Korreferent: Prof. Dr. Dieter Willbold

Tag der mündlichen Prüfung: 19.01.2016

Eidesstattliche Erklärung

Ich versichere an Eides Statt, dass die Dissertation von mir selbständig und ohne unzulässige fremde Hilfe unter Beachtung der „Grundsätze zur Sicherung guter wissenschaftlicher Praxis an der Heinrich-Heine-Universität Düsseldorf“ erstellt worden ist.

Düsseldorf, den

Anna Bronder

"If the brain were so simple we could understand it,

we would be so simple we couldn't."

-Emerson M. Pugh

Danksagung

Für den erfolgreichen Abschluss dieser Doktorarbeit (zumindest was den experimentellen und schriftlichen Teil angeht; für den Rest bedanke ich mich zu gegebener Zeit) muss ich vielen Menschen meinen herzlichsten Dank aussprechen. Zunächst danke ich Prof. Dr. Dieter Häussinger dafür, dass er diese Arbeit als mein Betreuer begleitet hat. Die Möglichkeit, mich dadurch mit der Medizin direkt auszutauschen, war sehr lehrreich für mich. Mein besonderer Dank gilt auch Prof. Dr. Dieter Willbold, nicht nur für die Bereitstellung seines Instituts, sondern auch für die Mitbetreuung dieser Arbeit. Dr. Filipp Oesterhelt möchte ich ebenfalls dafür danken, dass er mich vor mehr als sechs Jahren im Institut von Prof. Dr. Willbold vorgestellt und über einen so langen Zeitraum dort behalten hat (einmal abgesehen von der Tatsache, dass es mir dort viel zu sehr gefallen hat, als dass ich freiwillig das Institut gewechselt hätte). Ein großer Dank geht auch an Dr. Luitgard Nagel-Steger, welche zwar nicht offiziell aber dennoch erheblich an der Betreuung meiner Arbeit beteiligt war. Ihre Fachkompetenz aber auch Fürsorge und Geduld sorgten letztendlich dafür, dass während dieser Arbeit keine Morde begangen wurden.

Vielen Dank auch an Dr. Oleksandr Brener. Erst die Zusammenarbeit mit ihm hat einige der hier vorgestellten Ergebnisse möglich gemacht. Lieber Alex, die gemeinsamen Experimente haben sehr viel Spaß gemacht und ich verstehe nun mehr denn je, dass Zeit relativ ist. Vielen Dank auch an Mario Schneider und Dr. Adeline Bieker, welche die Kraftkurven in eine auswertbare Form gebracht haben. Auch die fachlichen (und weniger fachlichen) Gespräche und Aktivitäten (Mario kann tanzen UND singen!) haben zur Erheiterung meines Alltags beigetragen. Besonders möchte ich mich auch bei der Arbeitsgruppe von Dr. Manuel Etzkorn für ihre Expertisen bedanken. Ohne Euch, vor allem ohne Dich liebe Shantha Elter, wäre vieles nicht möglich gewesen (das Naschen an der Kapuzinerkresse im Botanischen Garten zum Besipiel). Auch Stefan Klinker möchte ich für seinen Versuch danken, mir die Proteinaufreinigung näher zu bringen. Ich befürchte aber, ich bin ein hoffnungsloser Fall. Vielen lieben Dank auch an alle Korrekturleser: Elke Reinartz, Nadine Rösner, Adeline, Mini und Havoc! Ein Dank und ein Gruß geht auch an Dr. Arpita Roychoudhury, an deren Dissertation ein Teil dieser Arbeit anknüpft. Besonders danken möchte ich auch Bernd Esters, Stefanie Schiefer, Gerhard Steger, Oliver Bannach, Michael Wördehoff, Heidi Gruber, Astrid Wies, Lothar Gremer, Christina Decker, Thomas Karcher, Sabine Arens, Cordula Kruse und Susanne Steeger. Auch an alle anderen, die ich nicht namentlich erwähnt habe, fühlt euch bitte angesprochen, wenn ich sage: Vielen Dank an den Seminarraum! Ihr ward alle eine (humorvolle) geistige und menschliche Bereicherung.

Ein ganz besonderer Dank gilt natürlich meinen Eltern, die mir so ziemlich alles in meinem Leben ermöglicht haben, was ich mir gewünscht habe. Es hat schon seine Vorteile die eigene Mutter als beste Freundin zu haben. Den Vater bekommt man ja immer mit einem „*Papinchen*“ und Augenklimpern auf seine Seit. Meinem kleinen Bruder möchte ich übrigens ganz lieb für die Kaffeeversorgung während des Schreibens danken! Das war die Rettung! Meinem Freund gebührt auch ein besonderer Dank für seine Unterstützung und die sprachliche Korrektur dieser Arbeit. Es ist schon faszinierend, wo überall ein Komma stehen kann.

Vielen Dank auch an alle meine Freunde (Sandra, Christin, Meli, Lama, Lauri, Alex, Anne, Jacky, Felix, Alex G., Franzi, Asja, Veit, Maia, Julia, *insertyournamehere*). Ich hoffe, ich habe jetzt niemanden vergessen, oder noch schlimmer, einen Namen falsch geschrieben.

“It is sometimes an appropriate response to reality to go insane.”

-Philip K. Dick, VALIS

Table of contents

TABLE OF CONTENTS **I**

List of Figures **III**

List of Abbreviation **IV**

1. INTRODUCTION **1**

1.1 Integral membrane proteins **1**
1.1.1 Protein folding 2
1.1.2 TGR5 4
1.1.3 Bacteriorhodopsin 5
1.1.4 Amyloid beta-peptide 7

1.2 Cellular membranes **8**
1.2.1 Phospholipids 9
1.2.2 Cholesterol 10

1.3 Artificial membrane mimetic systems **11**

1.4 CFE **13**

1.5 AFM **13**
1.5.1 Set up 14
1.5.2 Contact mode 15
1.5.3 Tapping mode 16
1.5.4 Force spectroscopy 17
1.5.5 Calibration 21
Cantilever resonance 21
Cantilever deflection 22
Spring constant 22

1.6 Motivation **24**

2. RESULTS **26**

2.1 Articles and Manuscripts **26**
2.1.1 Disruptive effect of specific Aβ1-42 Oligomers on Cholesterol-rich Membranes 26
2.1.2 Oriented Membrane Protein Reconstitution into Tethered Lipid Membranes for AFM Force Spectroscopy 58
2.1.3 Atomic force measurements on the specifically orientated membrane protein TGR5 reconstituted inside a tethered bilayer lipid membrane 80

2.2 Unpublished Results **84**

3. DISCUSSION **89**

3.1 Analyzing the influence of $A\beta_{1-42}$ oligomers on cholesterol-rich sBLMs **90**

3.2 Creating a model tBLM to study integral membrane proteins in a defined orientation 91

3.3 Expression of TGR5 92

4. PROSPECTS 93

5. SUMMARY 94

6. ZUSAMMENFASSUNG 95

7. LIST OF MANUSCRIPTS 96

8. REFERENCES 97

List of Figures

Figure 1: Different types of integral membrane proteins. ····· **1**

Figure 2: Energy landscape of the protein folding process. ····· **3**

Figure 3: Structure and mutation residues of the G protein-coupled bile acid receptor TGR5. ····· **5**

Figure 4: Purple membrane imaged with high resolution atomic force microscopy. ····· **6**

Figure 5: Schematic representation of the amyloid cascade hypothesis. ····· **7**

Figure 6: Schematic representation of the cellular membrane. ····· **8**

Figure 7: Examples of different types of phospholipids. ····· **9**

Figure 8: Ordered and disordered bilayers. ····· **10**

Figure 9: Schematic representation of the effect of cholesterol on lipid structure. ····· **11**

Figure 10: Different membrane mimetic systems. ····· **12**

Figure 11: Schematic representation of the reaction vessel for CFE. ····· **13**

Figure 12: The first scanning probe microscope. ····· **14**

Figure 13: Schematic set up of AFM. ····· **15**

Figure 14: Schematic representation of the movement and deflection of the cantilever during contact mode. ····· **16**

Figure 15: Schematic representation of tapping mode. ····· **16**

Figure 16: Schematic force curve on a non-repulsive, non-stick, hard surface. ····· **18**

Figure 17: Comparison between a force curve on different surfaces. ····· **19**

Figure 18: Force curve on a surface showing adhesion. ····· **20**

Figure 19: Force curve showing the unfolding and stretching of a polymer. ····· **21**

Figure 20: Purification results of TGR5 from HEK 293. ····· **85**

Figure 21: Results of TGR5 expression in *E. coli.* ····· **86**

Figure 22: Results of CFE using the pET28a vector. ····· **87**

Figure 23: Results of CFE using the pIVEX2.3d vector. ····· **88**

List of Abbreviation

Abbreviation	Definition
Aβ	amyloid beta-peptide
$A\beta_{1-42}$	amyloid beta-peptide 1-42
AD	Alzheimer's disease
AFM	atomic force microscopy
APTES	(3-aminopropyl)triethoxysilane
APP	amyloid precursor protein
BLM	black or bilayer lipid membrane
sBLMs	Solid supported bilayer lipid membranes
tBLMs	Tethered bilayer lipid membranes
BR	Bacteriorhodopsin
C-terminus	carboxyl-terminus
C-terminal	carboxyl-terminal
CF	carboxyfluorecein
CFE	cell free expression
DPC	dodecylphosphocholine
DPPC	1,2-dipalmitoyl-sn-glycero-3-phosphocholine
E. coli	*Escherichia coli*
ECL	extracellular loops
Egg PC	L-α-phosphatidylcholine
ELISA	enzyme-linked immunosorbent assay
FM	feeding mixture
GPCR	G protein coupled receptor
GST	glutathione S-transferase
HEK 293	human embryonic kidney cells
His	histidine
His6	hexahistidine

ICL	intracellular loop
IPTG	isopropyl β-D-1-thiogalactopyranoside
IMAC	immobilized metal affinity chromatography
LPT	long-term potentiation
Lyso PC	L-α-lysophosphatidylcholine
MP	membrane protein
IMP	integral membrane protein
N-terminus	amino-terminus
N-terminal	amino-terminal
Ni-NTA	nickle-nitrilotriacetic acid
trisNTA	tris-nitrilotriacetic acid
PEG	polyethylene glycol
PSC	primary sclerosing cholangitis
Q-factor	quality factor
RM	reaction mixture
RT	room temperature
SPM	scanning probe microscope
SuccinylPE	1,2-dipalmitoyl-sn-glycero-3-phosphoethanolamine-N-(succinyl) sodium salt
TGR5	G protein coupled bile acid receptor GPBAR-1
TMH	transmembrane-α-helices
UC	ulcerative colitis
WLC	worm-like chain
XPS	X-ray photoelectron spectroscopy

1. Introduction

1.1 Integral membrane proteins

Generally membrane proteins (MPs) are a class of proteins associated with the cellular membrane. MPs permanently associated with the membrane are called integral membrane proteins (IMPs). They can be bound, adsorbed or embedded into the membrane either as integral polytopic proteins (Figure 1a-c), spanning the whole membrane, or as integral monotopic proteins (Figure 1d-f), associating with the membrane unilaterally.

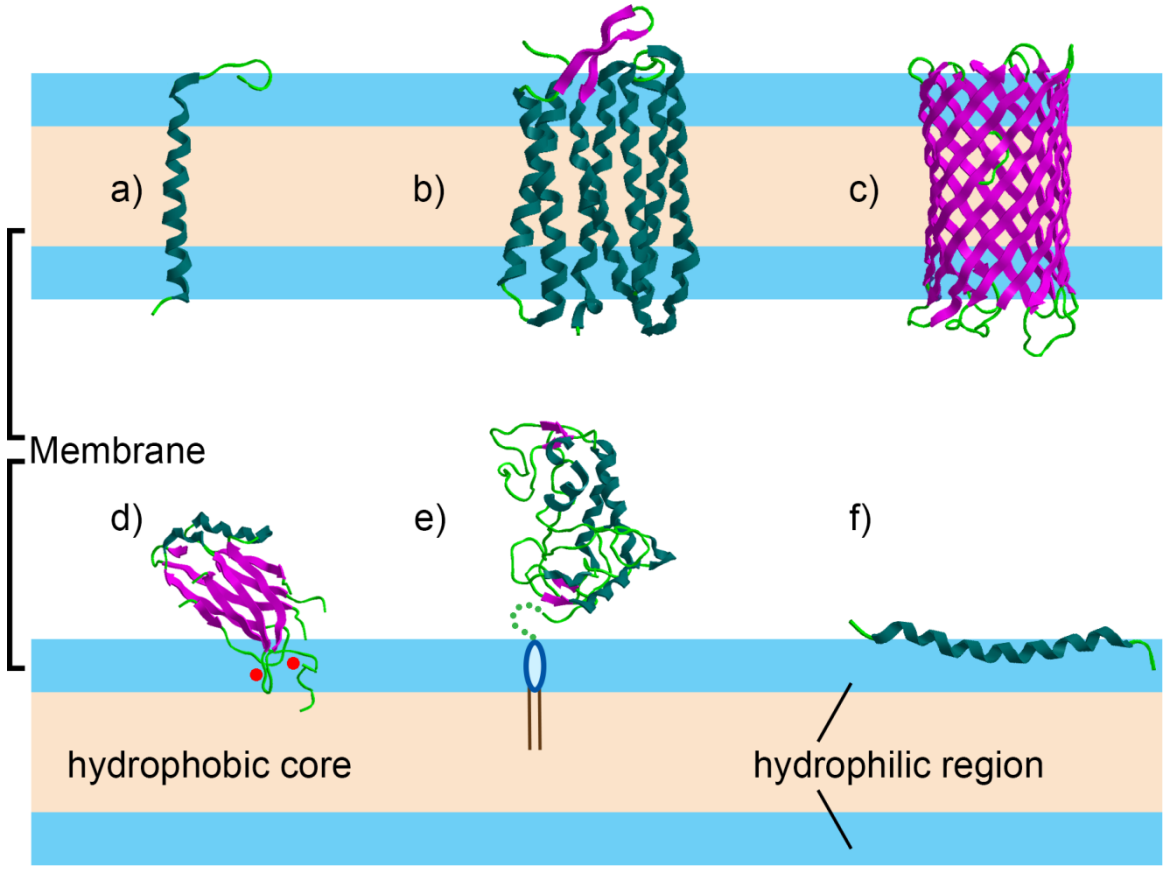

Figure 1: Different types of integral membrane proteins. (a) An example for a bitopic membrane protein with one α-helix (teal) spanning the membrane as its transmembrane domain (PDB: 2K1L). (b) A protein spanning the membrane with seven α-helices (PDB: 1PY6). (c) A membrane spanning beta barrel (beta sheets in pink) (PDB: 4D51). (d) Membrane proteins can interact with one side of the membrane through ionic interactions (red) with the hydrophilic region of the membrane (blue) and through hydrophobic residues in the loops (green) with the membrane's hydrophobic core (beige) (PDB: 2CM5). (e) Protein covalently bound to a lipid that can integrate into the cellular membrane (PDB: 4KM6). (f) A membrane protein can also interact with the membrane through an in-plane membrane anchor domain (PDB: IR7C).

IMPs account for around 30 % of all proteins (Liu, Rost 2001). They function as ion channels, proton pumps and enzymes and are responsible for many membrane related processes, e. g. cell adhesion, energy production and transmission, osmotic balance and photosynthesis. G protein coupled receptors (GPCRs) are one class of integral polytopic proteins. They consist of seven transmembrane-α-helices (TMHs) and trigger a variety of different intracellular and physiological responses, which makes them especially interesting as possible drug targets.

1.1.1 Protein folding

The three dimensional structure of a protein, and therefore its function, is governed by the protein's amino acid sequence. Several thermodynamic processes are needed to arrive from a protein's unfolded state at its folded conformation. These processes can be visualized by an energy landscape (Figure 2). At the end of the protein's folding process, the protein should reach its thermodynamically most stable state, also called the native conformation. However, on the way from the unfolded to folded state, there are several thermodynamically stable conformations a protein can reach. The number of these possible conformations increases exponentially with the length of the protein's amino acid sequence. In theory this means that the time the protein needs to fold into the native conformation is longer the higher its number of possible thermodynamically stable conformations. In contrast to this mathematical view of the protein folding process, a protein reaches its native conformation *in vivo* in a short period of time. This contradiction is described as the Levinthal-paradox (Zwanzig et al. 1992). However, it has to be considered that proteins start folding already during protein expression. Each new amino acid spontaneously takes on the energetically most favorable conformation very quickly after being added to the chain. This creates preordered domains and reduces the amount of possible conformations for the whole protein (Wolynes et al. 1995). Additionally, the folding process of some proteins can for example be governed by so called chaperones, which assist the protein in folding into the native conformation.

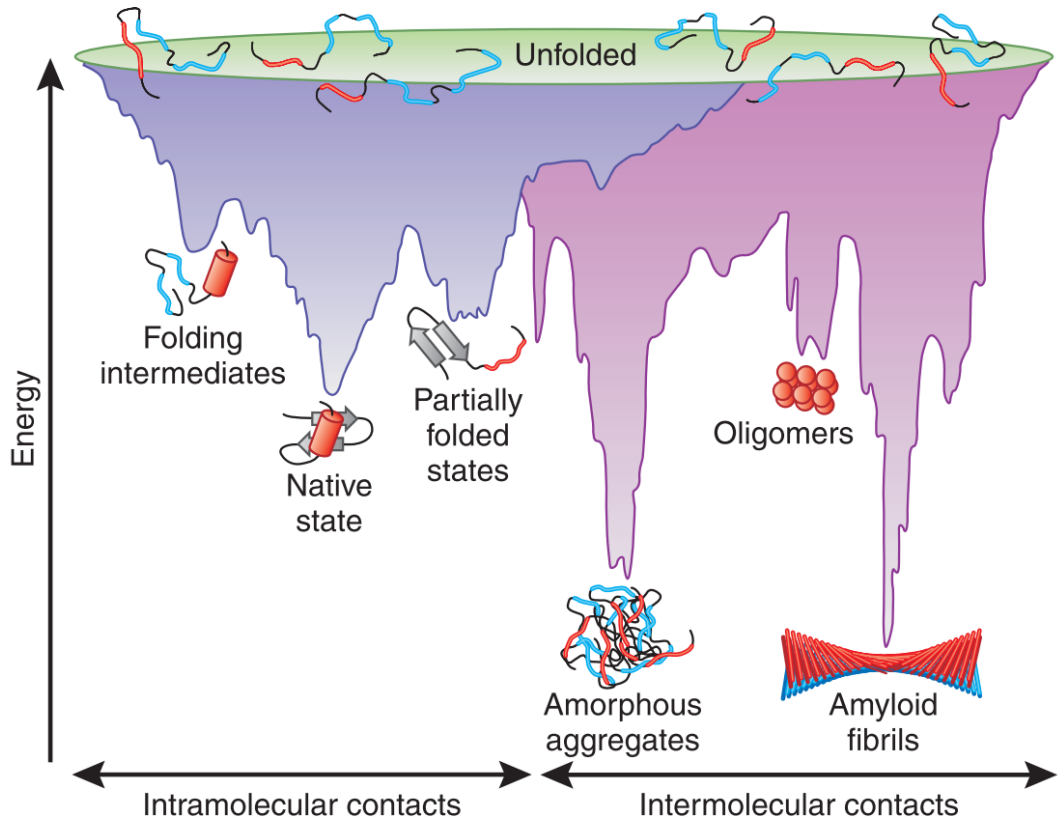

Figure 2: Energy landscape of the protein folding process. Starting from their unfolded state (green area) proteins can "funnel" to their native conformation through intramolecular interactions (blue area) or non-native conformation through intermolecular interactions (purple area). In both cases there are several stable conformations (energy minima) the proteins can reach (Hartl, Hayer-Hartl 2009).

A protein with a non-native conformation can be described as misfolded. Amorphous aggregates, fibrils and some oligomeric structures can also be considered as misfolded proteins. Misfolding of proteins can be the cause of diseases. The class of diseases caused by misfolding or abnormal oligomerization and aggregation of proteins is called proteopathy. It can be divided into two subgroups (Winklhofer et al. 2008). In the first subgroup the disease is caused by an abolished function of the misfolded protein ("loss-of-function"), while in the second subgroup the function of the protein is changed into a toxic form ("gain-of-toxicity"). Characteristic for the second group is the appearance and accumulation of aggregates (plaques) in tissue. Metabolic diseases and congenital myotonia are examples for the first subgroup of proteopathy (Segalat 2007), while Alzheimer's, Parkinson's and Creutzfeldt-Jacob disease all belong to the second subgroup of proteopathy (Chiti, Dobson 2006).

1.1.2 TGR5

The G protein coupled bile acid receptor (GPBAR-1, also known as TGR5) is a GPCR expressed in liver, adipose tissue, gall bladder, skeletal muscle and various cells of the gastro intestinal tract (Kawamata et al. 2003; Poole et al. 2010). Due to its ubiquitous expression, many functions are associated with TGR5, e. g. regulation of hepatic blood flow and anti-inflammatory responses (Keitel et al. 2007; Keitel et al. 2008). These associations can be used in disease treatment. One example for this is the potential role of TGR5 in the treatment of diabetes, due to its co-responsibility in the control of insulin release in the pancreas (Katsuma et al. 2005; Knop 2010; Kumar et al. 2012). It is also known, that TGR5 activation increases energy expenditure, counteracting the effects of metabolic disease (Pols, Thijs W H et al. 2011; Watanabe et al. 2012). Additionally, TGR5 deficiency or misfolding can be linked with various diseases. This is indicated by the role of TGR5 mutants in primary sclerosing cholangitis (PSC), a chronic inflammatory bile duct disease associated with ulcerative colitis (UC). Here the TGR5 mutants show a reduced or abolished function (Hov et al. 2011). Contrary to these findings it was also shown that TGR5 is over-expressed in most gastric intestinal type adenocarcinomas. Here, the activation of TGR5 increases cell proliferation and TGR5 staining was connected with decreased patient survival (Cao et al. 2013).

As is typical for GPCRs, TGR5 consists of seven TMHs (Figure 3). As crystal structures are known for the G protein-coupled receptor rhodopsin, which has shown to form dimers or larger oligomeric complexes (Fotiadis et al. 2004), it can be speculated that TGR5, a member of the same class A (Rhodopsin-like) G protein-coupled receptors forms similar complexes. To achieve a better understanding of TGR5 functionality and to develop TGR5 specific drugs, in depth knowledge about TGR5's structural details is of high importance. However, the structure and functionality of TGR5 are not fully resolved, yet.

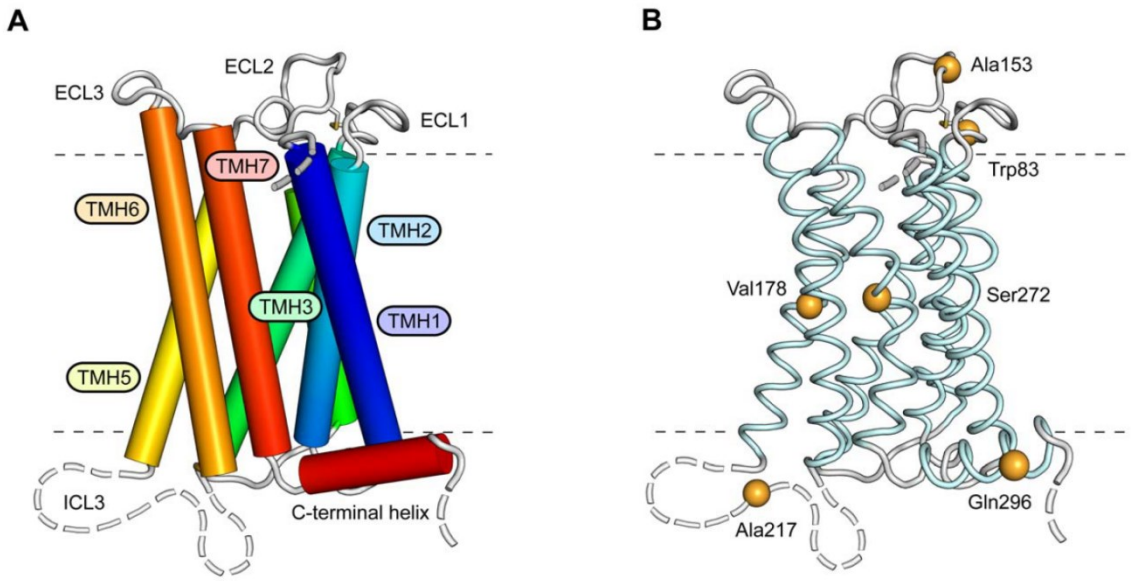

Figure 3: Structure and mutation residues of the G protein-coupled bile acid receptor TGR5. (A) A 3D structure was presented through comparative modeling. The receptor is generally composed of seven transmembrane helices (TMH1-7) connected by three loops on the extracellular (ECL1-3) and on the intracellular side (ICL1-3). (B) Six residues have been found to be mutated in PSC patients. Adapted from (Hov et al. 2010).

1.1.3 Bacteriorhodopsin

Bacteriorhodopsin (BR) represents a IMP that has been studied extensively (Roychoudhury et al. 2012; Roychoudhury et al. 2013; Wickstrand et al. 2015). It is expressed in *halobacterium salinarium* (Oesterhelt, Stoeckenius 1971), which is found in brine pools of high temperature, saturated salt conditions and bright sunlight. BR is also known as a light driven proton pump. It consists of the typical seven TMHs, named from A to G, and a retinal molecule that forms a Schiff base with a conserved lysine in TMH G. When the retinal absorbs a photon a conformational change occurs in BR, which results in a proton being transferred from inside the cell into the extracellular environment. The generated proton gradient across the membrane is then used to synthesize adenosine triphosphate. Inside the cellular membrane BR naturally forms 2D-crystals, the so called purple membrane (Figure 4). Due to BR's high stability and extensive knowledge about its structure and functionality, it is suitable as a model membrane protein. Additionally, BR has been expressed using cell free expression (CFE) (Etzkorn et al. 2013), which makes solubilized BR available outside of its crystal compound. Due to its characteristic absorption at 555 nm in BR's native conformation, stability and functionality can be controlled conveniently.

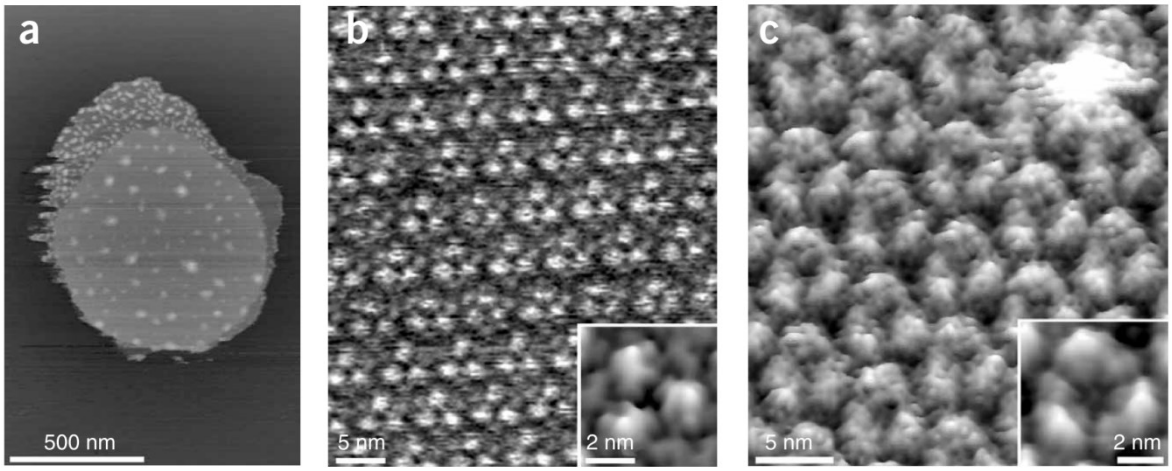

Figure 4: Purple membrane imaged with high resolution atomic force microscopy. (a) A patch of the purple membrane absorbed to a solid support. (b) The extracellular surface as well as the (c) intracellular surface show the trimerization of BR (Müller, Engel 2007).

1.1.4 Amyloid beta-peptide

Alzheimer's disease (AD) is characterized by the accumulation of amyloid aggregates (Ross, Poirier 2004; Soto, Estrada 2008) in the central nervous system. They mainly consist of amyloid beta-peptide (Aβ) (Schmidt et al. 1994). The amyloid cascade hypothesis (Selkoe 2001) (Figure 5) states that different aggregation states of Aβ initiate cellular events leading to cell death (Tanzi, Bertram 2005).

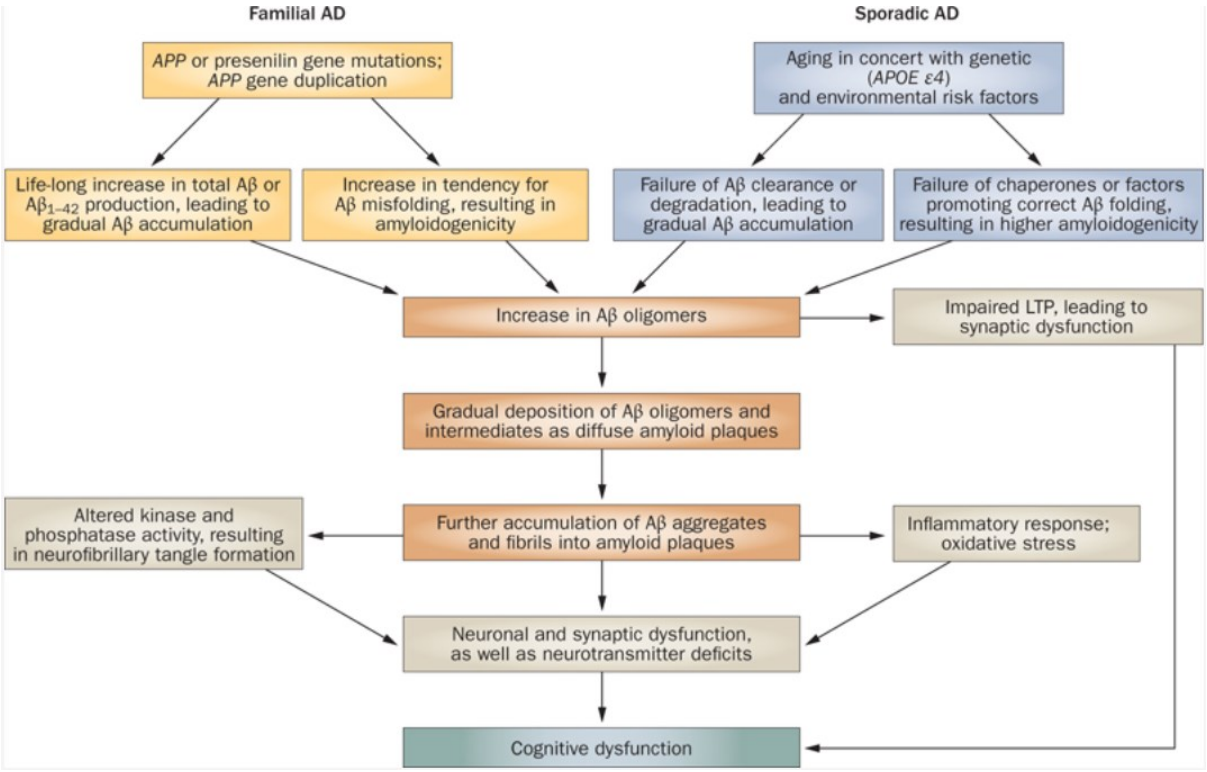

Figure 5: Schematic representation of the amyloid cascade hypothesis. An imbalance between production and clearance of Aβ in the brain is the initiating event in AD. In both familial and sporadic AD the misfolding of Aβ causes an increase in Aβ oligomers. Those oligomers can already induce an impaired long-term potentiation (LPT), which leads to synaptic dysfunction. Further aggregation of oligomers first leads to the formation of amyloid plaques, fibrils and higher aggregates. Together with the preceding synaptic dysfunctions they cause neurofibrillary tangle formation, neurotransmitter deficits, oxidative stress, inflammatory response and neuronal dysfunction, which lead to cognitive dysfunction (Blennow et al. 2010).

Soluble Aβ oligomers occupy a central role in AD pathogenesis (Walsh et al. 2002a; Walsh et al. 2002b; Walsh et al. 2005), consequently their study is of high interest. The formation of Aβ is catalyzed by the proteolytic cleavage of the amyloid precursor protein (APP) by β-secretase and γ-secretase (Milligan 2000). As the cleavage is not consistent, different Aβ species with a length of 17-46 amino acids are formed (Portelius et al. 2006; Portelius et al. 2011; Seubert et al. 1992; Zhao et al. 2007). Of these species mainly $Aβ_{1-42}$ is found in amorphous plaques and soluble oligomers (Haass, Selkoe 2007; Karran et al. 2011; Selkoe

2001). Even though Aβ is not inherently a membrane protein, studies have shown that Aβ oligomers can form pores when associated with a lipid membrane (Lin et al. 2001; Quist et al. 2005; Shafrir et al. 2010). Furthermore, there is evidence that the lipid composition of these membranes plays an important part in membrane association and development of AD (Berthelot et al. 2013). Especially cholesterol seems to promote membrane association and aggregation (Fantini et al. 2013; Tashima et al. 2004). When integrated into the cellular membrane, Aβ oligomers form ion channels and disrupt the calcium homeostasis in cells (Hardy, Higgins 1992). Additionally, it can bind to membrane cholesterol (Di Scala et al. 2014) and disrupt the membrane due to curvature stress (Gibson Wood et al. 2003). Therefore investigation of the connection between cellular membranes and $A\beta_{1-42}$ oligomers is of great interest to the scientific field.

1.2 Cellular membranes

The cellular membrane (Figure 6) is a lipid bilayer consisting of phospholipids, glycolipids and cholesterol. It has been described as a two dimensional liquid by S.J. Singer and G.L. Nicolson in 1972 in the fluid mosaic model. In this model lipids and proteins can diffuse freely through the lipid bilayer (Singer, Nicolson 1972). A membrane's stability is important to separate the cell from its environment, while a membrane's fluidity at an organisms preferred temperature is crucial for the integration and function of integral membrane proteins. Both factors are governed by the lipid composition of the membrane (Los, Murata 2004). Certain compositions of lipids and proteins can further promote the formation of structured domains, so called lipid rafts or protein complexes.

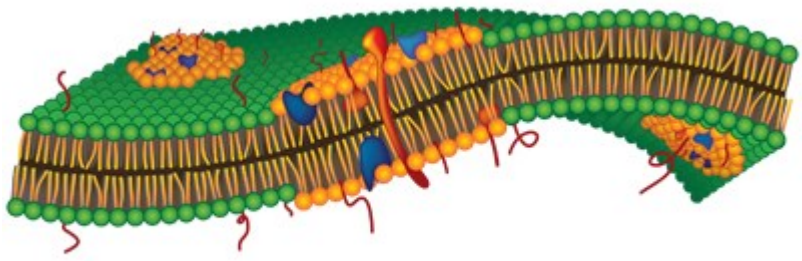

Figure 6: Schematic representation of the cellular membrane. The membrane consists of a lipid bilayer (green heads, yellow tails). Lipid rafts are depicted in orange. Various proteins (blue and red shapes) interact with the membrane. Adapted from http://www.lanl.gov/science/1663/august2011/story3full.shtml.

1.2.1 Phospholipids

Phospholipids consist of a polar head-group including a phosphate. The hydrophobic tail can either consist of a single or double hydrocarbon chain, which can be partially unsaturated. Due to their different structures they can be grouped into three categories: cylindrical (fully saturated hydrocarbon double chain) (Figure 7a), cone- (partially unsaturated hydrocarbon double chain) (Figure 7b) and inverted cone-(single hydrocarbon chain) (Figure 7c) like lipids. Depending on these three structural categories the lipid composition can influence the membrane curvature of the cell.

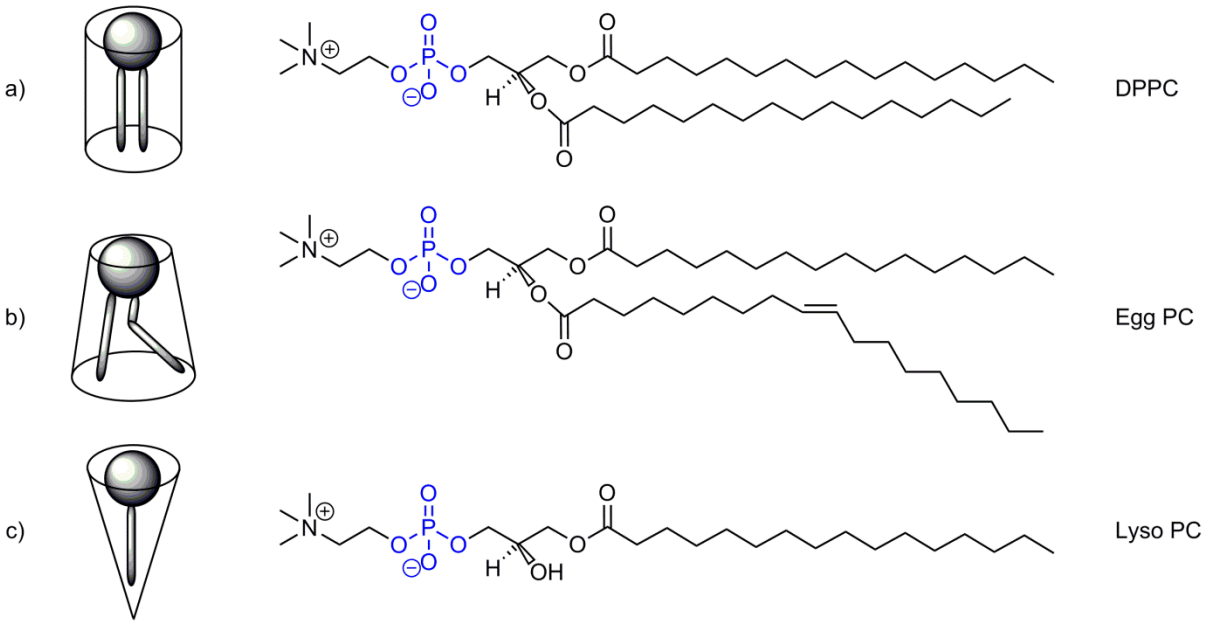

Figure 7: Examples of different types of phospholipids. Phosphate-group shown in blue. (a) 1,2-dipalmitoyl-*sn*-glycero-3-phosphocholine (DPPC) has a cylindrical shape due to its two fully saturated hydrocarbon chains. (b) L-α-phosphatidylcholine (Egg PC) has one unsaturated hydrocarbon chain, which gives it a cone-like shape. (c) L-α-lysophosphatidylcholine (Lyso PC) assumes an inverted cone-like shape as it has only one hydrocarbon chain.

Another effect of these structural differences is shown in a membrane's phase. A lipid membrane can generally be present in a fluid phase or a gel to crystal phase, depending on the environmental temperature. Lipids with fully saturated hydrocarbon double chains prefer an ordered conformation of these chains even at higher temperatures (Figure 8a). This higher order increases membrane thickness and stiffness, hence making the membrane more gel-like to crystalline. For partially unsaturated hydrocarbon chains and single chain lipids the ordered conformation of the chains is disturbed even at lower temperatures, therefore decreasing the membrane thickness and making the membrane more fluid (Figure 8b).

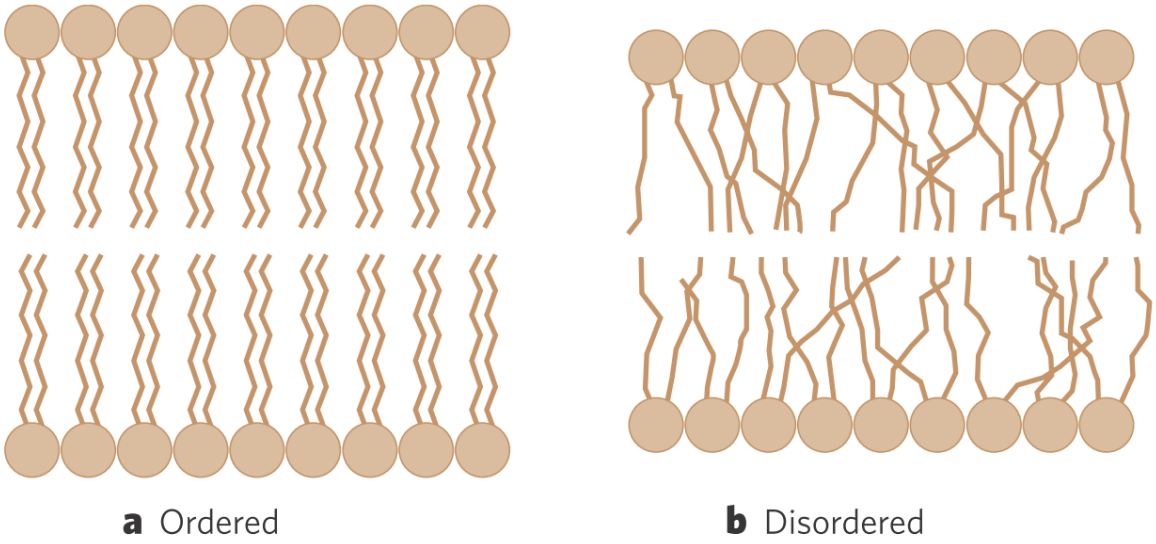

Figure 8: Ordered and disordered bilayers. (a) Straight, fully saturated hydrocarbon chains lead to high ordering of the lipid bilayer. (b) Through the presence of unsaturated chains or increased temperature the bilayer becomes disordered. As the chains can interlace, the bilayer thickness decreases. Adapted from (Maxfield, Tabas 2005).

1.2.2 Cholesterol

Cholesterol is an important component of the cellular membrane. It has a single hydrophilic hydroxyl-group while the rest of the molecule is comprised of hydrophobic rings. Due to its size and structure cholesterol will associate with its small hydrophilic group towards the polar head-groups of the other membrane lipids, while the rings move between the hydrophobic chains. Two effects can then be observed. If the lipid is partially unsaturated, hence making the chains unordered, cholesterol will stabilize the chains and facilitate a higher ordering (Figure 9a). This will increase the height of the membrane as well as move the phase transition temperature from fluid to gel to higher temperatures (Lodish 2000). If the lipid is fully saturated and prefers an ordered conformation of the hydrocarbon chains, cholesterol will break this order, decreasing the height of the membrane and moving the phase transition temperature from crystal to fluid to lower temperatures (Figure 9b). If the cholesterol content is high enough, the phase transition was shown to completely disappear (Redondo-Morata et al. 2012). Apart from lipids, cholesterol can also directly interact with or facilitate interaction between different proteins (Fantini et al. 2013).

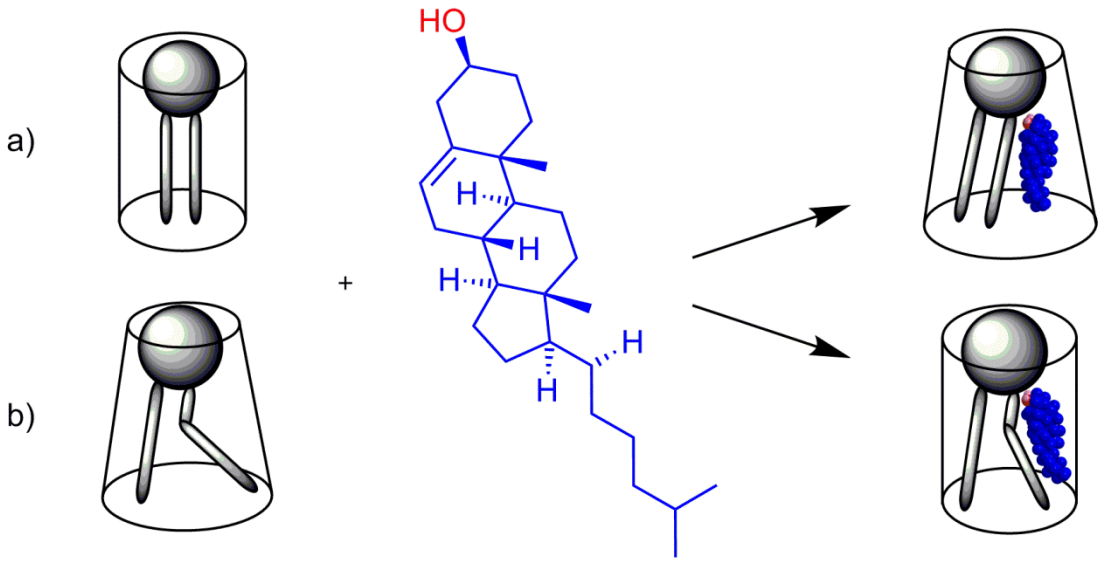

Figure 9: Schematic representation of the effect of cholesterol on lipid structure. Cholesterol interacts with its hydrophilic hydroxyl-group (red) with the polar headgroups of the lipids (ball). Cholesterole's hydrophobic tail moves between the hydrocarbon chains and either disturbes (a) or facilitates (b) a higher order by altering the general shape.

1.3 Artificial membrane mimetic systems

As cellular membranes are a very complex and intricate system, studying their components, e. g. integral membrane proteins, can be very challenging. Artificial membrane mimetic systems offer a suitable alternative, as they decrease the complexity but offer enough customization options to study different proteins of interest in their functional conformation. These artificial membrane mimetic systems can be comprised solely of lipids or, as recent studies have shown, a mixture of lipids and lipid-like detergents. Outside of their natural environment, a cellular membrane, integral membrane proteins have been known to be stabilized by detergents (Seddon et al. 2004). These detergents can also be mixed with lipids to modify artificial lipid membranes. As they weaken the lipid-lipid interactions, detergents make the membrane more permeable to proteins, thus increasing the possibility of integral membrane proteins to integrate into artificial membrane mimetic systems.

The simplest system of an artificial membrane is the generation of large vesicles formed of lipid bilayers (Figure 10a), which allows for efflux experiments, study of protein binding processes and the interaction between proteins. However, the electric control over the membrane and the recording of electric currents due to protein function is highly restricted (Koper 2007). Another membrane mimetic system is a free standing lipid film in aqueous phase, a so called black or bilayer lipid membrane (BLM) (Figure 10b). This system offers the

possibility to measure currents, as ion channels can be integrated into the BLM. However, BLMs in general, are not very stable (Koper 2007).

Solid supported bilayer lipid membranes (sBLMs) use a solid substrate onto which the membrane is deposited (Figure 10c). The substrate offers higher stability for the membrane and can be functionalized with a polymer brush before membrane deposition. This polymer brush can mimic the cytoskeleton of a natural membrane and reduce the interactions between proteins and the substrate (Koper 2007).

Tethered bilayer lipid membranes (tBLMs) use an anchoring lipid, which is covalently bound to the surface (Figure 10d). Due to this anchor the stability of the membrane is increased further. Additionally, an anchoring lipid will support the fusion of vesicles on surfaces that are generally desired for different techniques but do not facilitate vesicle fusion of the desired lipid composition. The density of the lipid anchor has to be modified according to the substrate, lipid composition of the membrane and the integration possibility of membrane proteins. A high coverage with lipid anchor might otherwise hinder the successful incorporation of integral membrane proteins (Koper 2007).

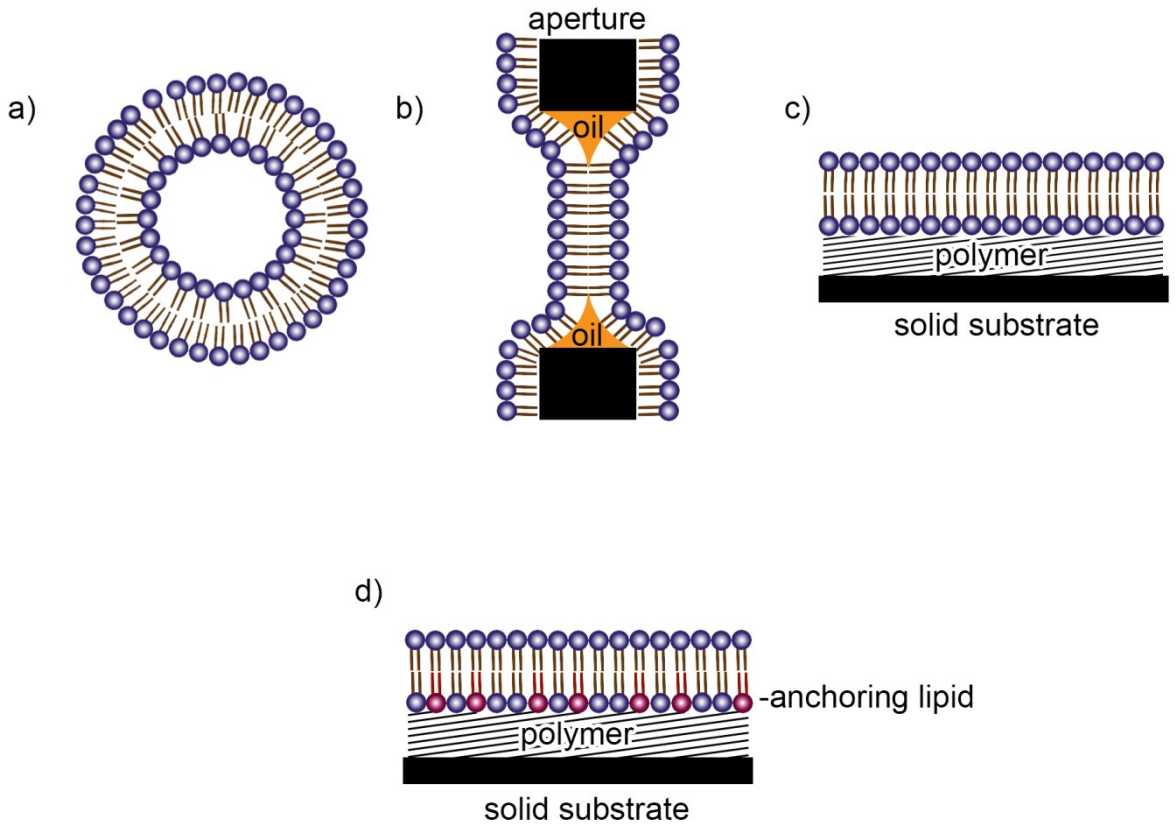

Figure 10: Different membrane mimetic systems. Membrane mimetic systems can be (a) simple unilamellar vesicles, (b) a lipid bilayer film spanning an aperture, (c) an sBLM resting on a polymer cushion or (d) a tBLM, partially bound to the polymer cushion through an anchoring lipid (pink).

1.4 CFE

CFE offers an expression of proteins with high yield, while avoiding the key problems of a cellular host system, e. g. inclusion bodies, toxic proteins and degradation. CFE facilitates protein-expression through a coupled transcription/translation system. It uses two compartments, which are separated by a semi-permeable membrane (Figure 11). One compartment is filled with the so called reaction mixture (RM), while the other compartment is filled with the feeding mixture (FM). The RM contains high molecular weight compounds like proteins and nucleic acids, while the FM is comprised of low molecular weight precursors like nucleotides and amino acids. During the expression precursors from the FM can penetrate into the RM and small inhibitory breakdown products can diffuse from the RM into the FM. There are three different modes of CFE. Precipitation CFE allows water insoluble membrane proteins to precipitate during expression. The proteins can later be refolded under specific conditions. Detergent assisted CFE uses detergent micelles to stabilize membrane proteins after expression, while lipid assisted CFE utilizes lipid vesicles, into which the membrane proteins can integrate during expression (Schneider et al. 2010).

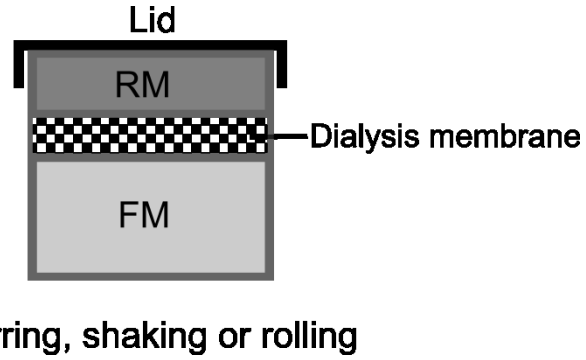

Figure 11: Schematic representation of the reaction vessel for CFE.

1.5 AFM

The scanning probe microscope (SPM) (Figure 12) was invented by G. Binning, C.F. Quate and C. Gerber in 1986 (Binnig et al. 1986). The name originates from the general setup of the microscope. An SPM does not use conventional optics or an incident beam, as is typical for classical microscopes. Instead, a probe with a nanometer sharp tip is used to scan the sample of interest point per point and line per line by direct contact with the sample. This way it enables three-dimensional sub-molecular surface imaging in real time. Scanning conditions can be adjusted to fit the sample of interest, e. g. aqueous buffer and physiological temperatures for the investigation of proteins. As the ultimate interaction that is measured between the tip and the sample is force, the technique is called atomic force microscopy (AFM). This measured force can not only be used to image a sample's topography but also

provides the possibility of studying physical properties, e. g. hydrophobicity, charge and mechanical properties of a surface. Furthermore spectroscopic measurements can be performed.

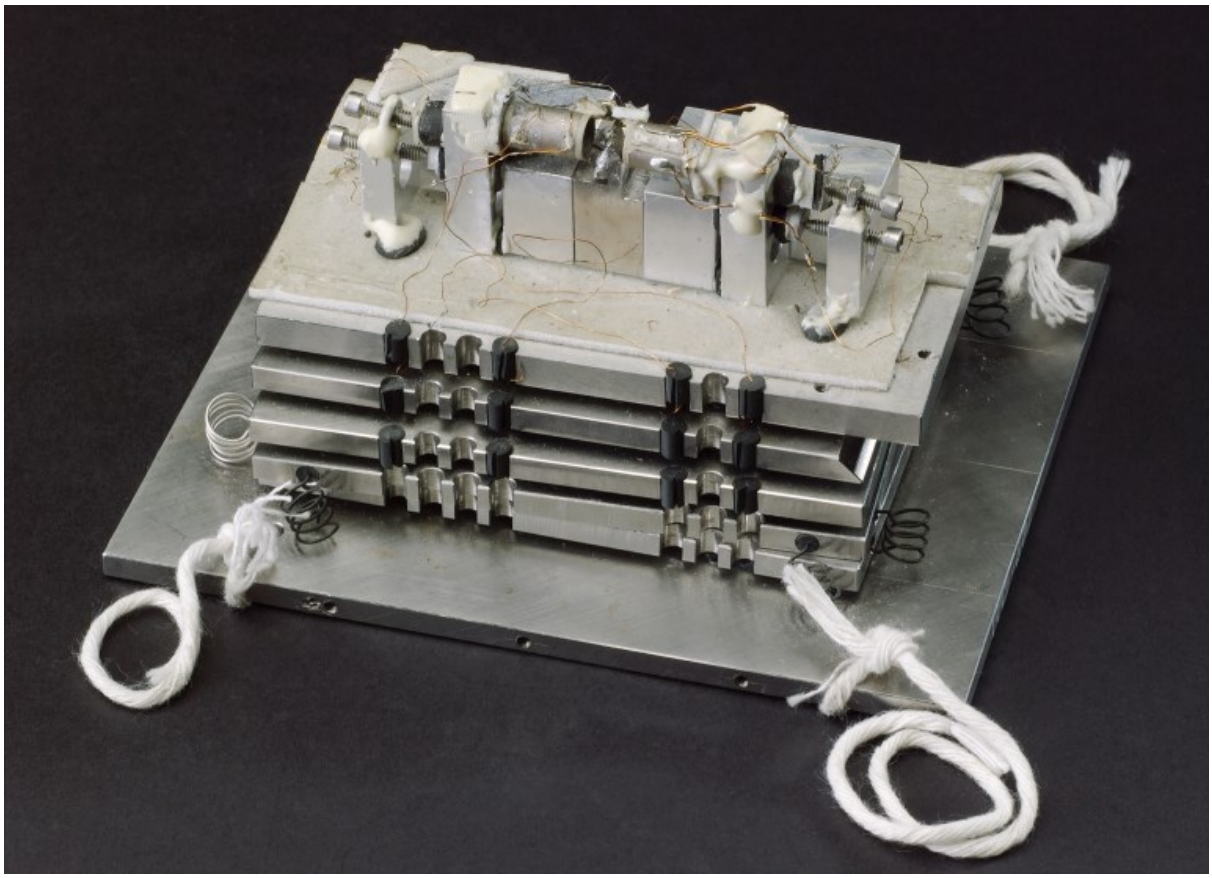

Figure 12: The first scanning probe microscope. Build by G. Binning, C.F. Quate and C. Gerber. http://www.sciencemuseum.org.uk/online_science/explore_our_collections/objects/index/smxg-8685?agent=smxg-50271

1.5.1 Set up

Since AFM is a surface dependent technique, the sample of interest needs to be immobilized onto a flat substrate. A nanometer sharp tip, which is mounted onto a flexible cantilever is then used as a probe. A laser is focused onto the back of the cantilever and reflected onto a position-sensitive photodetector. Either the sample itself or the cantilever is moved in x, y and z direction using piezo crystals. Whenever the flexible cantilever deflects up or down, the position of the laser on the photodetector changes. The voltage difference between the segments of the detector is linearly related to the cantilever deflection, which allows for the precise detection of the cantilever deflection. This leads to a resolution under optimal conditions down to 0.1 Å, if the deflection is translated into a distance (Sarid 1994). The

deflection can also be translated into a force using Hook's law and knowledge about the cantilever's spring constant. This way forces in the piconewton range acting upon the cantilever can be detected. Movement and detection are governed by a control element connected to a computer with the appropriate software to allow for real-time detection and operation (Figure 13). AFM can be used to investigate the properties of various samples, e. g. nanoparticles, tissue, cells and single molecules. There are several AFM modes to detect the different properties, however, in this study contact mode, tapping mode and force spectroscopy have been used.

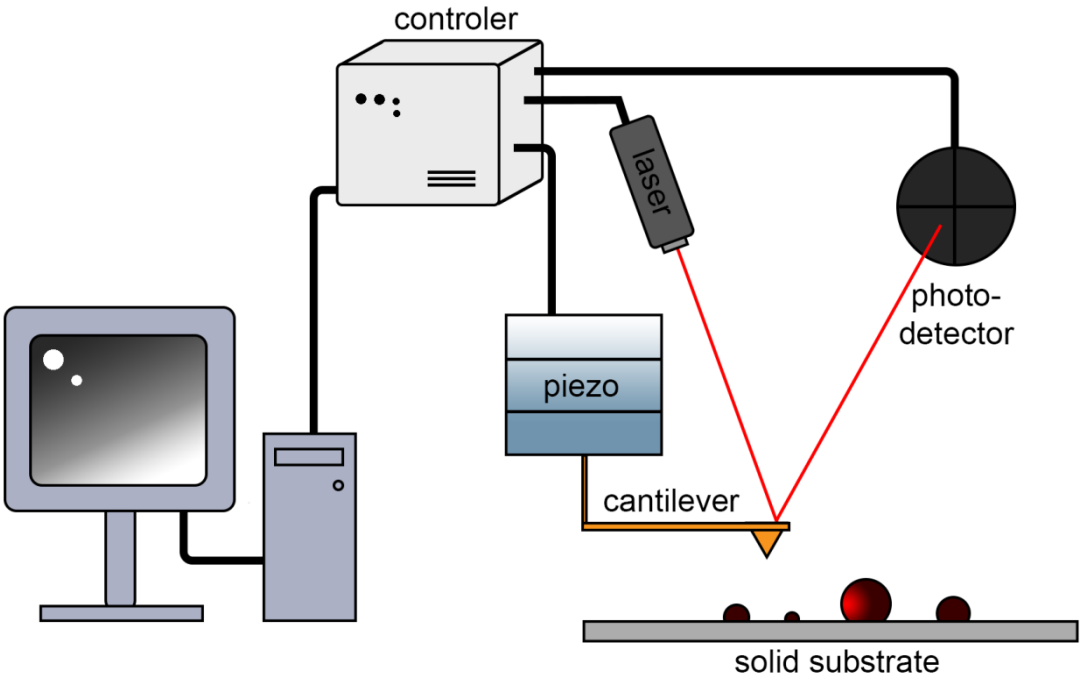

Figure 13: Schematic set up of AFM. While the sample (red) is immobilized on a solid substrate the cantilever moves over it, controlled by piezo elements. A laser is focused onto the back of the cantilever and reflected onto a photodetector. As the cantilever deflects, the position of the laser on the detector changes. All signals pass through a controller and finally give the height or force data that is recorded.

1.5.2 Contact mode

Contact mode is mainly used to create a topographical image of the surface. As the name implies the cantilever propagates over the surface in continuous contact. Contact mode is performed using a mixture of two operation principles (Figure 14). One principle is to move the cantilever over the surface at a constant height and only measure the deflection. The second principle is to continuously adjust the height of the cantilever to adapt for the surface topography. This would lead to no change in the deflection of the cantilever and only the

piezo displacement in z direction would indicate the topography of the sample. However, the first principle puts a high strain on both the sample and the cantilever, potentially leading to damage of both. The second principle demands an infinitely fine sensitivity, which cannot be achieved in practice. Thus a combination of both principles is used, recording the piezo displacement to adjust to the surface topography and the cantilever deflection. A maximum deflection is set by the operator to indicate the force with which the cantilever presses down onto the surface, while a feedback response will adjust the cantilever z position to the samples topography with finite sensitivity. The aim hereby is to minimize the deflection of the cantilever and thus the forces between sample and tip. Deflection and z displacement are then used together to calculate the real height properties of the sample.

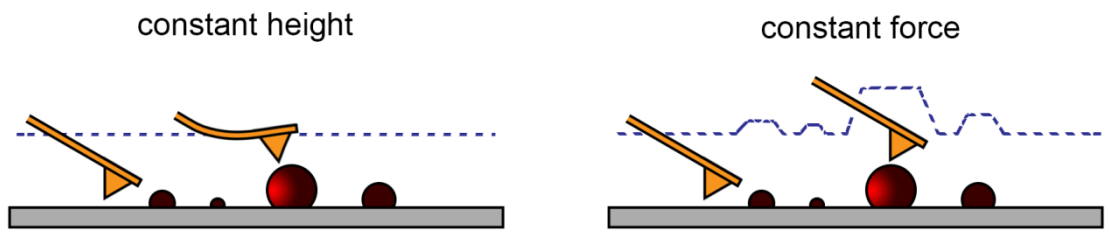

Figure 14: Schematic representation of the movement and deflection of the cantilever during contact mode. While scanning the sample with constant height only the cantilever deflection is responsible for the height image. During constant force mode the cantilever deflection is held constant and the piezo regulates the height of the cantilever according to sample topography. Only the piezo displacement in z direction (blue dashed line) is responsible for the height image.

1.5.3 Tapping mode

Tapping mode (Figure 15) was first proposed in the early 1990s by D. J. Keller (Bustamante et al. 1994), Q. Zhong (Zhong et al. 1993) and C. A. J Putman (Putman et al. 1994) independently. In this mode the cantilever is excited to exhibit vertical sinusoidal oscillations with amplitudes of a few nanometers and at frequencies close to its resonance frequency. When the cantilever comes into contact with the sample, the amplitude is dampened. Here a feedback

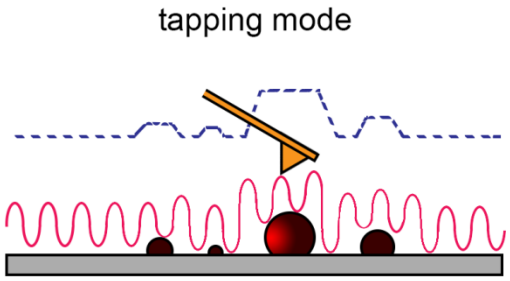

Figure 15: Schematic representation of tapping mode. In tapping mode the cantilever is oscillating (pink line) while moving over the surface. Dampening of the oscillation amplitude due to the sample topography guide the piezo displacement in z direction.

loop again aims to keep the decrease of the amplitude to a preset value. Apart from a topographic image, the recorded change in amplitude and phase of the cantilever oscillation can give information on softness/hardness and chemical properties of the sample. As the cantilever is only in contact with the sample intermittently and for short periods of time, the lateral shear forces during the scanning process are minimized. Thus, tapping mode enables the investigation of fragile biological samples, e. g. living cells (Putman et al. 1994), in physiological conditions.

1.5.4 Force spectroscopy

Apart from scanning a sample in x and y direction, AFM is used to analyze the forces acting upon the cantilever while moving just in z direction. Using this method, force-distance curves are measured. The cantilever deflection is recorded during the process and plotted against the z piezo displacement, or distance (Figure 16). In the so called force spectroscopy measurements the cantilever starts its measurement a fixed distance away from the surface and moves downwards at a preset speed (Figure 16a). The deflection remains zero until the cantilever comes into contact with the surface (Figure 16b). At this point the deflection will increase with distance. When a preset deflection of the cantilever pressing down onto the surface is reached, the cantilever starts moving back, away from the surface (Figure 16c).

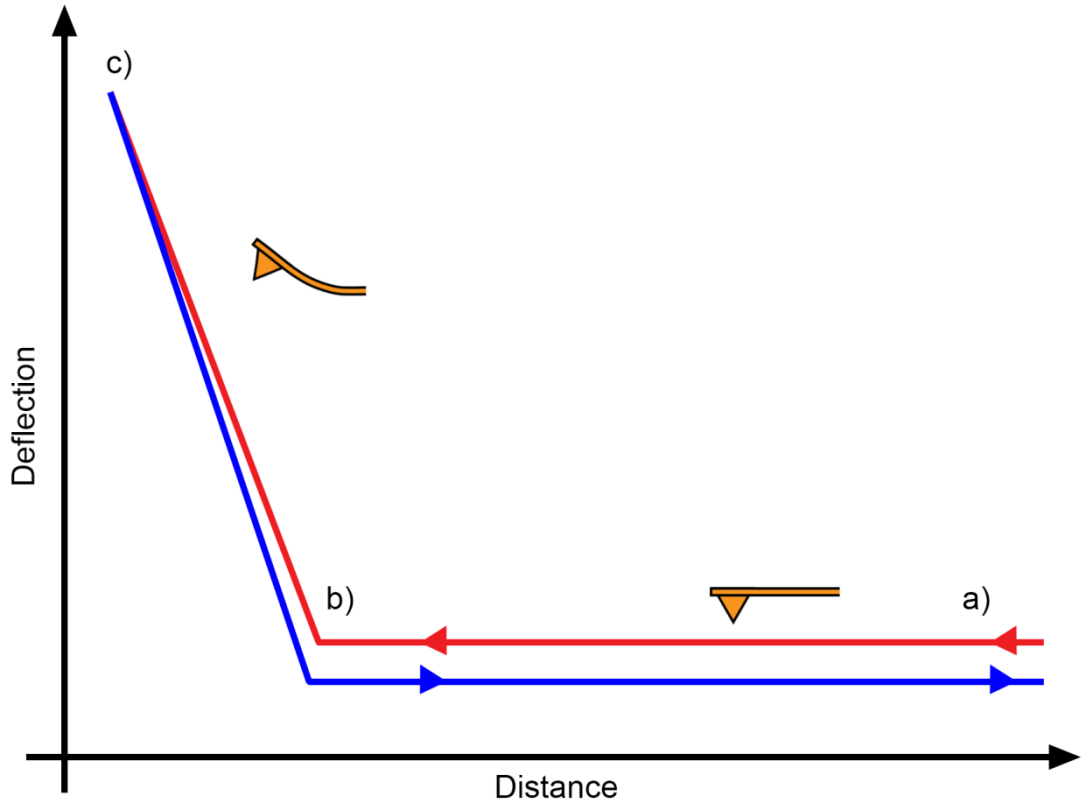

Figure 16: Schematic force curve on a non-repulsive, non-stick, hard surface. The red line represents the deflection of the cantilever while moving towards the surface (extend) and the blue line represents the way back (retract). While the cantilever (orange) is away from the surface (a) it remains straight and the deflection is zero. Upon contact with the surface (b) the cantilever deflects upwards, while piezo displacement in z direction (distance) still persists downwards. The deflection of the cantilever increases until a preset value is reached (c) and the cantilever retracts.

The deflection of the cantilever on its way towards the surface (extend) can be analyzed to give information about the stiffness of the sample. In contact with a hard surface the increase in deflection will be linear with distance (Figure 17a), while on a soft surface the resulting curve will be bent (Figure 17b). Using Young's modulus, for example, the curve can then be analyzed in terms of stiffness.

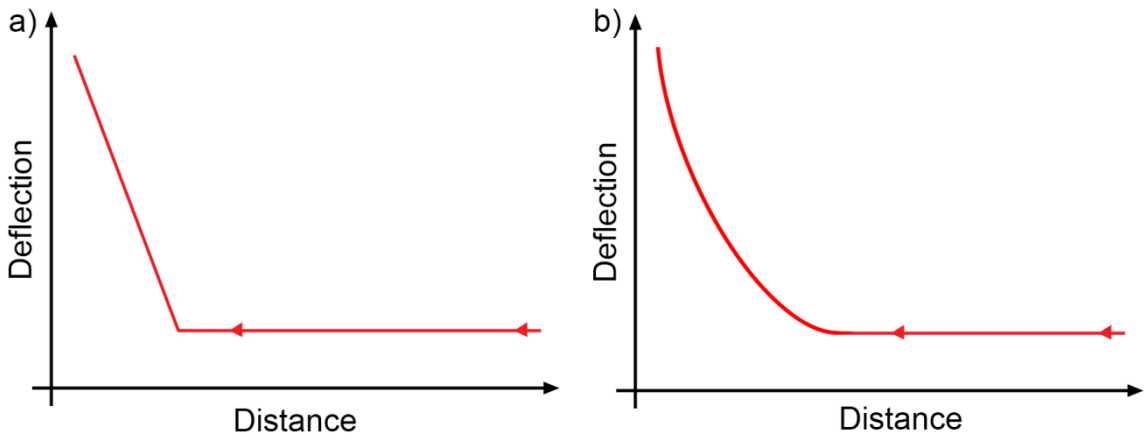

Figure 17: Comparison between a force curve on different surfaces. (a) On a hard surface the increase in deflection is linear with distance. (b) On a soft surface, e. g. a cell, the force increase is dampened by the softness of the sample.

The deflection of the cantilever on its way away from the surface (retrace) can be used to analyze possible adhesion forces between the cantilever and the sample. If adhesion between cantilever and surface exists, the cantilever will "stick" to the surface, deflecting downwards, until the force of the z piezo retraction is high enough to overcome the adhesion. Once this point is reached, the deflection will revert back to zero as the cantilever straightens (Figure 18).

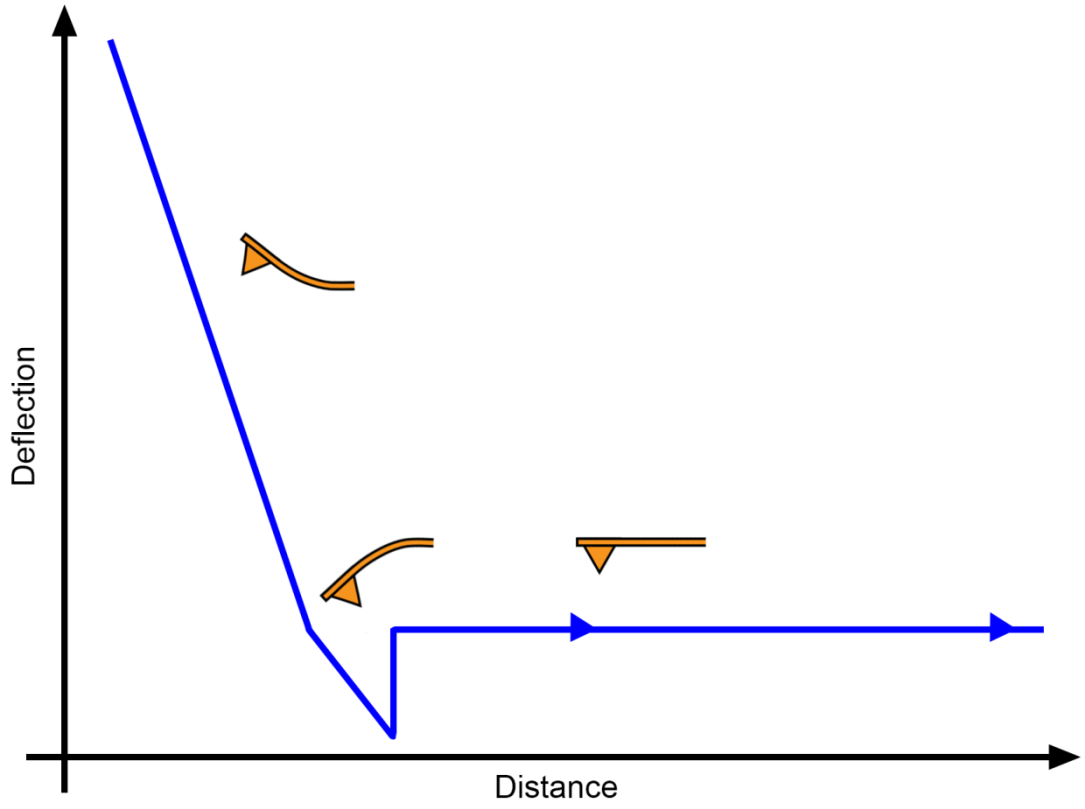

Figure 18: Force curve on a surface showing adhesion. While retracting from a surface, the cantilever can interact with the surface due to adhesion. As adhesion persists, the cantilever will bend downwards while the piezo pulls backwards. When the pull of the piezo is strong enough to overcome the adhesion, the cantilever straightens suddenly. The adhesion can be seen in the deflection of the retrace through a negative deflection peak.

The retrace can further be used to study interaction forces between the cantilever and single molecules or structural properties of polymers (Figure 19). Due to unspecific adsorption single molecules, immobilized on the surface, can "stick" to the tip. Additionally, the cantilever can be functionalized to study intermolecular forces between two molecules. Due to the elasticity of polymers the increase in deflection while the cantilever retracts is slow and non-linear over the length of the molecule. Possible intramolecular interactions can also lead to characteristic changes in deflection during stretching or unfolding. As proteins can be considered biological polymers, this method can be used to study their structure and inter- and intramolecular interactions. During stretching, a protein behaves like a non-linear elastic spring, which can be described by theoretical models, e. g. the worm-like chain model (WLC).

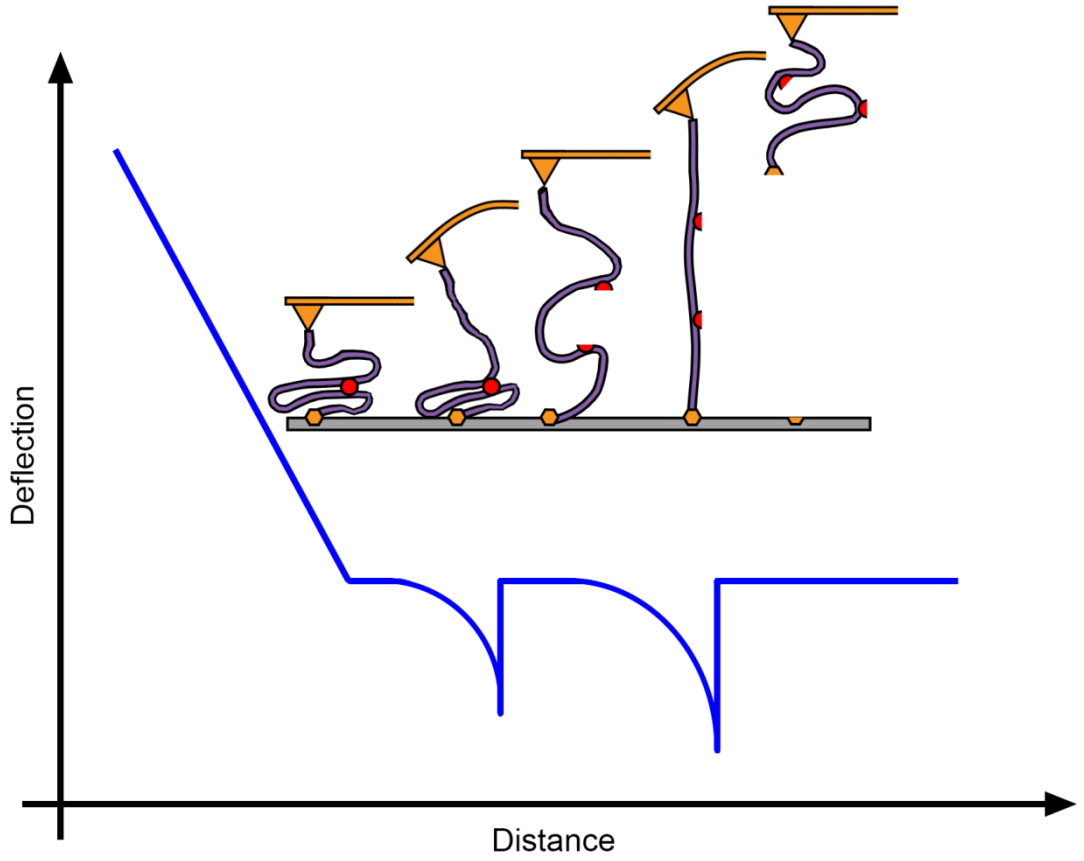

Figure 19: Force curve showing the unfolding and stretching of a polymer. When a polymer (purple), that is bound to the substrate (grey) adsorbes to the cantilever tip during retrace, unfolding and stretching of the polymer occures. An interaction between segments of the polymer (red) first leads to the stretching until the interaction can be broken. This is indicated be the straightening of the cantilever. The cantilever then bends again during further stretching until the bond between the surface and the polymer (orange) is broken. The two stretching events can be seen in the retrace through two non-linear increases in negative deflection followed by a sudden relaxation.

1.5.5 Calibration

To calculate the measured deflection into a distance or force the so called InVols value (nm/V) as well as the knowledge about the cantilever's spring constant (N/m) is needed. Even though standard values are given by cantilever manufacturers, due to variances during production these values have to be calibrated before each measurement for every new cantilever.

Cantilever resonance

Measuring the amplitude and phase of the cantilever oscillation away from the surface dependent on frequency enables us to determine the resonance frequency of the cantilever. The measured cantilever resonance curve can be fit with using a harmonic oscillator function:

$$y(f) = A \cdot \frac{f_0^2}{\left(f^2 - f_0^2\right)^2 + \left(\frac{f_0 f}{Q}\right)^2}. \quad 1$$

With A being the amplitude, f the frequency, f_0 the resonance frequency and Q the quality factor (Q-factor) of the resonance. The Q-factor of the resonance is a measure of the damping in the oscillating system and can be calculated as follows:

$$Q = \frac{energy\ stored\ in\ an\ oscillation}{energy\ lost\ per\ cycle}. \quad 2$$

This translates into a measure of how sharp the resonance curve is:

$$Q \approx \frac{f_0}{full\ width\ at\ half\ max.}. \quad 3$$

A large Q-factor means a sharp resonance curve, which in turn means a higher sensitivity of the cantilever in tapping mode. AFM cantilevers for tapping mode usually have a Q-factor of a few hundred in air. However, in water or aqueous buffer a much higher damping, due to the viscosity of the liquid, reduces the Q-factor to smaller values of 1-5. Additionally, the effective mass of the cantilever increases as the cantilever has to carry the surrounding liquid as it oscillates. Therefore the shape of the resonance curves depends not only on the chosen cantilever, but also on the surrounding medium.

Cantilever deflection

Especially for force measurements it is important to know the precise distance a cantilever deflects for a certain measured change in photodetector voltage. This relationship depends on the type of cantilever and the optical path of the laser. To calibrate cantilever deflection a force-distance curve is measured on the surface. The linear slope of the increase in deflection displays the change in piezo height with change in deflection. From this, a factor can be determined easily to convert Volts into nanometers.

Spring constant

The basic method of thermal noise spring constant calibration has been described in the past (Hutter, Bechhoefer 1993). The thermal vibration of the cantilever can be measured as a vertical deflection of the cantilever over time. However, to exclude low-frequency components and specific noise sources, the thermal vibrations are analyzed dependent on

frequency. The resonance peak of the frequency dependent thermal vibrations is fit using a harmonic oscillator function:

$$A^2(f) = \eta^2 + A_{DC}^2 \frac{f_0^4}{\left(f^2 - f_0^2\right)^2 + \left(\frac{f_0 f}{Q}\right)^2}. \quad 4$$

Wherein η is the white noise background and A_{DC} is the direct current amplitude. The area under the fit curve is used to calculate the value $\Delta\chi^2$, which is the mean square cantilever deflection. The equipartition theorem states that the energy in any degree of freedom in a system has to be equal to the thermal energy $E_{Thermal}$:

$$E_{Thermal} = \frac{1}{2} k_B T. \quad 5$$

k_B is the Boltzmann constant and T is the temperature in Kelvin. In turn, the thermal Energy of the cantilever can be described by the spring constant k_c and $\Delta\chi^2$:

$$E_{Thermal} = \frac{1}{2} k_c \langle \Delta x^2 \rangle. \quad 6$$

With higher vibrational modes neglected, the cantilever stiffness can therefore be described as:

$$k_c = \frac{k_B T}{\langle \Delta x^2 \rangle}. \quad 7$$

Knowing the cantilever's spring constant, the deflection can now be converted into force using Hook's law:

$$F = -k_c \cdot d, \quad 8$$

with F being the force acting on the cantilever and d its deflection in nanometers.

1.6 Motivation

The study of proteins is a topic of high interest in the scientific field. Due to misfolding, proteins can be the cause for various diseases, e. g. Alzheimer's disease and metabolic disease. Knowledge about their structure gives insight into their function and intra- and intermolecular interactions. Only if this information is available, disease treatment and drug design can be conducted accordingly. Proteins associated with the cellular lipid membrane are one specific group that this study has been focused on. They are exceptionally difficult to study as they need a lipid membrane to retain their native conformation. Studying MPs in whole cells on a single molecule level is improbable. However, once removed from the membrane, most of these proteins lose their functionality. One way to make MPs available for investigation outside of the cell is the development of membrane mimicking systems. The aim of this work was to study different membrane associated proteins, $A\beta_{1-42}$, BR and TGR5, with AFM. To achieve this, two different membrane mimicking systems should be developed: One such system based on sBLMs to study the cholesterol and temperature dependent membrane association of $A\beta_{1-42}$ oligomers in comparison with monomers and fibrils. A method to separate oligomers, monomers and fibrils was previously established in our group.

The second membrane mimicking system should be based on a tBLM with an integrated specifically orientated IMP on quartz glass. Solubilized BR, which was available due to cell free expression from the group of Manuel Etzkorn, was to be used as a model for GPCRs. Simultaneously, the medically relevant human GPCR TGR5 should be expressed and purified in its native conformation using cell free expression, to make it available for studies with the here developed tBLM.

2. Results

2.1 Articles and Manuscripts

2.1.1 Disruptive effect of specific Aβ1-42 Oligomers on Cholesterol-rich Membranes

Journal: PLoS ONE (Manuscript prepared for submission)

Impact Factor: 3.234

Own contribution: 50 %

Carrying out and analysis of AFM, preparation of artificial membranes, SUV preparation, ELISA, size exclusion chromatography of SUVs, co-authoring the manuscript

Changes to the manuscript: Figures have been placed at the designated places in the text.

Disruptive effect of specific $A\beta_{1-42}$ Oligomers on Cholesterol-rich Membranes

Anna Bronder[1*], Alexander Brener[1,2], Luitgard Nagel-Steger[1,2], Dieter Willbold[1,2]

[1]Institut für Physikalische Biologie, Heinrich-Heine-Universität Düsseldorf, 40225 Düsseldorf, Germany

[2]Institute of Complex Systems, Structural Biochemistry (ICS-6), Research Centre Jülich, 52425 Jülich, Germany

* Corresponding author

E-mail: anna.bronder@hhu.de (AB)

Abstract

A key feature of Alzheimer's disease is the formation of extracellular amyloid deposits of aggregated cellular proteins, mainly consisting of the amyloid β-protein (Aβ). There is evidence that Aß membrane interactions play a pivotal role for aggregate formation as well as for Aβ mediated cell toxicity. It has been shown previously that Aβ oligomers associate with the cellular membrane, which leads to subsequent cell death. The interactions of Aβ with the cellular membrane are dependent on membrane composition. Additionally, cholesterol levels seem to play an important role during the course of Alzheimer's disease.

We studied the influence of $A\beta_{1-42}$ oligomers on a solid supported bilayer membrane consisting of the phospholipid 1,2-dipalmitoyl-sn-glycero-3-phosphocholine, cholesterol and n-dodecylphosphocholine with atomic force microscopy. Our results show a destabilizing effect of specific $A\beta_{1-42}$ oligomers on the model membrane at 37 °C, with the presence of cholesterol playing a key role in this process. In contrast $A\beta_{1-42}$ monomers and fibrils did not show any effect on the model membrane. Our findings emphasize the difference of the influence of $A\beta_{1-42}$ oligomers on membranes in comparison with monomers and fibrils. Furthermore, we could link high cholesterol levels to a strong interaction between $A\beta_{1-42}$ oligomers and cellular membranes.

Introduction

The main characteristic of neurodegenerative disorders is the slowly progressing, irreversible damage of neural tissue. Their most common form is Alzheimer's disease (AD), which accounts for 60 % of all dementia cases [1]. One of the major risk factors of AD is age. Facing an ever increasing life expectancy, studies helping us to understand mechanisms underlying the development of AD are of great interest for drug development. One of the hallmarks of AD is the accumulation of amyloid aggregates [2,3] in the central nervous system, mainly consisting of the amyloid β-protein (Aβ) [4]. According to the amyloid cascade hypothesis [5,6] different aggregation states of Aβ initiate cellular events leading to cell death [7]. Especially Aβ oligomers are thought to play a central role in AD pathogenesis [8–10]. Thus, studying their properties and structure is of high interest. Aβ is generated by the proteolytic cleavage of the amyloid precursor protein (APP) [11]. Several species of Aβ exist, depending on the imprecise location of the cleavage sites [12–15]. Although $A\beta_{1-40}$ is the more abundant form in blood and cerebrospinal fluid, $A\beta_{1-42}$ is found as the prevailing and more toxic species in amorphous plaques and soluble oligomers [5,16,17].

Previous studies have shown that Aβ oligomers can form pores when associated with a lipid membrane [18–20]. There is evidence that the lipid composition of the membrane plays an important part in Aβ membrane association and development of AD [21]. Especially cholesterol seems to promote membrane association and aggregation of Aβ [22,23]. Thus, we are interested to investigate the interaction of $A\beta_{1-42}$ oligomers with membranes. Cellular membranes are lipid bilayers consisting of phospholipids, glycolipids and cholesterol. The fluidity of a membrane is dependent on temperature and its lipid composition [24]. Depending on these factors artificial membranes have been observed to either be in an unordered fluid-like phase or a more rigid and ordered gel- to crystal-like phase. Especially the cholesterol content plays a decisive role in phase transitions [25,26]. Artificial membranes can be formed on solid supports through self-assembly, creating solid supported bilayer lipid membranes (sBLM) [27]. Such supported bilayers can be studied by surface dependent techniques, like atomic force microscopy (AFM). AFM uses the interaction between the sample and a nanometer sharp cantilever tip to study a sample's topography and properties. Complex molecules as

well as molecular layers can be visualized at the nanometer scale.

In this study we aimed to investigate the effect of $A\beta_{1-42}$ oligomers on a model sBLM with a high ratio of cholesterol to phospholipid (1:1) at physiological temperatures by AFM. Our findings clearly indicate cholesterol-dependent membrane disruptive properties of specific $A\beta_{1-42}$ oligomers, which were absent for $A\beta_{1-42}$ monomers and fibrils.

Materials and Methods

All experiments were reproduced independently at least twice.

Peptides and Lipids

$A\beta_{1-42}$ with 95.2 % purity was purchased from Bachem (Heidelberg, Germany). 1,2-dipalmitoyl-sn-glycero-3-phosphocholine (DPPC), >99 % purity, n-dodecylphosphocholine (DPC), >99 % purity, and cholesterol, from ovine wool, >98 % purity, were purchased as powders from Avanti Polar Lipids (Alabaster, U.S.). Water was purified by the Milli-Q Integral Water Purification System (milli-Q; Merck Millipore, Darmstadt, Germany). Iodixanol was purchased from Sigma-Aldrich. Primary antibody Beta Amyloid, 1-16 (6E10), monoclonal, mouse IgG, was purchased from Covance (Princeton, U.S), and secondary antibody peroxidase-conjugated AffiniPure goat anti-mouse IgG (H+L) (GAM-PO) was purchased from Dianova (Hamburg, Germany).

Pre-incubation of $A\beta_{1-42}$

Dried $A\beta_{1-42}$ (S1 File) was re-suspended in 10 mM sodium phosphate buffer, pH 7.4 in a final concentration of 80 μM. For the maximum amount of $A\beta_{1-42}$ monomers the solution was directly used for density gradient centrifugation. To yield a high amount of oligomers the solution was incubated for 4.5 h, at room temperature (RT) with shaking (600 rpm). In order to generate $A\beta_{1-42}$ fibrils the solution was incubated for 48 h, at 37 °C with shaking (600 rpm). Fibril formation was verified by AFM imaging in tapping mode, before and after density gradient centrifugation.To investigate $A\beta_{1-42}$ oligomers, monomers and fibrils independently, the different types of $A\beta_{1-42}$ assemblies were separated according to size and shape by density gradient centrifugation [28–30]. After defined incubation times of $A\beta_{1-42}$ and subsequently performed density gradient centrifugation, monomeric $A\beta_{1-42}$ can be found in the top gradient fractions, slightly larger oligomers will move towards the

middle, while fibrils and higher order oligomers will sediment to the bottom fractions. A discontinuous gradient of iodixanol was pre-formed by layering 260 µl of 50 % (v/v) iodixanol at the bottom of an 11 × 34 mm polyallomer centrifuge tube, overlaid by 260 µl of 40 %, 260 µl of 30 %, 780 µl of 20 %, 260 µl of 10 %, and 100 µl of 5 % iodixanol. The total volume of the phosphate-buffered, non-linear gradient was 1920 µl. The top of the gradient was overlaid by a 100 µl aliquot of incubated $A\beta_{1-42}$. The samples were spun at 259,000 × g for 3 h at 4 °C in a TL 100 ultracentrifuge with a TLS-55 rotor (both Beckman Instruments, Brea, USA). After centrifugation, 14 fractions of 140 µl were harvested with a pipette by downward displacement. The leftover of each tube (ca. 60 µl remaining volume) eventually including a pellet was mixed with 60 µl 6 M guanidine hydrochloride and boiled for 10 min. The resulting solution yielded the 15 th fraction. Fraction 1 from the top of the gradient was the least dense, and fraction 14 from the bottom was the densest fraction. Fractions 4-6, where oligomers accumulate, contain about 20 % iodixanol, which corresponds to a density of 1.112 g/cm³. The $A\beta_{1-42}$ content per fraction was determined by RP-HPLC as described in [28] (S1 File). Thus purified and characterized monomers, oligomers and fibrils were used for the membrane interaction studies.

Floatation Density Gradient Centrifugation

In order to characterize the state of $A\beta_{1-42}$ oligomers after incubation on the cholesterol containing sBLM a 100 µl sample was taken from the surface and loaded onto preformed gradient as described before. In addition, an inverse sample application scheme for density gradient centrifugation was used. Likewise a 100 µl sample taken from the surface of an $A\beta_{1-42}$ oligomer treated cholesterol containing sBLM was loaded either as a first fraction at the bottom of a iodixanol gradient. Due to the low amount of $A\beta_{1-42}$ per fraction the concentration had to be determined by an enzyme-linked immunosorbent assay (ELISA) instead of RP-HPLC. As a control a sample containing freshly prepared $A\beta_{1-42}$ without any lipids was loaded at the bottom of a density gradient and analyzed with ELISA after centrifugation.

ELISA

For the quantification of sub-nanomolar $A\beta_{1-42}$ amounts the A specific immunoassay based on the detection antibody 6E10 was chosen. The assay was prepared on black 96-well immuno plates with flat bottom suitable for usage with the QuantaBluTM Fluorogenic Peroxidase Substrate Kit (Thermo Scientific, Rockfolf, Illinois USA). The detailed procedure was described previously [33] and in supporting information (S1 File).

Preparation of sBLMs for AFM and incubation of $A\beta_{1-42}$ peptide

Aqueous DPPC and cholesterol suspensions (S1 File) were mixed 2:1 (v/v) for cholesterol containing sBLMs, while aqueous DPPC suspension alone was used for sBLMs without cholesterol. A volume of 50 µl suspension was incubated on freshly cleaved mica for 2 h, RT before rinsing with 5 x 100 µl of 10 mM sodium phosphate buffer, pH 7.4 by carefully pipetting up and down on the surface. After the last rinsing step 50 µl of 10 mM sodium phosphate buffer, pH 7.4 were added onto the surface for direct AFM measurements. For incubation with $A\beta_{1-42}$ monomers, oligomers and fibrils only a thin layer of 10 mM sodium phosphate buffer pH 7.4 (approximately 10 µl) was left on the surface after rinsing. After determination of the concentration of $A\beta_{1-42}$ in the fractions of interest the concentration was adjusted to 4 µM with 10 mM sodium phosphate buffer pH 7.4 and 5 µl of this solution were incubated on the membranes for 1 h, RT. The mica surface was rinsed again with 5 x 100 µl 10 mM sodium phosphate buffer pH 7.4 by carefully pipetting up and down on the surface. Finally, 50 µl 10 mM sodium phosphate buffer pH 7.4 were left on the surface for AFM measurements. To test the effect of iodixanol on cholesterol containing sBLMs 5 µl of a 30 % (v/v) iodixanol solution in 10 mM sodium phosphate buffer, pH 7.4 were incubated on a freshly constituted sBLM for 1 h, RT. The sample was rinsed again with 5 x 100 µl 10 mM sodium phosphate buffer pH 7.4 by carefully pipetting up and down on the surface. 50 µl 10 mM sodium phosphate buffer pH 7.4 were left on the surface for AFM measurements. After imaging at RT all samples were placed at 37 °C in a humid environment to prevent drying of the samples. After 1 h incubation the samples were again imaged by AFM. For floatation density gradient centrifugation from the bottom the samples on mica were covered with 50 µl 10 mM sodium phosphate buffer pH 7.4 containing 55 % iodixanol to adjust the density of the sample to the density of the bottom fraction of the gradient before incubation of the samples for 1 h at 37 °C in a humid environment.

Preparation of $A\beta_{1-42}$ fibrils for AFM

5 µl of a 40 µM $A\beta_{1-42}$ fibril solution, before and after density gradient centrifugation respectively, were incubated on freshly cleaved mica for 1 h, RT. The sample was rinsed 5 x 100 µl milli-Q-water and dried under nitrogen.

Imaging by AFM

AFM images of sBLMs were taken at RT with a Nanowizard III (JPK Instruments, Berlin, Germany) and SNL-10 probes (Cantilever A, triangle, Bruker, Massachusetts, US) with a nominal spring constant (k_c) of 0.18-0.35 N/m, a resonance frequency (f) of 50 -80 kHz and a tip radius (r) of 2-12 nm using tapping mode in 10 mM sodium phosphate buffer, pH 7.4. Fibrils were imaged at RT with a Multimode Atomic Force Microscope (Bruker, Massachusetts, US) and OMCL-AC160TS probes (rectangular, $k_c = 0.012$ to 0.103 N/m, $f = 200$ to 400 kHz, $r = 7$ to 11 nm, Asylum Research, Mannheim, Germany) using tapping mode in air.

Results

Membrane formation and stability

The membrane composition for this study (DPPC:cholesterol 1:1 (n/n) with 0.1 % DPC (w/v)) was specifically chosen to yield a homogenous bilayer on the mica surface, consisting predominantly of a single lipid phase. A homogeneous lipid phase for a DPPC bilayer with 50 % cholesterol on mica was previously demonstrated [31]. To test membrane formation on mica and ensure a homogenous lipid phase, imaging with AFM was performed. In Fig 1A an AFM image of a membrane, consisting of DPPC, cholesterol and DPC can be seen. Imaging was done directly after membrane formation at RT. Coverage of the surface was disrupted only by a few small holes of 4 nm depth, indicating the successful formation of an almost completely intact lipid bilayer. To test temperature dependent stability over time, the surface was subsequently incubated for 2 h at 37 °C. In Fig 1B the same surface after incubation can be seen. A change in membrane coverage was not observed, however the lipid membrane shows two domains, one main domain (light gray) which is interspersed with both linear and round nanodomains (dark gray). These nanodomains have been shown to occur in

membranes made of DPPC and cholesterol mixtures [32].

Further, the membrane was tested for its stability towards the density gradient material iodixanol, since the different Aβ species are purified by a density gradient centrifugation procedure. Fig 1C shows a surface completely covered with membrane, imaged after incubation of 30 % iodixanol in 10 mM sodium phosphate buffer pH 7.4 (v/v). Fig 1D shows the same surface after 2 h incubation at 37 °C. The surface shows some holes of about 4 nm depth. All surfaces show small round particles on top of the membrane (white arrows) that are attributed to small unfused lipid vesicles, which remained from the lipid membrane production procedure.

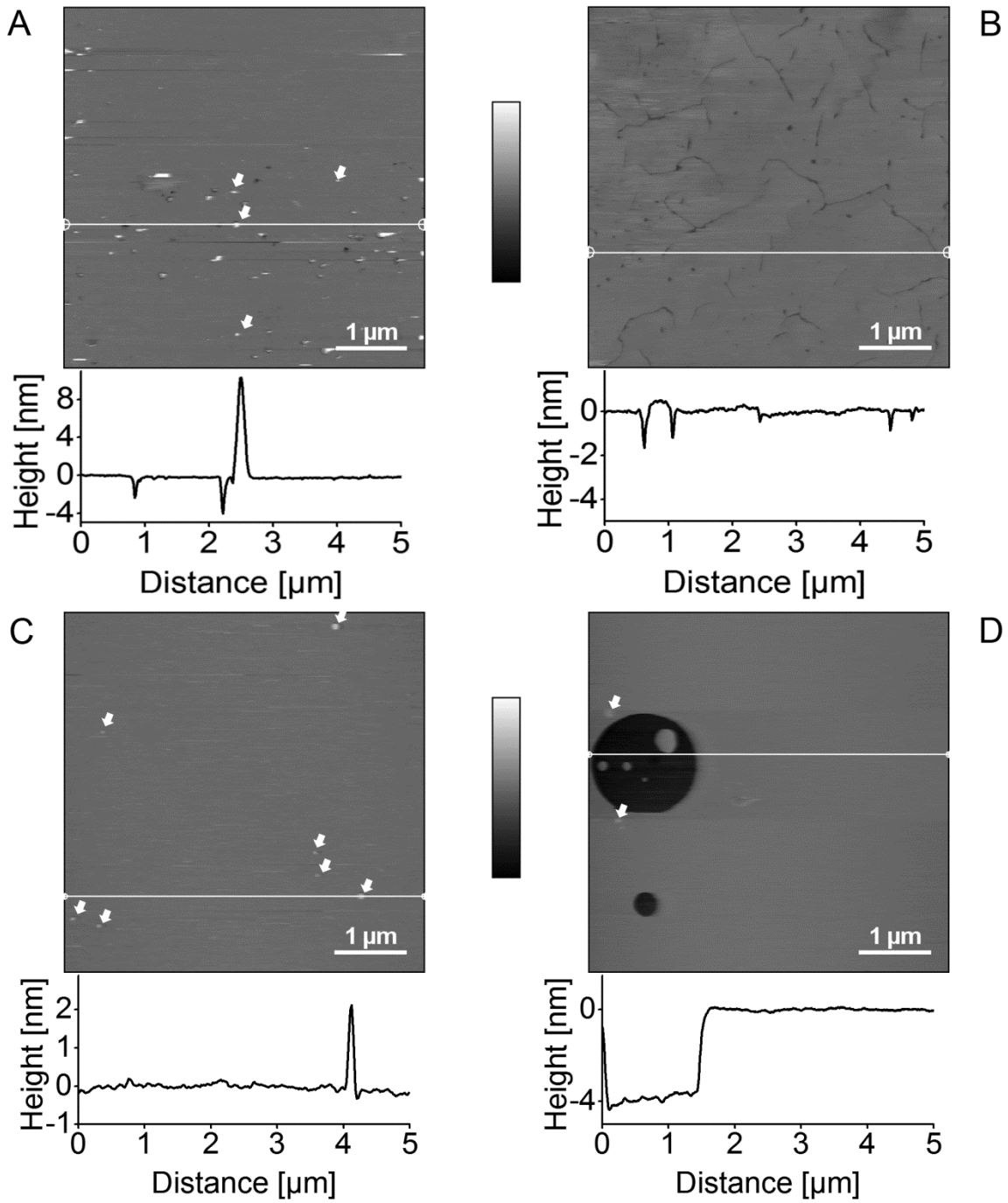

Fig 1 Membrane stability. AFM images of DPPC/cholesterol/DPC membranes on mica. All images show an area of 5 µm x 5 µm each. A few round particles of 1 to 10 nm height can be observed (white arrows) on the surfaces, which can be attributed to small unfused vesicles. Defects or holes in the membrane correspond to the dark grey to black area, while the membrane is depicted in grey. The white line in all images corresponds to the height profile under each image. All color scales represent 10 nm. (A) The membrane imaged directly after formation at RT shows a small defect of 4 nm depth. (B) The same surface after incubation at 37 °C for 2 h does not indicate a change in surface coverage. (C) A membrane incubated with 30 % iodixanol for 1 h shows no

observable defects. (D) The same surface after 2 h incubation at 37 °C shows a similar integrity with holes of 4 nm depth.

Oligomeric $A\beta_{1-42}$ and membranes

The oligomeric $A\beta_{1-42}$ used here was characterized in a previous study [28]. The $A\beta_{1-42}$ oligomers have been described as oblate spheroids with a height of 4.7 nm and a diameter of 8.7 nm. With a sedimentation coefficient of 7 S and a molecular weight of about 104 kDa they consist of approximately 23 monomeric units with β-sheet secondary structure. These oligomers were incubated on a pre-formed DPPC/cholesterol/DPC membrane to investigate possible effects. Fig 2A shows an AFM image of a membrane after incubation with $A\beta_{1-42}$ oligomers at RT. The membrane does not show any visible defects. One small round particle (white arrow) is visible, which is typical for a small vesicle. Slightly darker areas (black arrow) are visible throughout the membrane. The corresponding height profile shows a depth of these areas of 0.2 nm (black arrow). This height difference is indicative of a second lipid phase [34]. The same surface after 1 h incubation at 37 °C (Fig 2B) shows complete absence of membrane. Only a few round objects with a height of 2 nm are visible on the surface. Zoomed in areas of 150 nm x 150 nm before (Fig 2C) and after incubation at 37 °C (Fig 2D) show a distinct difference in surface topography. Fig 2C shows the presence of small round objects (white arrows), protruding 0.2 to 0.3 nm out of the membrane. Fig 2D shows a homogenously flat surface with the typical roughness of mica.

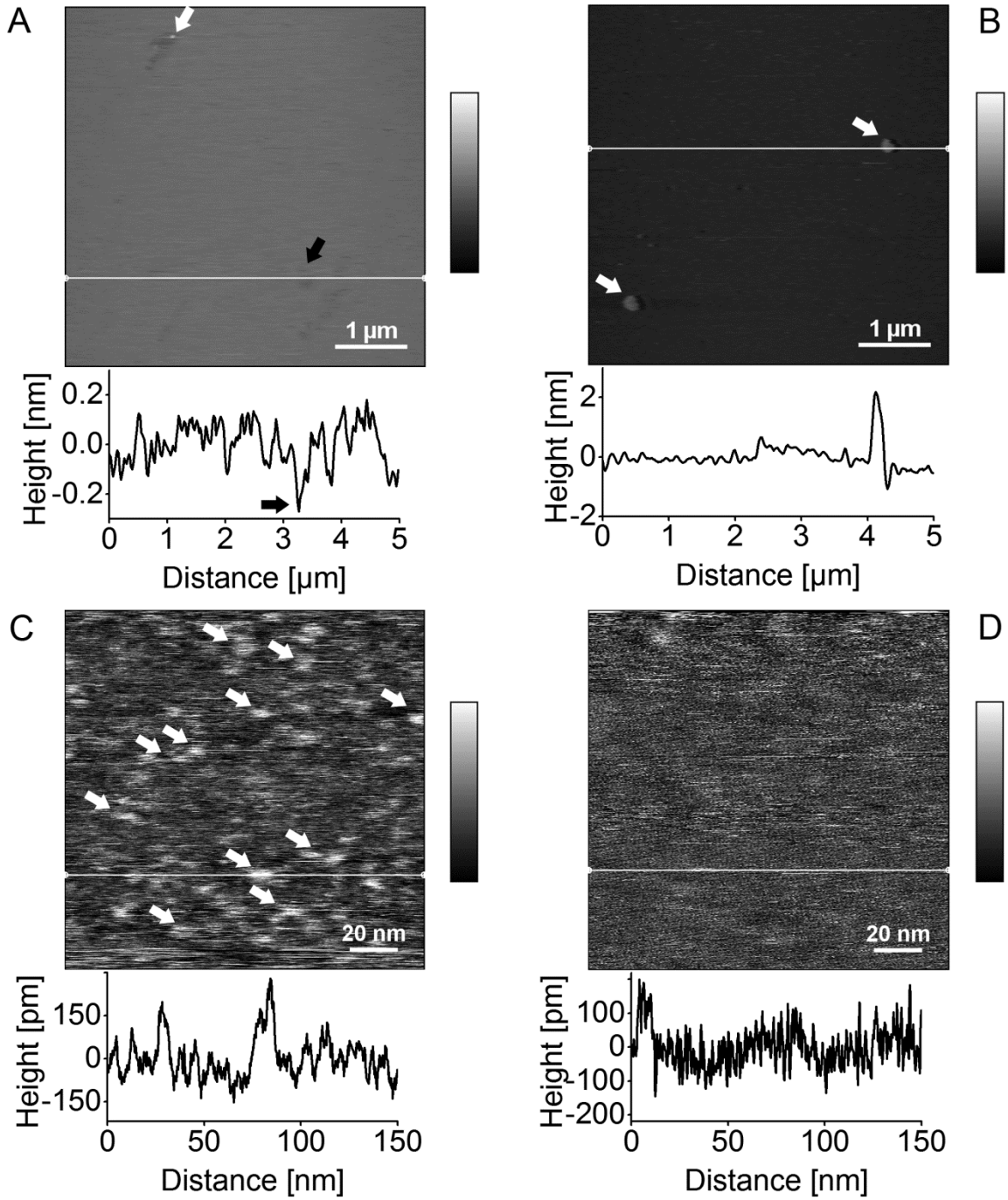

Fig 2 Effect of oligomeric $A\beta_{1-42}$ on supported bilayers. AFM images, of DPPC/cholesterol/DPC membranes on mica incubated with oligomers. Upper images show an area of 5 µm x 5 µm each, while lower images show zoomed in areas of 150 nm x 150 nm. The horizontal white line in all images corresponds to the height profile under each image. Color scales of A and B represent 10 nm, while color scales for C and D represent 300 pm. (A) The surface after 1 h incubation at RT with $A\beta_{1-42}$ oligomers shows full coverage with a bilayer membrane. One round particle (white arrow) and a few darker areas (black arrow) with a depth of ~0.2 nm are visible. (B) The surface after further incubation for 1 h at 37 °C shows no membrane but round objects of 2 nm height are

visible (white arrows). (C) The detailed scan of the membrane after incubation with $A\beta_{1-42}$ oligomers indicates small round structures (white arrows) protruding ~0.3 nm from the membrane. (D) The free mica surface, imaged in detail, shows a homogenous topography with an average roughness of 0.1 nm on a scale of 20 nm and height differences of 0.2 nm throughout the whole dimensions of the image.

Monomers and fibrils on membranes

$A\beta_{1-42}$ monomers and fibrils were incubated on a pre-formed DPPC/cholesterol/DPC membrane to compare their possible effects with the one observed for oligomeric $A\beta_{1-42}$. Fig 3A shows a membrane with $A\beta_{1-42}$ monomers after 1 h at 37 °C. An incomplete coverage is visible with darker areas corresponding to the mica surface. A membrane height of 5 nm can be seen in the height profile. Fig 3B shows a membrane incubated with $A\beta_{1-42}$ fibrils after 1 h at 37 °C. A few small holes (black) and a few dark gray areas can be distinguished from the membrane surface (light gray). The height profile shows the depth of the wholes to be 5 nm, while the dark gray areas have a depth of ~2 nm (black arrows). The holes show the bilayer thickness while the dark gray areas can be related to a second lipid phase or lipid monolayer. There was no difference in surface coverage to a bilayer membrane before incubation at 37 °C (S1 Fig). Fibril formation and presence of fibrils after density gradient centrifugation was verified by AFM (S2 Fig) before incubation of fibrils on the membrane. Small round particles (white arrows), which correspond to unfused vesicles can be seen on all surfaces.

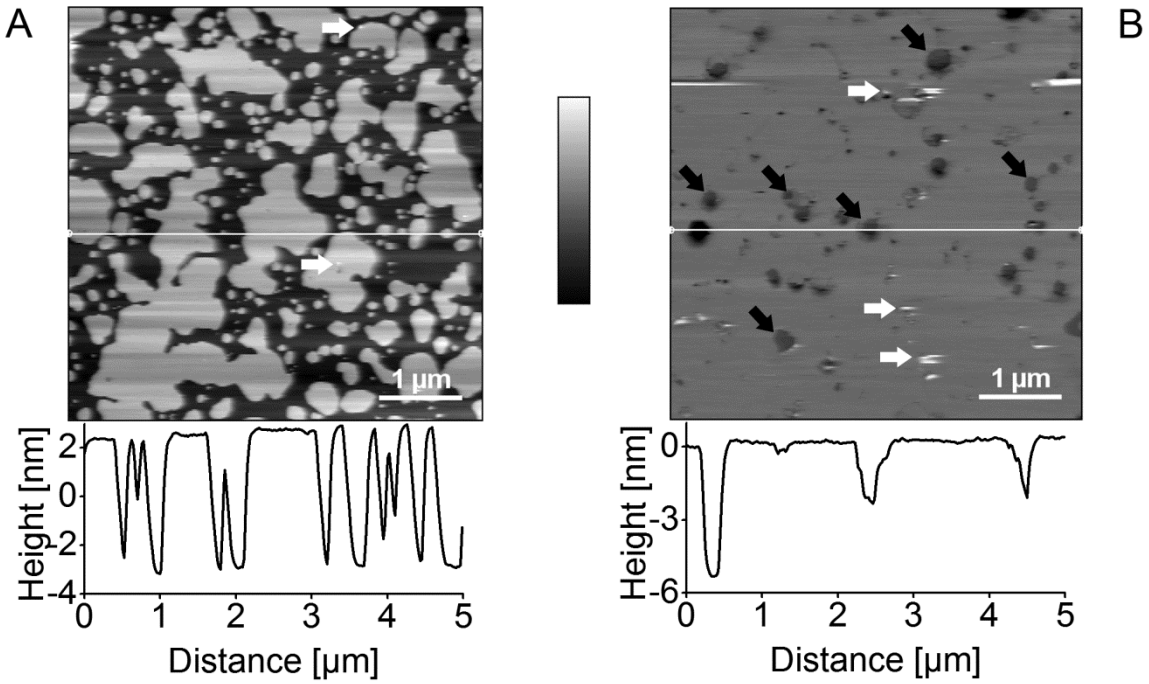

Fig 3. Effect of $A\beta_{1-42}$ monomers and fibrils on supported bilayers. AFM images of DPPC/cholesterol/DPC membranes on mica incubated with monomers and fibrils. Both images show an area of 5 µm x 5 µm each. The horizontal white line in both images corresponds to the height profile under each image. The color scale represents 10 nm. (A) The membrane after 1 h incubation with $A\beta_{1-42}$ monomers at RT and further incubation for 1 h at 37 °C. Light gray colored membrane patches can be seen interspersed with dark gray areas with a depth of 5 nm. Some white round particles can be found on top of the membrane patches (white arrows). (B) The membrane after 1 h incubation with $A\beta_{1-42}$ fibrils at RT and further incubation for 1 h at 37 °C. The membrane (light gray) shows only a few defects (dark gray) and some lower gray areas (black arrows). The height of the bilayer is 5 nm. The gray areas have a depth of 2 nm. White arrows indicate particles on top of the membrane, which have been disturbed during the scanning process.

Role of cholesterol

Oligomeric $A\beta_{1-42}$ was incubated on a pre-formed DPPC/DPC membrane to investigate possible effects in absence of cholesterol. Fig 4A shows an AFM image of the membrane directly after 1 h incubation at RT with $A\beta_{1-42}$ oligomers. The membrane has an incomplete coverage of the surface as well as some double-stacked membrane patches. The membrane patches have a height of 5 nm as shown by the height profile. This is again interpreted as a bilayer. In Fig 4B the same surface is shown after incubation at 37 °C. The surface coverage is still incomplete and the height of the membrane

remains at 5 nm. Zoomed in areas of the membrane before incubation at 37 °C (Fig 4C) and after (Fig 4D) do not show any protruding particles or a difference in surface topography.

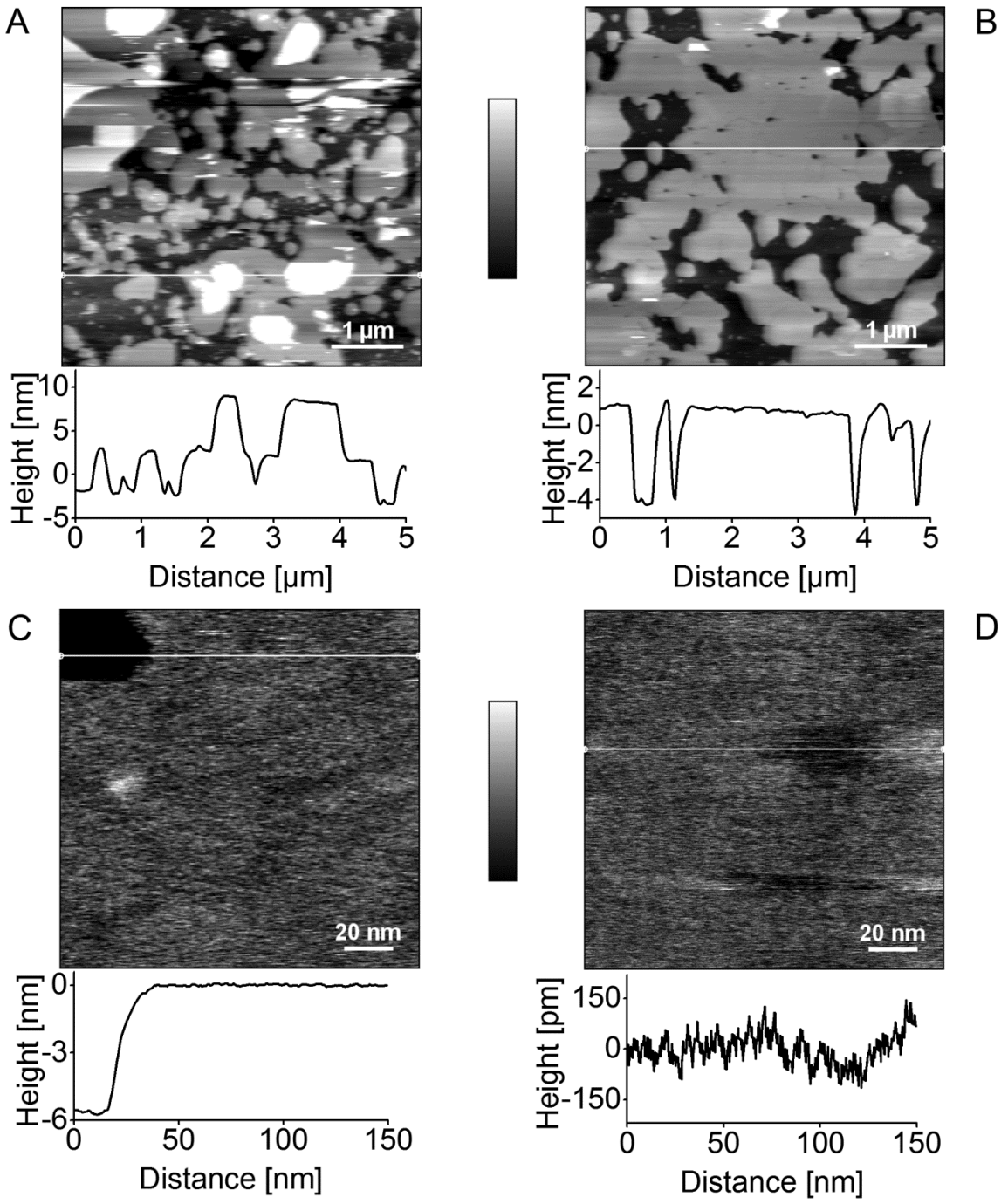

Fig 4. Effect of $A\beta_{1-42}$ oligomers on membranes in the absence of cholesterol. AFM images of DPPC/DPC membranes on mica incubated with oligomers. Upper images show an area of 5 µm x 5 µm each, while lower images show zoomed in areas of 150 nm x 150 nm. The horizontal white line in all images corresponds to the height profile under each image. Color scale for A and B represents 10 nm, while color scale for C and D represents 300 pm. (A) The membrane after incubation with $A\beta_{1-42}$ oligomers at RT shows membrane patches

(light gray) interspersed with mica (dark gray). A second layer of smaller membrane patches can be found on top of the other (white). The height profile indicates a membrane height of around 5 nm. (B) The membrane after incubation at 37 °C shows a more homogenous surface coverage with membrane patches (light gray) and only a few membrane patches left on top (white). The height of the membrane is 5 nm. (C) A detailed scan of the membrane before incubation at 37 °C shows a homogenous surface. The height profile shows a more precise membrane height of 5.5 nm. (D)The detailed scan of the membrane after incubation at 37 °C shows again a homogenous surface.

Floatation density gradient centrifugation

To analyze whether $A\beta_{1-42}$ oligomers still interact with the lipid membrane after dissociation from the solid support, the liquid covering the mica surface after incubation at 37 °C was collected. The sample was loaded onto preformed density gradients, one time at the top and the other time at the bottom. After centrifugation the 15 fractions of each gradient were collected and analyzed with ELISA together with a buffer control.

The results from ELISA with the sample loaded on the top are depicted in Fig 5. The bars show the relative amount of total fluorescence signal detected. Starting at the top fraction 1 shows a relative fluorescence of 15.9 %. This signal decreases towards a minimum in fractions 5 and 6 (1.0-1.1 %) before increasing again until a maximum in fraction 11 of 17.7 %. The fluorescence decreases again until 2.5 % in fraction 14 and shows a slightly higher signal of 4.9 % in the pellet (fraction 15).

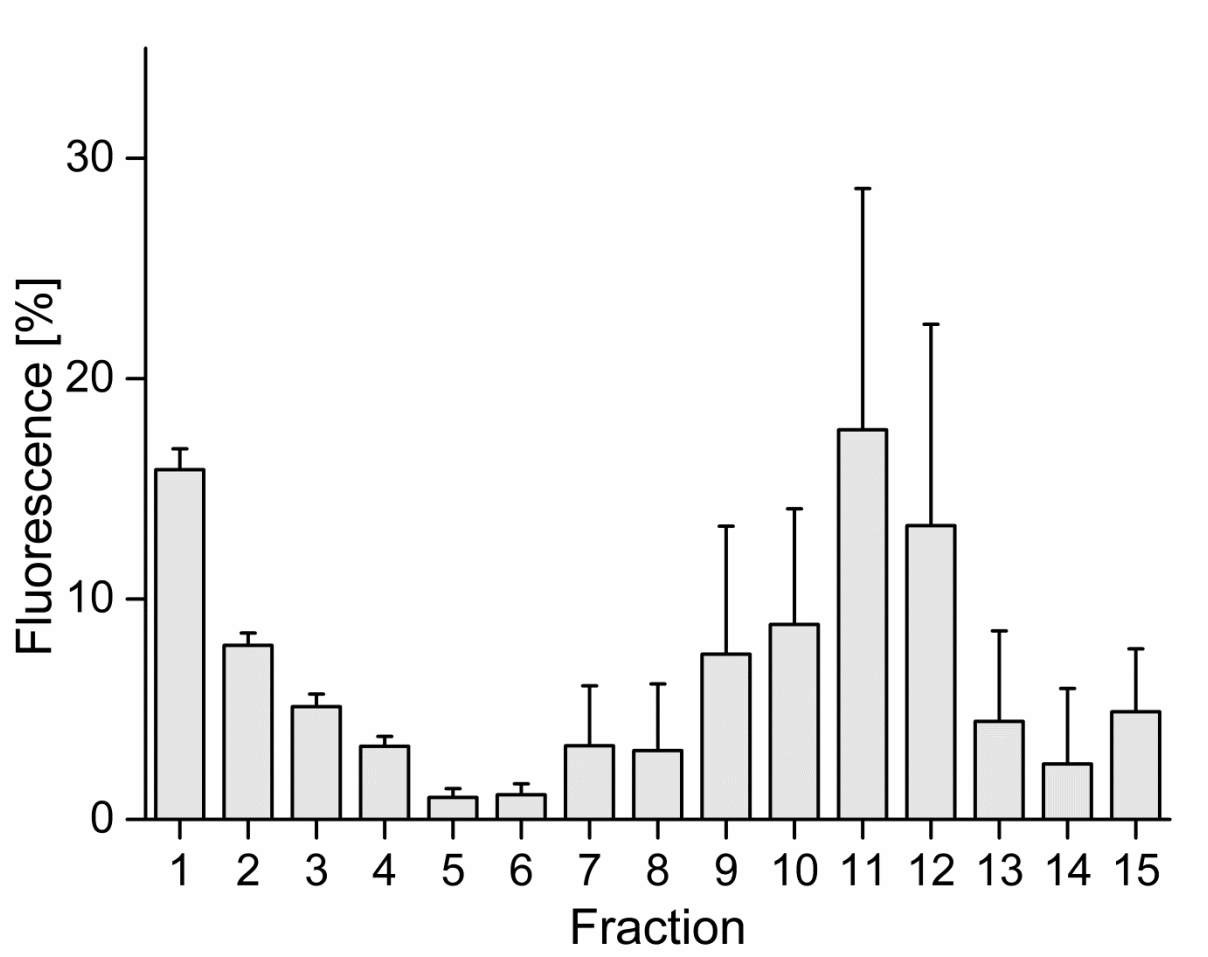

Fig 5. Results of floatation density gradient centrifugation from the top: The histogram shows the results of the floatation density gradient centrifugation of DPPC/cholesterol/DPC membranes with $A\beta_{1\text{-}42}$ oligomers, which dissociated from the support after 1 h incubation at 37 °C. A blank was subtracted and the fluorescence signals were normalized to the total fluorescence. The histogram shows the results of the sample loaded from the top. Three maxima are visible: one at the pellet fraction 15, one around fraction 12 and one at the top fraction 1. The lowest fluorescence was detected in fractions 2-8.

The results from ELISA with the sample loaded on the bottom are depicted in Fig 6. The bars show the amount of $A\beta_{1\text{-}42}$ as calculated by a fit (S3 Fig.). It is notable that most of the protein is detected infractions 13-15 (~64 pg). Only a small amount can be detected in fraction 1 (~2 pg).

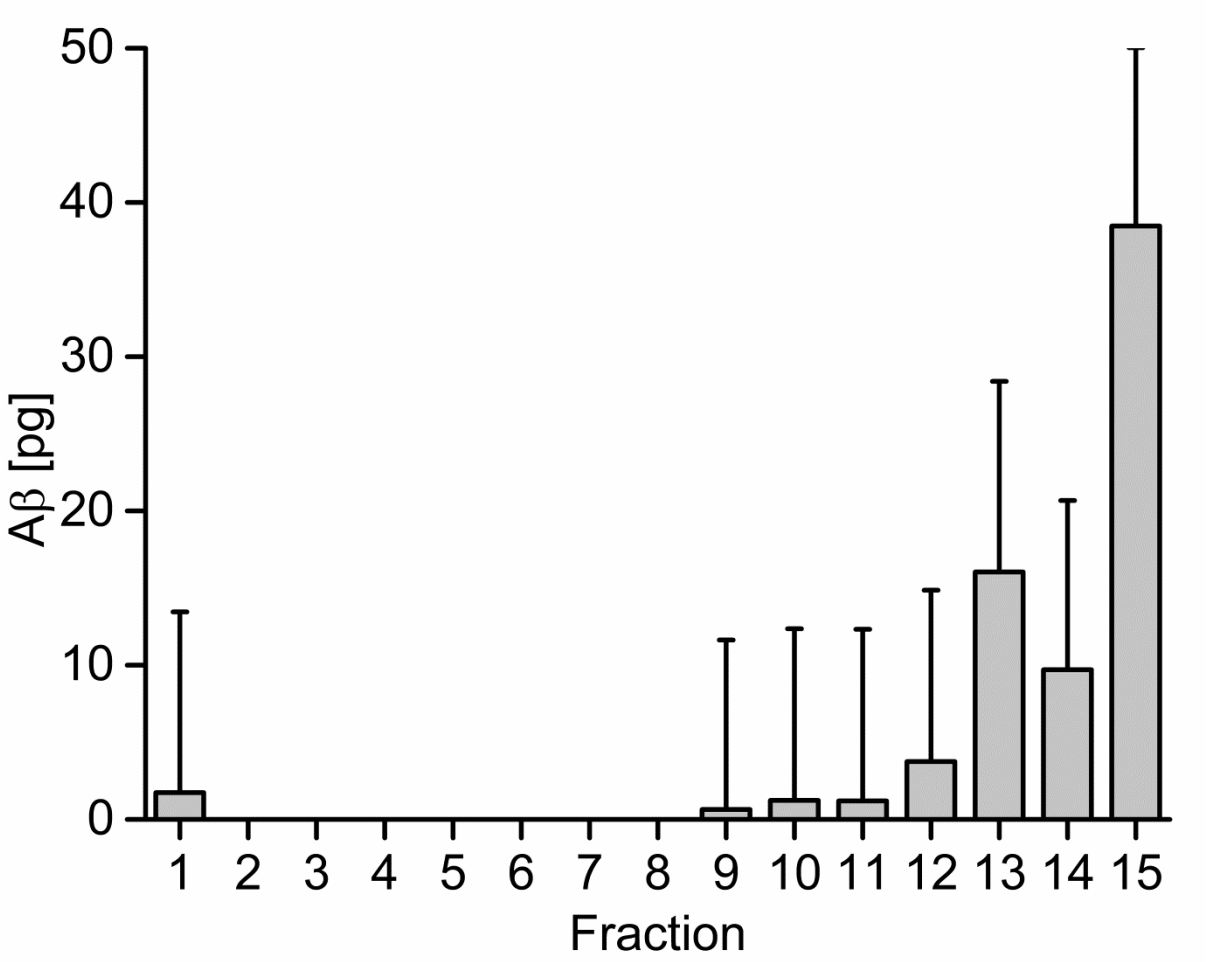

Fig 6. Results of floatation density gradient centrifugation from the bottom: The histogram shows the results of the floatation density gradient centrifugation of DPPC/cholesterol/DPC membranes with $A\beta_{1-42}$ oligomers, which dissociated from the support after 1 h incubation at 37 °C. A blank was subtracted and the fluorescence signals were recalculated into pictogram using a fit (S3 Fig.). The histogram shows the results of the sample loaded from the bottom. Most of the signal is detected in the bottom fractions, while a small amount floats upwards into fraction 1.

As a control a sample containing only $A\beta_{1-42}$ oligomers (without any lipids) was loaded onto a density gradient from the bottom as well. The result of the subsequent ELISA is depicted in Fig 7. Again most of the protein is detected in fractions 13-15 (~1705 pg), while a small amount floats upwards into fraction 1 (~4 pg).

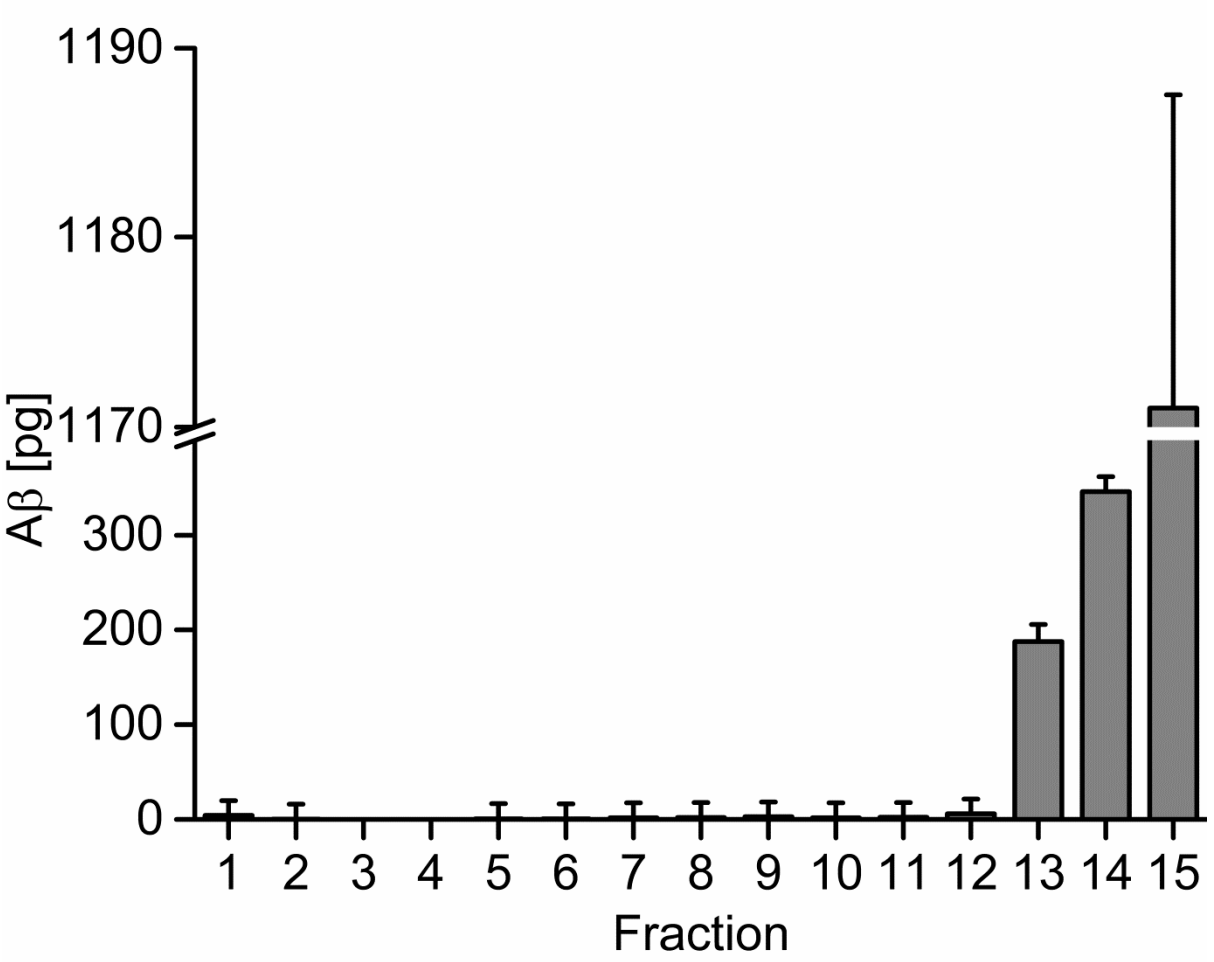

Fig 7. Results of the control floatation density gradient centrifugation from the bottom: The histogram shows the results of the floatation density gradient centrifugation of $A\beta_{1\text{-}42}$ oligomers. A blank was subtracted and the fluorescence signals were recalculated into pictogram using a fit (S4 Fig.). The histogram shows the results of the control loaded from the bottom. Most of the signal is detected in the bottom fractions, while a small amount floats upwards into fraction 1.

Discussion

Membrane formation and stability

The aim of this study was to investigate, whether different aggregation states of $A\beta_{1\text{-}42}$ show different types of interactions with supported lipid bilayers by AFM. The chosen model membrane was composed of the phospholipid DPPC and cholesterol in order to mimic natural membranes in the brain as well as to guarantee a stable non-phase separated membrane as starting condition. Similar sBLM models have been used successfully in the past for other studies [25] and demonstrated high stability.

With a phase transition temperature between gel and liquid phase of 41 °C, DPPC membranes are very rigid and ordered at RT. The addition of cholesterol at the high ratio as found in brain myelin [35] was shown to lower the temperature at which membranes become fully crystalline, or even completely inhibit the crystallization process [36,37]. However, it also moves the phase transition from gel to fluid to higher temperatures. The fluidity of a membrane is of high importance and has to be controlled precisely, as membrane transport processes, enzyme activities or the integration of proteins into the membrane decrease or even cease completely with increasing viscosity. Because the high rigidity of our model sBLM might hinder the integration or interaction of $A\beta_{1-42}$ oligomers, a small amount of DPC, was added as an additional third component. Adding a detergent like DPC weakens lipid-lipid interactions and makes the bilayer more permeable to proteins [38] while the functionality as a membrane mimetic system remains [39]. The results show a membrane consisting of DPPC:cholesterol 1:1 (n/n) and 0.8 mol % DPC formed by self-assembly on mica (Fig 1A). It is stable for at least 5 h, representing the average total time of an experiment and withstands temperatures up to 37 °C (Fig 1B). After incubation at 37 °C the membrane surface coverage apparently remains the same. To exclude the possibility of an effect of the gradient material iodixanol on the membrane, a solution of 30 % iodixanol was incubated on a preformed sBLM. Again, the membrane did not show any changes directly after the incubation at RT or after a further incubation period at 37 °C (Fig 1C-1D).

$A\beta_{1-42}$ and membranes

AFM images of $A\beta_{1-42}$ oligomers incubated on sBLMs containing cholesterol show a membrane on mica (Fig 2A). Upon further inspection of smaller areas of the membrane a distribution of elevated protrusions (~0.3 nm) was detectable (Fig 2C). Aβ oligomers are known to integrate into bilayer lipid membranes and form pores, which can be visualized by AFM [19,20]. Even though a pore like structure could not be identified, the protrusions did neither appear on membranes without oligomeric $A\beta_{1-42}$ nor in presence of monomers or fibrils. Additionally, incubating the membranes containing oligomeric $A\beta_{1-42}$ at 37 °C led to dissociation of the membrane from the mica support after 1 h (Fig 2B). Further inspection of smaller areas of the surface (Fig 2D), as well as scratching on the surface with the cantilever (data not shown) revealed that only the mica surface was left. Pores of Aβ

oligomers described previously [19,20] have a protrusion of 1 nm out of the membrane. As the protrusions in our study had a height of 0.3 nm, a pore like structure could not be identified. The height discrepancy between previous studies [19,20] and our results could on the one hand mean that the $A\beta_{1-42}$ oligomers did not assemble into pore like structures in our case. On the other hand different membrane mimetic systems could lead to different integration depths of the $A\beta_{1-42}$.

The sBLMs incubated with $A\beta_{1-42}$ monomers or fibrils appeared to be stable after incubation at 37 °C (Fig 4). We can however not exclude a possible reversible temperature induced effect. Even though a possible membrane interaction between monomers and lipids could not be visualized with AFM, it cannot be fully excluded. Fig 3A at least indicates a partial disruption of the membrane as compared to a membrane without any $A\beta_{1-42}$ (Fig 1A and B). The resolution achieved in our experiments was high enough to visualize supposed oligomeric protrusions from the model sBLM. Monomers, however, could not be distinguished from background noise. Another indication for a possible effect of $A\beta_{1-42}$ monomers on the presented sBLM is the incomplete coverage of the mica surface by the membrane before incubation at 37 °C. The incomplete surface coverage of the membrane after monomer incubation can also be indicative of a possible effect of the $A\beta_{1-42}$ monomers on the membrane. However, it is unclear whether this is the same, albeit weakened effect, as observed from $A\beta_{1-42}$ oligomers, or a completely different, monomer specific effect. An interaction of fibrils with the membranes could not be confirmed, though fibril formation and content in the appropriate fractions was controlled by AFM prior to incubation on membranes (S2 Fig). Our results so far lead to the conclusion that interaction of $A\beta_{1-42}$ and membrane relies on the oligomeric state of $A\beta_{1-42}$ and a dissociation of the membrane from the solid support is dependent on a temperature of at least 37 °C. Considering theses results it is possible to assume that the aggregation process itself could be the reason for membrane disruption.

A further factor in membrane association of $A\beta_{1-42}$ which has been investigated is the presence of cholesterol. To test whether membrane association of Aβ is possible without cholesterol, sBLMs built only of DPPC/DPC were prepared on mica. AFM images of these sBLMs after incubation with $A\beta_{1-42}$ oligomers (Fig 4A and 4C) and after incubation at 37 °C (Fig 4B and 4D) neither showed a distinct topography indicative of oligomer integration nor membrane dissociation from the support.

This leads us to the conclusion that the presence of cholesterol in this model membrane is another necessity for integration and subsequent induction of membrane dissociation by $A\beta_{1-42}$ oligomers.

Interaction of $A\beta_{1-42}$ oligomers with lipids after dissociation of the membrane

The next question we aimed to answer was whether the interaction between $A\beta_{1-42}$ and the membrane persists after the membrane dissociates from the support. A membrane or lipid association of proteins can be shown by floatation gradient centrifugation [40–43]. Here the sample of interest is loaded at the bottom and the gradient layered on top. Due to the low density of lipid structures they float into the top fractions during centrifugation, including any associated $A\beta_{1-42}$. Proteins not associated with lipids will remain in the bottom fractions. The supernatant of the dissociated sBLM was layered on the bottom of a density gradient and the distribution of $A\beta_{1-42}$ after centrifugation was controlled by ELISA. We could show that $A\beta_{1-42}$ potentially at least still partially (~3 % of total amount of $A\beta_{1-42}$ as shown in S5 Fig) interacted with the lipid environment after the dissociation of the membrane. A comparison between a control of $A\beta_{1-42}$ oligomers loaded on the bottom of a gradient without any lipid (S5 Fig) shows that in the absence of lipid, 15 times less oligomeric $A\beta_{1-42}$ floats into fraction 1. However, most of $A\beta_{1-42}$ was found distributed in the lower fractions 9-15. The lower fractions of a floatation density gradient were previously described as the loading zone [42]. As the sample was loaded at the bottom the fluorescence can be attributed to any aggregation state of $A\beta_{1-42}$, as long as the peptide is not associated with lipids.

To investigate these aggregation states further, a density gradient centrifugation was performed with the sample loaded on the top. In this case only $A\beta_{1-42}$ associated with lipids, $A\beta_{1-42}$ monomers and small oligomers will remain in the top fractions, while the rest of the sample would sediment through the gradient according to its density and sedimentation coefficient. Again fluorescence of each fraction was measured after ELISA (Fig 5). 15.9 % of the total fluorescence signal was detected in fraction 1. This can be attributed to lipid associated $A\beta_{1-42}$ and $A\beta_{1-42}$ monomers. In a density gradient of $A\beta_{1-42}$ only, oligomers will move to fractions 4-6 [28]. In the here performed

floatation gradient, with the sample loaded at the top, fractions 4-6 show the least amount of fluorescence (~5.4 % total fluorescence). This indicates that most of the still present $A\beta_{1-42}$ oligomers stayed lipid associated in fraction 1-3. Fractions 9-12 show the highest amount of fluorescence (~50 % total fluorescence). Fluorescence in these fractions is indicative of larger scale oligomers, and fibrils. Thus it can be concluded that a large part of the applied $A\beta_{1-42}$ oligomers aggregated further throughout the course of the experiment. This is expected, as cholesterol is known to promote $A\beta_{1-42}$ aggregation [22,23].

Conclusion

Our studies showed the disruptive effect of $A\beta_{1-42}$ on a model sBLM consisting mainly of phospholipids and cholesterol. Regarding the aggregation state, only an interaction between $A\beta_{1-42}$ oligomers and the sBLMs has an effect on the membrane. Our results indicate that $A\beta_{1-42}$ oligomers integrate into the sBLM at RT. It is indicated that subsequent changes in interaction between $A\beta_{1-42}$ and the membrane lipids, as well as a further aggregation of $A\beta_{1-42}$ oligomers lead to a dissociation of the sBLM from the solid support at physiological temperatures of 37 °C. The presence of cholesterol plays a key role in this process as model membranes without a cholesterol component showed no incorporation of $A\beta_{1-42}$ oligomers and were stable after incubation at 37°C. $A\beta_{1-42}$ monomers and fibrils did not contribute to a dissociation of the membrane. Floatation gradient experiments from the bottom indicate that the applied $A\beta_{1-42}$ oligomers might remain associated with lipid after membrane disruption. Floatation gradient experiments from the top reveal further aggregation of $A\beta_{1-42}$ oligomers or dissociated monomers into larger oligomers and fibrils. All in all our results emphasize the difference between $A\beta_{1-42}$ oligomers and its monomeric and fibrillar structures with regard to membrane interactions, as well as further fortify the importance of cholesterol for a membrane disrupting effect of $A\beta_{1-42}$.

Acknowledgements

We gratefully acknowledge support (and training) from the Deutsche Forschungsgemeinschaft through Sonderforschungsbereich 974 and through the Forschungskommission Düsseldorf.

References

1. Ferri CP, Prince M, Brayne C, Brodaty H, Fratiglioni L, Ganguli M, et al. Global prevalence of dementia: a Delphi consensus study. The Lancet. 2005; 366: 2112–2117. doi: 10.1016/S0140-6736(05)67889-0.

2. Ross CA, Poirier MA. Protein aggregation and neurodegenerative disease. Nat Med. 2004; 10 Suppl: S10-7. doi: 10.1038/nm1066.

3. Soto C, Estrada LD. Protein misfolding and neurodegeneration. Arch Neurol. 2008; 65: 184–189. doi: 10.1001/archneurol.2007.56.

4. Schmidt ML, DiDario AG, Otvos L, JR, Hoshi N, Kant JA, Lee VM, et al. Plaque-associated neuronal proteins: a recurrent motif in neuritic amyloid deposits throughout diverse cortical areas of the Alzheimer's disease brain. Exp Neurol. 1994; 130: 311–322. doi: 10.1006/exnr.1994.1209.

5. Selkoe DJ. Alzheimer's disease: genes, proteins, and therapy. Physiol Rev. 2001; 81: 741–766.

6. Hardy JA, Higgins GA. Alzheimer's disease: the amyloid cascade hypothesis. Science. 1992; 256: 184–185.

7. Tanzi RE, Bertram L. Twenty years of the Alzheimer's disease amyloid hypothesis: a genetic perspective. Cell. 2005; 120: 545–555. doi: 10.1016/j.cell.2005.02.008.

8. Walsh DM, Klyubin I, Fadeeva JV, Rowan MJ, Selkoe DJ. Amyloid-beta oligomers: their production, toxicity and therapeutic inhibition. Biochem Soc Trans. 2002; 30: 552–557.

9. Walsh DM, Klyubin I, Fadeeva JV, Cullen WK, Anwyl R, Wolfe MS, et al. Naturally secreted oligomers of amyloid beta protein potently inhibit hippocampal long-term potentiation in vivo. Nature. 2002; 416: 535–539. doi: 10.1038/416535a.

10. Walsh DM, Klyubin I, Shankar GM, Townsend M, Fadeeva JV, Betts V, et al. The role of cell-derived oligomers of Abeta in Alzheimer's disease and avenues for therapeutic intervention. Biochem Soc Trans. 2005; 33: 1087–1090. doi: 10.1042/BST20051087.

11. Milligan CE. Caspase cleavage of APP results in a cytotoxic proteolytic peptide. Nat Med. 2000; 6: 385–386. doi: 10.1038/74644.

12. Portelius E, Zetterberg H, Andreasson U, Brinkmalm G, Andreasen N, Wallin A, et al. An Alzheimer's disease-specific beta-amyloid fragment signature in cerebrospinal fluid. Neurosci Lett. 2006; 409: 215–219. doi: 10.1016/j.neulet.2006.09.044.

13. Portelius E, Mattsson N, Andreasson U, Blennow K, Zetterberg H. Novel abeta isoforms in Alzheimer's disease - their role in diagnosis and treatment. Curr Pharm Des. 2011; 17: 2594–2602.

14. Seubert P, Vigo-Pelfrey C, Esch F, Lee M, Dovey H, Davis D, et al. Isolation and quantification of soluble Alzheimer's beta-peptide from biological fluids. Nature. 1992; 359: 325–327. doi: 10.1038/359325a0.

15. Zhao G, Tan J, Mao G, Cui M, Xu X. The same gamma-secretase accounts for the multiple intramembrane cleavages of APP. J Neurochem. 2007; 100: 1234–1246. doi: 10.1111/j.1471-4159.2006.04302.x.

16. Haass C, Selkoe DJ. Soluble protein oligomers in neurodegeneration: lessons from the Alzheimer's amyloid beta-peptide. Nat Rev Mol Cell Biol. 2007; 8: 101–112. doi: 10.1038/nrm2101.

17. Karran E, Mercken M, Strooper B de. The amyloid cascade hypothesis for Alzheimer's disease: an appraisal for the development of therapeutics. Nat Rev Drug Discov. 2011; 10: 698–712. doi: 10.1038/nrd3505.

18. Shafrir Y, Durell S, Arispe N, Guy HR. Models of membrane-bound Alzheimer's Abeta peptide assemblies. Proteins. 2010; 78: 3473–3487. doi: 10.1002/prot.22853.

19. Lin H, Bhatia R, Lal R. Amyloid beta protein forms ion channels: implications for Alzheimer's disease pathophysiology. FASEB J. 2001; 15: 2433–2444. doi: 10.1096/fj.01-0377com.

20. Quist A, Doudevski I, Lin H, Azimova R, Ng D, Frangione B, et al. Amyloid ion channels: a common structural link for protein-misfolding disease. Proc Natl Acad Sci U S A. 2005; 102: 10427–10432. doi: 10.1073/pnas.0502066102.

21. Berthelot K, Cullin C, Lecomte S. What does make an amyloid toxic: morphology, structure or interaction with membrane. Biochimie. 2013; 95: 12–19. doi: 10.1016/j.biochi.2012.07.011.

22. Fantini J, Yahi N, Garmy N. Cholesterol accelerates the binding of Alzheimer's β-amyloid peptide to ganglioside GM1 through a universal hydrogen-bond-dependent sterol tuning of glycolipid conformation. Front Physiol. 2013; 4: 120. doi: 10.3389/fphys.2013.00120.

23. Tashima Y, Oe R, Lee S, Sugihara G, Chambers EJ, Takahashi M, et al. The effect of cholesterol and monosialoganglioside (GM1) on the release and aggregation of amyloid beta-peptide from liposomes prepared from brain membrane-like lipids. J Biol Chem. 2004; 279: 17587–17595. doi: 10.1074/jbc.M308622200.

24. Los DA, Murata N. Membrane fluidity and its roles in the perception of environmental signals. Biochim Biophys Acta. 2004; 1666: 142–157. doi: 10.1016/j.bbamem.2004.08.002.

25. Asakawa H, Fukuma T. The molecular-scale arrangement and mechanical strength of phospholipid/cholesterol mixed bilayers investigated by frequency modulation atomic force microscopy in liquid. Nanotechnology. 2009; 20: 264008. doi: 10.1088/0957-4484/20/26/264008.

26. Yip CM, Elton EA, Darabie AA, Morrison MR, McLaurin J. Cholesterol, a modulator of membrane-associated Abeta-fibrillogenesis and neurotoxicity. J Mol Biol. 2001; 311: 723–734. doi: 10.1006/jmbi.2001.4881.

27. Sackmann E. Supported membranes: scientific and practical applications. Science. 1996; 271: 43–48.

28. Brener O, Dunkelmann T, Gremer L, van Groen T, Mirecka EA, Kadish I, et al. QIAD assay for quantitating a compound's efficacy in elimination of toxic Aβ oligomers. Sci Rep. 2015; 5: 13222. doi: 10.1038/srep13222.

29. Aileen Funke S, van Groen T, Kadish I, Bartnik D, Nagel-Steger L, Brener O, et al. Oral treatment with the d-enantiomeric peptide D3 improves the pathology and behavior of Alzheimer's Disease transgenic mice. ACS Chem Neurosci. 2010; 1: 639–648. doi: 10.1021/cn100057j.

30. Funke SA, Liu H, Sehl T, Bartnik D, Brener O, Nagel-Steger L, et al. Identification and characterization of an aβ oligomer precipitating peptide that may be useful to explore gene therapeutic approaches to Alzheimer disease. Rejuvenation Res. 2012; 15: 144–147. doi: 10.1089/rej.2011.1262.

31. Redondo-Morata L, Giannotti MI, Sanz F. Influence of cholesterol on the phase transition of lipid bilayers: a temperature-controlled force spectroscopy study. Langmuir. 2012; 28: 12851–12860. doi: 10.1021/la302620t.

32. Kim K, Choi SQ, Zell ZA, Squires TM, Zasadzinski JA. Effect of cholesterol nanodomains on monolayer morphology and dynamics. Proc Natl Acad Sci U S A. 2013; 110: E3054-60. doi: 10.1073/pnas.1303304110.

33. Streich C, Akkari L, Decker C, Bormann J, Rehbock C, Muller-Schiffmann A, et al. Characterizing the Effect of Multivalent Conjugates Composed of Abeta-Specific Ligands and Metal Nanoparticles on Neurotoxic Fibrillar Aggregation. ACS Nano. 2016; 10: 7582–7597. doi: 10.1021/acsnano.6b02627.

34. Sullan, Ruby May A, Li JK, Hao C, Walker GC, Zou S. Cholesterol-dependent nanomechanical stability of phase-segregated multicomponent lipid bilayers. Biophys J. 2010; 99: 507–516. doi: 10.1016/j.bpj.2010.04.044.

35. Björkhem I, Meaney S. Brain cholesterol: long secret life behind a barrier. Arterioscler Thromb Vasc Biol. 2004; 24: 806–815. doi: 10.1161/01.ATV.0000120374.59826.1b.

36. Róg T, Pasenkiewicz-Gierula M, Vattulainen I, Karttunen M. Ordering effects of cholesterol and its analogues. Biochim Biophys Acta. 2009; 1788: 97–121. doi: 10.1016/j.bbamem.2008.08.022.

37. Hung W, Lee M, Chen F, Huang HW. The condensing effect of cholesterol in lipid bilayers. Biophys J. 2007; 92: 3960–3967. doi: 10.1529/biophysj.106.099234.

38. Seddon AM, Curnow P, Booth PJ. Membrane proteins, lipids and detergents: not just a soap opera. Biochim Biophys Acta. 2004; 1666: 105–117. doi: 10.1016/j.bbamem.2004.04.011.

39. Vasudevan SV, Schulz J, Zhou C, Cocco MJ. Protein folding at the membrane interface, the structure of Nogo-66 requires interactions with a phosphocholine surface. Proc Natl Acad Sci U S A. 2010; 107: 6847–6851. doi: 10.1073/pnas.0911817107.

40. Brignati MJ, Loomis JS, Wills JW, Courtney RJ. Membrane association of VP22, a herpes simplex virus type 1 tegument protein. J Virol. 2003; 77: 4888–4898.

41. Ali A, Avalos RT, Ponimaskin E, Nayak DP. Influenza virus assembly: effect of influenza virus glycoproteins on the membrane association of M1 protein. J Virol. 2000; 74: 8709–8719.

42. Jasenosky LD, Neumann G, Lukashevich I, Kawaoka Y. Ebola virus VP40-induced particle formation and association with the lipid bilayer. J Virol. 2001; 75: 5205–5214. doi: 10.1128/JVI.75.11.5205-5214.2001.

43. Spearman P, Horton R, Ratner L, Kuli-Zade I. Membrane binding of human immunodeficiency virus type 1 matrix protein in vivo supports a conformational myristyl switch mechanism. J Virol. 1997; 71: 6582–6592.

Supporting information

Disruptive effect of specific Aβ1-42 Oligomers on Cholesterol-rich Membranes

Anna Bronder[1*], Alexander Brener[1,2], Luitgard Nagel-Steger[1,2], Dieter Willbold[1,2]

[1]Institut für Physikalische Biologie, Heinrich-Heine-Universität Düsseldorf, 40225 Düsseldorf, Germany

[2]Institute of Complex Systems, Structural Biochemistry (ICS-6), Research Centre Jülich, 52425 Jülich, Germany

* Corresponding author

E-mail: anna.bronder@hhu.de (AB)

S1 File. Detailed experimental procedures.

Preparation of lipid stock solutions

0.022 g of DPPC and cholesterol were dissolved in 1 ml chloroform (anhydrous, stabilized with amylenes, ≥99 %, Sigma-Aldrich, Munich, Germany) respectively in separate brown sample vials (4 ml Rotilabo sample vials, borosilicate glass, brown, Carl Roth, Karlsruhe, Germany) and stored at -80 °C until use. From these chloroform stocks 230 µl were transferred into fresh sample vials. The chloroform was evaporated under nitrogen and the dried lipid film was resuspended in 1 ml 10 mM sodium phosphate buffer pH 7.4, 0.1 % DPC (w/v) for formation of sBLMs. These aqueous stocks were stored at -20 °C until use.

Preparation of $A\beta_{1-42}$ peptide solutions

In order to dissolve any pre-existing aggregates of $A\beta_{1-42}$ and to assure the monomeric state of $A\beta_{1-42}$, the sample was pre-dissolved in 1,1,1,3,3,3-hexafluoro-2-propanol (HFIP; Sigma-Aldrich, Munich, Germany) at 1.43 mg/ml and incubated over night at room temperature. HFIP was removed by evaporation for 30 min in the hood followed by a drying step in a centrifugal evaporator (RVC 2-18, Christ, Mainz, Germany) for a further 30 min. The dried $A\beta_{1-42}$ was stored at −20 °C until use.

Analytical RP-HPLC

Quantification of $A\beta_{1-42}$ present in density gradient centrifugation fractions was performed by reversed-phase high performance liquid chromatography (RP-HPLC) on a Zorbax SB-300 C8 column (5 µ, 4.8 × 250 mm) connected to an Agilent 1260 Infinity system, both from Agilent, (Böblingen, Germany). Denaturation of $A\beta_{1-42}$ assemblies and separation of $A\beta_{1-42}$ from other compounds, especially from the density gradient forming iodixanol, was achieved using 30 % (v/v) acetonitrile, 0.1 % (v/v) trifluoroacetic acid in H_2O as the mobile phase, an elevated column temperature of 80 °C and a flow rate of 1 ml/min. Applied sample volumes were 20 µl. Eluting substances were detected by their UV absorbance at 215 nm. Data recording and peak area integration was achieved by the program package ChemStation (Agilent, Böblingen, Germany). Calibration of the column was achieved with $A\beta_{1-42}$ solutions of known concentrations (0 to 25 µM $A\beta_{1-42}$) and the resulting linear

equation from a plot of peak area vs. $A\beta_{1-42}$ concentration allowed the calculation of molar $A\beta_{1-42}$ concentrations (from corresponding peak areas).

ELISA

Washing means an incubation of 200 µl/well phosphate buffered saline with Tween 20 (PBS-T; 136.9 mM NaCl, 2.7 mM KCl, 1.9 mM KH_2PO_4, 11.4 mM Na_2HPO_4, 0.2 % Tween 20, pH 7.4) for 2 min, RT and shaking (400 rpm). Removal of excess liquid means inverting the plate and tapping firmly on absorbent paper. 22 µl of each fraction from the floatation density gradient centrifugation was diluted with 78 µl 10 mM sodium phosphate buffer pH 7.4 and loaded onto the plate together with a buffer control as fourfold detection. Incubation was done overnight at 4 °C and shaking (100 rpm). Excess liquid was removed, followed by washing. Excess liquid was removed again and blocking was done with 100 µl/well 0.25 % (w/v) powdered milk (blotting grade, Carl Roth, Karlsruhe, Germany) in milli-Q for 35 min at RT and shaking (400 rpm). Removal of excess liquid was followed by washing. Afterwards excess liquid was removed again and an incubation with 100 µl/well of a 1:5000 (v/v) dilution of primary antibody 6E10 in 10 mM sodium phosphate buffer pH 7.4 for 2 h, RT and shaking (400 rpm) followed. After removing excess liquid, a washing step was performed. Removal of excess liquid was followed by an incubation with a 1:6000 (v/v) dilution of secondary antibody GAM-PO in 10 mM sodium phosphate buffer pH 7.4 for 2 h, RT and shaking (400 rpm). Excess liquid was removed, followed by washing and a final removal of excess liquid. Incubation with 100 µl/well QuantaBlu-Substrate-Peroxide-solution for 30 min, RT and shaking (400 rpm) was followed by stopping with 100 µl/well stop-solution before detection of fluorescence directly afterwards.

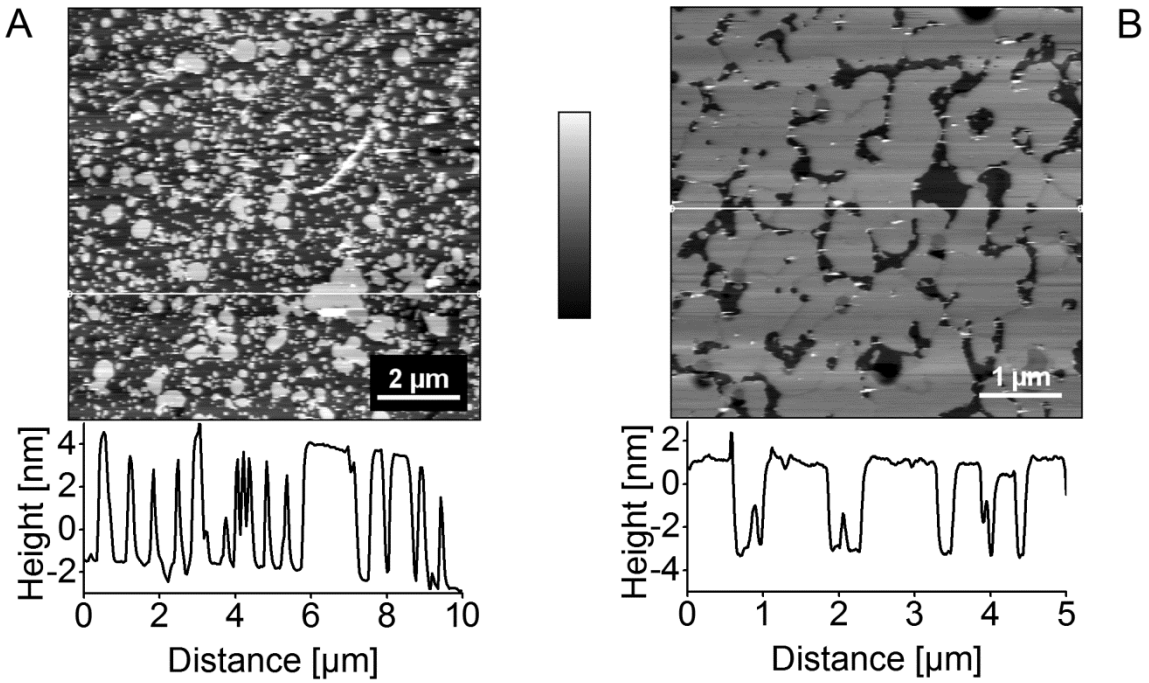

S1 Fig. sBLMs with monomers and fibrils before incubation at 37 °C. (A) sBLM with monomers (10 µm x 10 µm). (B) sBLM with fibrils (5 µm x 5 µm). Color scale represents 10 nm.

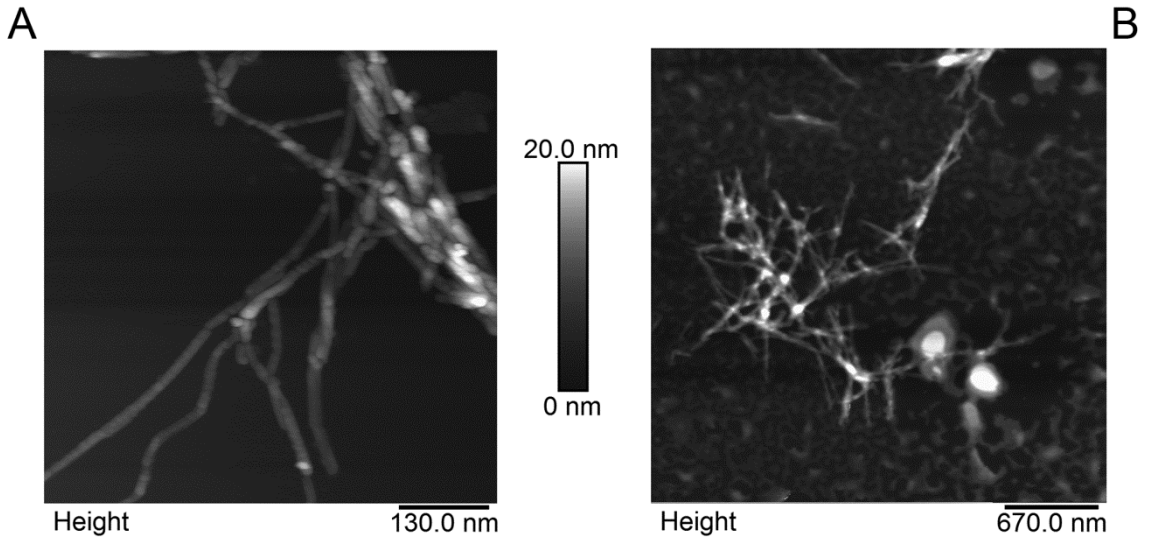

S2 Fig. Test of fibril formation. (A) $A\beta_{1\text{-}42}$ fibrils imaged with AFM before density gradient centrifugation. (B) $A\beta_{1\text{-}42}$ fibrils imaged with AFM after density gradient centrifugation.

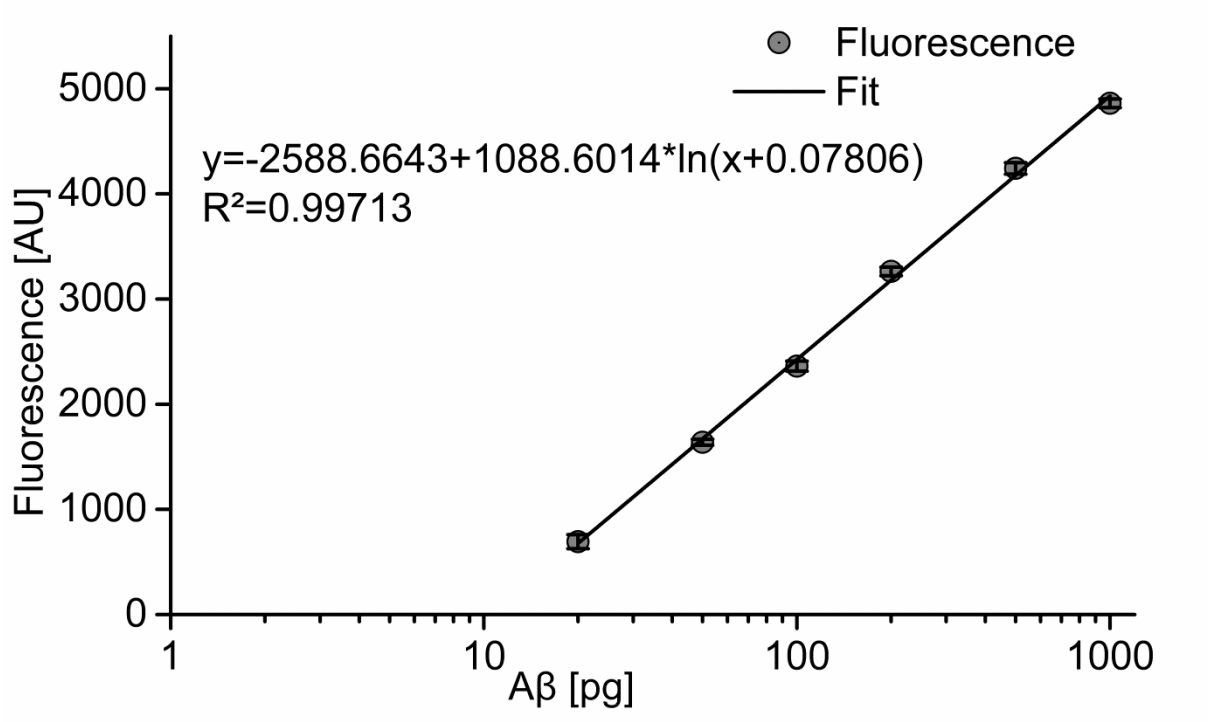

S3 Fig. Fit for histogram showing the results of the floatation density gradient centrifugation of DPPC/cholesterol/DPC membranes with $A\beta_{1-42}$ oligomers (Fig 6).

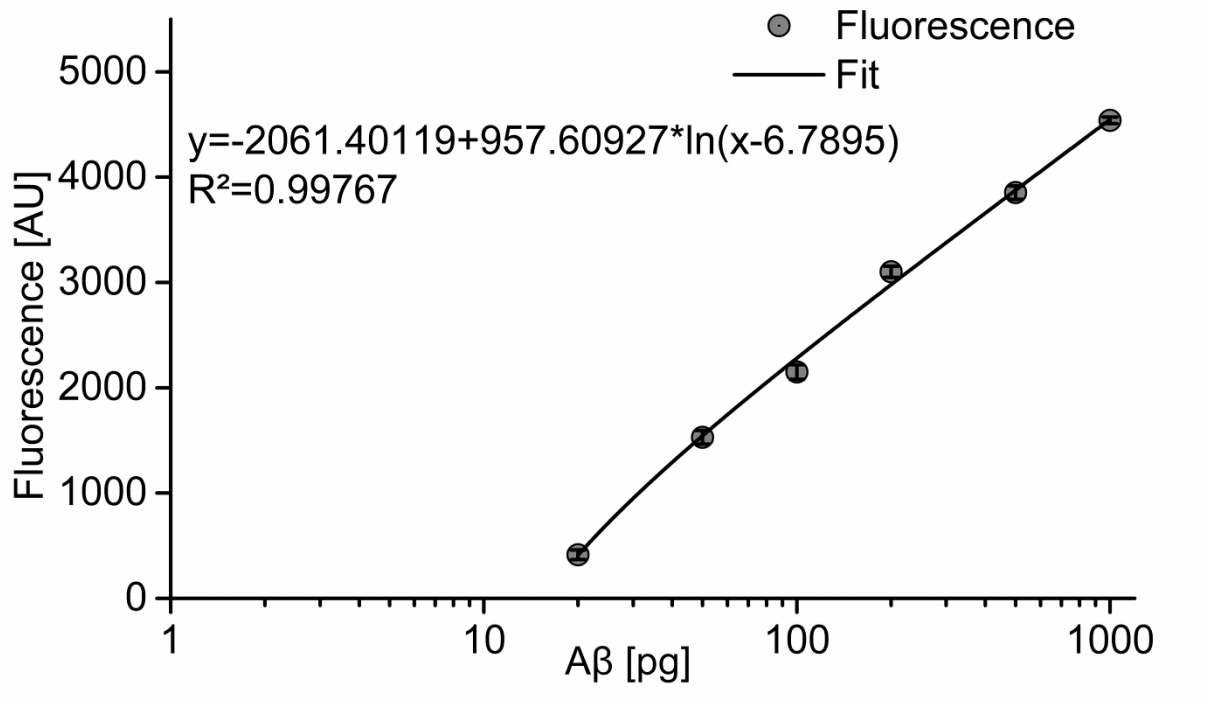

S4 Fig. Fit for histogram showing the results of the floatation density gradient centrifugation of $A\beta_{1-42}$ oligomers (Fig 7).

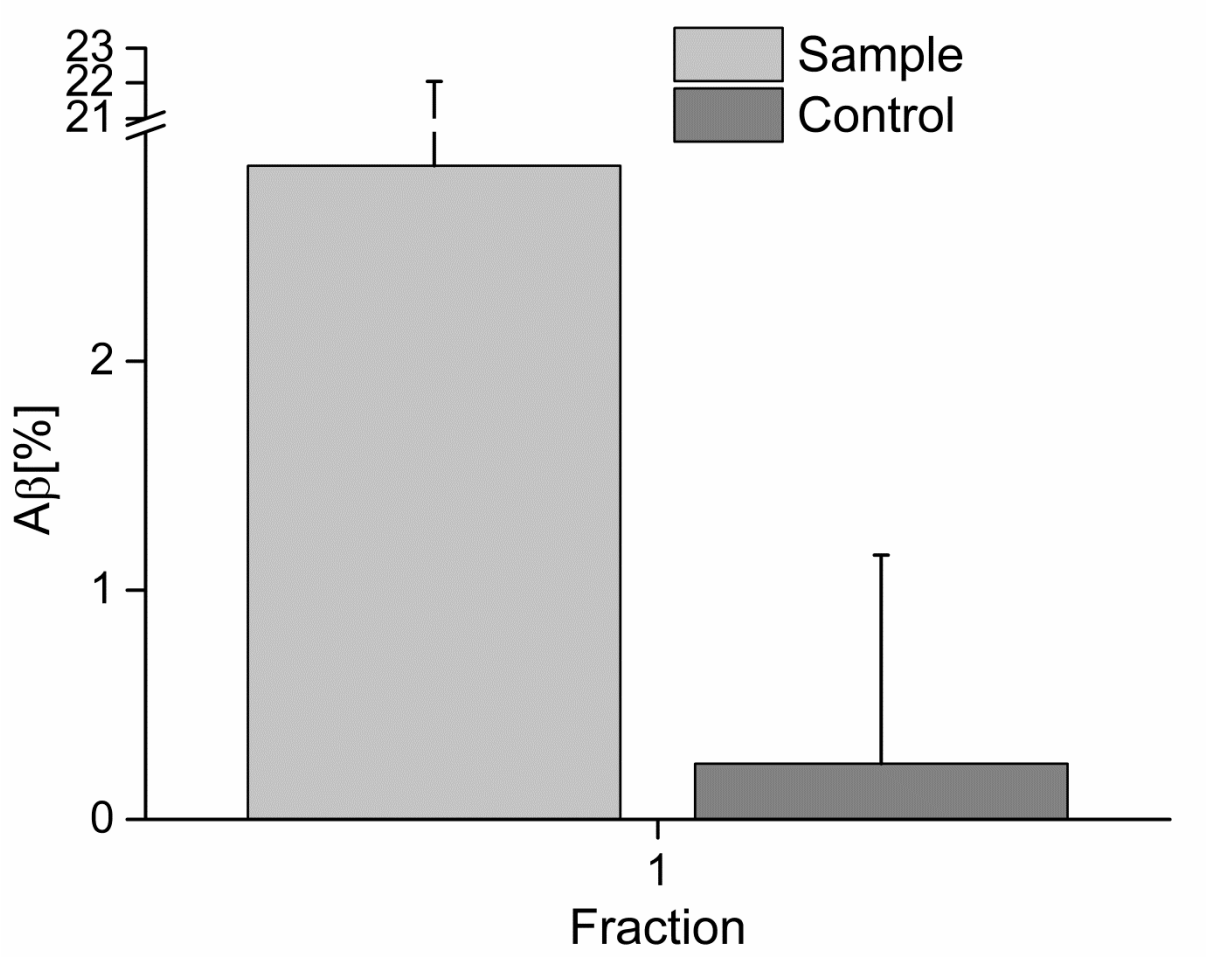

S5 Fig. Comparison of fraction 1between control density gradient centrifugation and density gradient centrifugation of lipid associated $A\beta_{1-42}$ oligomers. The amount of $A\beta_{1-42}$ in each fraction was normalized to the total amount of $A\beta_{1-42}$ in each gradient.

2.1.2 Oriented Membrane Protein Reconstitution into Tethered Lipid Membranes for AFM Force Spectroscopy

Biophysical Journal

Impact Factor: 3.632

Own contribution: 80 %

Carrying out and analysis of AFM imaging and force spectroscopy, surface functionalization, preparation of artificial membranes, XPS measurements and analysis, Dot Blot, refolding and purification of BR, co-authoring the manuscript, cleaning procedure

Biophysical Journal
Article

Oriented Membrane Protein Reconstitution into Tethered Lipid Membranes for AFM Force Spectroscopy

Anna M. Bronder,[1,*] Adeline Bieker,[1] Shantha Elter,[1] Manuel Etzkorn,[1] Dieter Häussinger,[2] and Filipp Oesterhelt[1,3]

[1]Institut für Physikalische Biologie and [2]Clinic for Gastroenterology, Hepatology and Infectiology, Heinrich-Heine-Universität, Düsseldorf, Germany; and [3]Department for Microbial Bioactive Compounds, Interfaculty Institute for Microbiology and Infection Medicine, University of Tuebingen, Tuebingen, Germany

ABSTRACT Membrane proteins act as a central interface between the extracellular environment and the intracellular response and as such represent one of the most important classes of drug targets. The characterization of the molecular properties of integral membrane proteins, such as topology and interdomain interaction, is key to a fundamental understanding of their function. Atomic force microscopy (AFM) and force spectroscopy have the intrinsic capabilities of investigating these properties in a near-native setting. However, atomic force spectroscopy of membrane proteins is traditionally carried out in a crystalline setup. Alternatively, model membrane systems, such as tethered bilayer membranes, have been developed for surface-dependent techniques. While these setups can provide a more native environment, data analysis may be complicated by the normally found statistical orientation of the reconstituted protein in the model membrane. We have developed a model membrane system that enables the study of membrane proteins in a defined orientation by single-molecule force spectroscopy. Our approach is demonstrated using cell-free expressed bacteriorhodopsin coupled to a quartz glass surface in a defined orientation through a protein anchor and reconstituted inside an artificial membrane system. This approach offers an effective way to study membrane proteins in a planar lipid bilayer. It can be easily transferred to all membrane proteins that possess a suitable tag and can be reconstituted into a lipid bilayer. In this respect, we anticipate that this technique may contribute important information on structure, topology, and intra- and intermolecular interactions of other seven-transmembrane helical receptors.

INTRODUCTION

The characterization of transmembrane proteins is key to a better understanding of essential processes in life. Transmembrane proteins account for ~30% of all proteins (1) and act as sensors, catalysts, receptors, transporters, and channels. Thus, they play an important role in almost all cellular processes and are associated with a broad range of different diseases (2–5). Among the membrane proteins, the class of seven-transmembrane helical (7TM) proteins, which includes G-protein-coupled receptors (GPCRs), have a very central part in a variety of sensing and signaling pathways, as well as physiological responses, making them a prominent target for drug development.

Transmembrane proteins easily lose their functionality and denature when removed from their natural membrane environment. One approach to study functional membrane proteins is the development of simple artificial membrane systems that reduce the complexity but still mimic the most important properties of biological membranes. A promising system is a tethered bilayer lipid membrane (tBLM). Lipids of the first layer of the membrane are anchored covalently to a solid substrate through a spacer. This spacer, e.g., a polymer, acts as a cushion that compensates surface roughness, mimicking a cytoskeleton, and can additionally create an ion reservoir beneath the membrane (6–8). The spacer can be bound to the substrate first, binding the lipid to the spacer in a subsequent step (9). tBLMs have proven to be stable for days and can even be used for weeks when covered by a hydrogel (9). Binding of the membrane to the spacer occurs through an anchoring molecule, a lipid or hydrophobic chain. Important while binding the anchoring molecule is the grafting density, i.e., the ratio of anchored to not-anchored lipids. Although a high grafting density leads to high electrical resistance, it can also hinder the incorporation of proteins (8) or the diffusion of

Submitted February 28, 2016, and accepted for publication August 22, 2016.

*Correspondence: anna.bronder@hhu.de

Editor: Simon Scheuring.

http://dx.doi.org/10.1016/j.bpj.2016.08.051

incorporated proteins through the membrane (10). In addition to tBLMs, so-called protein tethered membranes can be formed as well. In this case, the anchoring lipid or hydrophobic chain is directly substituted with the membrane protein, which is coupled to the surface, e.g., through a complex between a surface bound nitrilotriacetic acid (NTA) and the protein histidine-tag (His-tag) (11).

Alternatively, membrane proteins can be studied in other artificial membrane systems, e.g., liposomes (12), nanodiscs (13), black or bilayer lipid membranes (BLMs) (8), and solid supported BLMs (sBLM) (8).

The formation of a tBLM can be done by self-assembly (14). One way of self-assembly is to adsorb and then spread out whole vesicles over the surface (15,16). This way, proteins can be reconstituted already into the prepared vesicles before the final bilayer formation (17) or can be added to the finished bilayer on the surface (18).

Proteins embedded in a tBLM can be studied by atomic force microscopy (AFM). AFM-based single-molecule force spectroscopy can be used to obtain information on dissociation rates (19), energy barriers (20,21), Gibbs free energy (19,21), the form of a binding potential (21), and inter- and intramolecular interactions (20,22–24), as well as the folding of proteins and their constitution inside a membrane (20).

In this study, we demonstrate a method of forming a tBLM on quartz glass with the incorporated 7TM model membrane protein bacteriorhodopsin (BR) in a defined orientation. BR has been studied extensively (25–27) and offers high stability. In addition, the covalently bound retinal allows direct insight into its folding state through absorption measurements (e.g., at 555 nm). We investigated the conformation of BR inside the presented tBLM by AFM-based force spectroscopy. Our data are in accordance with expected force-distance curves of a 7TM membrane protein (13,28). The orientation of BR in purple membranes can be predetermined through AFM imaging (29,30). Thus, the characteristics of force-distance curves of BR pulled from the extracellular side and the cytoplasmic side are already known, which in turn can be used to process the data of statistically oriented BR. In general, knowledge of the orientation will substantially facilitate data analysis and interpretation. In our model system, predefined orientation is achieved through first functionalizing the quartz glass by silanization. Afterwards, a polyethylene glycol (PEG) is coupled as a spacer. To reconstitute the protein on the surface in a defined orientation, a protein anchor is bound to the spacer in addition to the lipid anchors. We make use of cell-free protein expression, a method that is suitable to produce 1) a broad range of different membrane proteins (31), and 2) large amounts of protein in the presence or absence of cofactors such as ligands, detergents, or lipids. We could show before that cell-free expression of BR enables analysis of the pure protein that is not biased by copurification of, e.g., coordinated lipids, which are normally present when BR is extracted from the native purple membrane (32). To test our model system, we use cell-free expressed BR that contains a His-tag and a surface-coupled protein anchor consisting of Tris-NTA (trisNTA). Our results show the specific coupling of the protein to the surface and the successful formation of a tBLM containing the membrane protein in a defined orientation.

MATERIALS AND METHODS

All water used was purified by the Milli-Q Integral Water Purification System (Merck Millipore, Darmstadt, Germany). Specific buffer compositions are described in the Supporting Material. All given cantilever values are nominal values.

Lipids, detergents, and stock solutions

1,2-dipalmitoyl-*sn*-glycero-3-phosphocholine (DPPC; >99% purity), 1,2-dipalmitoyl-*sn*-glycero-3-phosphoethanolamine-N-(succinyl) Sodium salt (SuccinylPE; >99% purity), and *n*-dodecylphosphocholine (DPC; >99% purity) were purchased as powders from Avanti Polar Lipids (Alabaster, AL). *n*-Dodecyl-β-D-maltopyranoside (DDM; Anagrade) was purchased from Affymetrix (Santa Clara, CA). Carboxy-functionalized *tert*-butyl ester (OtBu)-protected trisNTA (33) was provided by the group of Prof. Dr. Jacob Piehler of the University of Osnabrück. Stock solutions in chloroform (for spectroscopy, 99+% purity, stabilized with amylene; Acros Organics, Geel, Belgium) were created as follows: 0.026 g SuccinylPE, 0.022 g DPPC, and 0.005 g trisNTA were dissolved in 1 mL chloroform and stored at −80°C.

AFM

AFM images were taken with an AFM Nanowizard III (JPK Instruments, Berlin, Germany). Imaging was done at room temperature (RT) using contact mode with the probe OMCL-TR400PSA (Cantilever 2, Asylum Research, Mannheim, Germany) with a spring constant (k_c) of 0.02 N/m, a resonance frequency (f) in water of 11 kHz, and a tip radius (r) of 15 nm, or using tapping mode with the probe SNL-10 (Cantilever A, $k_c = 0.35$ N/m, f = 65 kHz in air, r = 2 nm; Bruker, Billerica, MA) in buffer P1.

AFM-based force spectroscopy

Force-distance curves were measured using a Nanowizard III (JPK Instruments). The same probes as for imaging in contact mode (OMCL-TR400PSA, Cantilever 2) were used. All experiments were performed at RT in buffer P1. Force-distance curves were acquired as follows. Starting away from the surface, the cantilever is moved downward at a constant speed (200 nm/s). When the surface is reached, the cantilever is moved farther until it reaches a defined maximal deflection (0.4 mV). This position is held for 1 s before retraction of the cantilever (200 nm for force-distance curves unfolding BR, 100–400 nm for force-distance curves measuring adhesion). This cycle is repeated at different positions on the surface (acquiring ~500 force-distance curves per position for experiments unfolding BR and ~100 force-distance curves per position during adhesion experiments). The position on the surface was changed two to three times per experiment. Experimental conditions were repeated in two independent measurements. A fresh cantilever was used for each measurement. As force measurements require the precise knowledge of the cantilever's spring constant, k_c, the thermal noise method (34) is used for calibration. Additionally, the cantilever's sensitivity (deflection → force) is calibrated by measuring the deflection of the cantilever approached against the surface. Calibration was performed at the beginning of each experiment and between positions on the surface.

X-ray photoelectron spectroscopy

Cleaned quartz glass surfaces and silanized quartz glass surfaces were characterized with x-ray photoelectron spectroscopy (XPS) using an ESCALAB MK II spectrometer (Thermo Fisher Scientific, Oberhausen, Germany).

Functionalization steps

Cleaning of quartz glass according to a previously described protocol (35) was followed by silanization with (3-aminopropyl)trimethoxysilane (APTES; 97%, Sigma Aldrich, St. Louis, MO) and subsequent binding of the spacer Mmt-NH-PEG$_{12}$-COO-Tfp (PEG; Iris Biotech, Marktredwitz, Germany). To this spacer was coupled the protein anchor trisNTA alone, the lipid anchor SuccinylPE alone, and a mixture of both anchors 1:2 (mol/mol). The detailed coupling steps are described in the Supporting Material.

Lipid suspension

30 mM DPPC stock (230 μL) was transferred into a sample vial and the chloroform was evaporated under nitrogen. Buffer P1 (1 mL) with 0.1% DPC (w/v) was added to create the final lipid suspension.

Binding of BR and membrane formation on functionalized quartz glass

After rinsing the functionalized slides (1 cm^2) 10 times with water, the surface was covered with 50 mM EDTA (disodium salt dehydrate, molecular biology grade; AppliChem, Darmstadt, Germany) solution for 5 min. After removal of the EDTA solution, a 10 mM nickel(II) chloride (98%, for analysis; Grüssing, Filsum, Germany) solution was added to the surface for 5 min. The solution was removed from the surface and replaced with buffer DDM-W1. The surface was rinsed once with protein buffer DDM-P1, and 20 μL of a 10 μM BR solution in buffer DDM-P1 was added to 180 μL lipid suspension. This solution was placed onto the surface and allowed to incubate for 2 h. The sample was rinsed 10 times with 250 μL buffer P1 and covered with 50 μL of the same buffer for AFM measurements.

Membrane formation on mica

Lipid suspension (50 μL) was incubated on a round mica surface (Ø 10 mm, Ted Pella, Redding, CA) for 2 h. The surface was rinsed five times with 100 μL P1 and covered with 50 μL of the same buffer for AFM measurements.

Membrane formation with reconstituted BR on mica

A 10 μM BR solution in buffer DDM-P1 (5 μL) was added to 45 μL lipid suspension. The mixture was incubated on a round mica surface (Ø 10 mm) for 2 h. The surface was rinsed five times with 100 μL P1 and covered with 50 μL of the same buffer for AFM measurements.

Dot blot

Specifically bound BR should only be rinsed from a functionalized surface with a buffer containing imidazole. After rinsing the surface once with buffer missing imidazole and once with buffer containing imidazole, a simplified Western blot (dot blot) was utilized to test the specific binding of BR to the functionalized surface. The procedure is described in detail in the Supporting Material.

Cloning and cell-free expression

Cell-free expression of BR was carried out as described before (32). An *Escherichia coli*-based system following previously published protocols (36) was used. Dialysis-mode reactions were carried out in the absence of retinal and detergents. The resulting protein pellet was washed with S30 buffer and directly refolded or stored at −20°C. The refolding procedure is described in more detail in the Supporting Material.

RESULTS

In our study, we aimed to reconstitute BR as a model membrane protein in a defined orientation in artificial tBLMs to perform single-molecule force spectroscopic studies. The process is depicted schematically in Fig. 1. The clean quartz glass surface (Fig. 1 *a*) is coated with APTES for amino functionalization (Fig. 1 *b*). After this, a PEG with an activated carboxyl group and a protected amino group is coupled to the surface (Fig. 1 *c*). Following the deprotection of the PEG's amino group, the binding of an anchoring lipid (SuccinylPE) (Fig. 1 *d*) and a protein anchor (trisNTA) (Fig. 1 *e*) were investigated both separately and as a mixture of both anchors (Fig. 1 *f*). The protein is reconstituted on the surface together with the free lipid (DPPC) supported by detergent (DPC).

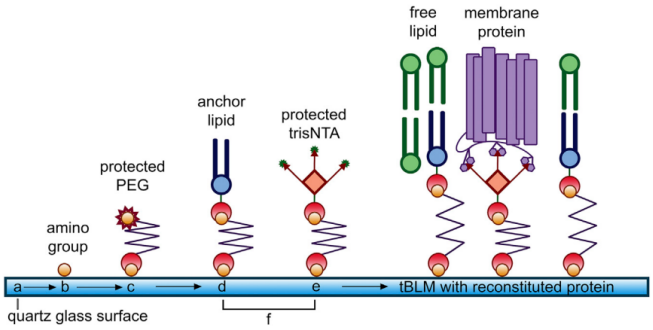

FIGURE 1 Schematic representation of the functionalization and coupling steps. The cleaned quartz glass surface (*a*) is first functionalized using APTES (*b*) to create amino groups. To these amino groups a PEG linker (*c*) is coupled with its activated carboxyl group and protected amino group. After deprotection of the PEG linker amino group, the surface can be functionalized in three ways, with only the lipid anchor bound to PEG (*d*), with only the protein anchor (protected trisNTA) bound to PEG (*e*), or with both anchors bound simultaneously to PEG (*f*). Afterward, a mixture of the protein with free lipid is applied to the surface, forming the final tBLM with reconstituted protein. To see this figure in color, go online.

Surface composition before and after silanization

The atomic composition of a pure quartz glass surface was compared to a silanized surface using XPS. In the survey spectrum of cleaned quartz glass (Fig. S1 *a*), binding energies corresponding to fluorine (F), sodium (Na), and carbon (C) levels are detected apart from expected silicon (Si) and oxygen (O) levels. A survey spectrum after silanization with APTES shows binding energies corresponding to levels in O and Si (Fig. S1 *b*). Additionally, there is an increase of C from 12.8 atomic percent (at.%) to 41.6 at.% and an appearance of 7.2 at.% N.

Changes in surface topography

The functionalization of quartz glass surfaces was controlled by AFM to be able to observe the changes in surface topography after each functionalization step. The surface roughness is calculated as the arithmetic mean (i.e., the average roughness, R_a) of absolute height values for each surface. The AFM image of quartz glass (Fig. 2 *a*) after the cleaning procedure shows the standard surface topography of quartz glass. The average surface roughness is 511 picometers (pm). Holes and scratches, which are typical for quartz glass, are also visible. The surface topography of cleaned quartz glass is similar after silanization (Fig. 2 *b*), which is also represented by the average surface roughness. A surface functionalized with PEG is shown in Fig. 2 *c*. The average surface roughness has decreased to 154.1 pm and there are no longer holes or scratches visible.

The surface was functionalized further with the lipid anchor SuccinylPE only (Fig. 2 *d*), with trisNTA only (Fig. 2 *e*), and with a mixture of 2:1 (mol/mol) SuccinylPE/trisNTA (Fig. 2 *f*). The surface with the lipid anchor alone shows an increased average roughness of 585.5 pm compared to the previous step (Fig. 2 *c*). Some small regions indicate an additional depth of 1 nm (*arrows*). The surface functionalized solely with trisNTA also shows a generally higher average roughness and round structures of 4–10 nm height and 200 nm diameter distributed over the whole surface. A mixture of SuccinylPE and trisNTA yields an average roughness of 332.6 pm, but distributed protruding structures of 1–3 nm height can be seen (*arrows*).

Changes in adhesion

Force-distance curves were performed between surface functionalization steps to observe the changes in cantilever-surface interaction (adhesion). This was done to observe whether adhesion on the functionalized surfaces remained constant over the majority of the surface, which would be an indication of complete and homogeneous functionalization. In Fig. 3, the mean adhesion of the cantilever on the surface is depicted for all functionalization steps, and for surfaces functionalized with SuccinylPE only, trisNTA only, or a mixture of the two. For quartz glass (Fig. 3 *a*), no adhesion can be observed. APTES-functionalized surfaces (Fig. 3 *a*) show a strong increase in adhesion force, from −25 pN ± 8 pN to 12,420 pN ± 1039 pN. After the second functionalization step, the strong adhesion forces diminish to 212 pN ± 125 pN for PEG (Fig. 3 *c*). From this step on, three functionalization ways were chosen. Surfaces functionalized with the lipid anchor SuccinylPE (Fig. 3 *d*) show an increase of adhesion forces to 556 pN ± 262 pN. Surfaces functionalized only with the protein anchor trisNTA (Fig. 3 *e*) show a higher increase in adhesion to 4160 pN ± 1152 pN, whereas surfaces with both anchors in a 2:1 (mol:mol) SuccinylPE:trisNTA mixture (Fig. 3 *f*) show an adhesion force of 669 pN ± 300 pN. Detailed distribution of adhesion forces as well as exemplary force-distance curves for each functionalization step can be seen in Fig. S2.

Protein complex formation

To test the successful immobilization of BR through a complex between the protein's N-terminal deca-histidine-tag (His10-tag) and the trisNTA on the surface, specific elution of the protein by imidazole-containing buffer was performed and visualized by dot blot. To accomplish this, BR was first immobilized on the surface functionalized with the protein anchor and the lipid anchor. Then the surface was rinsed first with a buffer without imidazole. The volume of this rinsing step was collected as the rinsing fraction. Afterward, the surface was rinsed again with the buffer containing imidazole. The volume of this elution step was collected as the elution fraction. Together with a buffer control of the buffer containing imidazole, the fractions were distributed on a dot blot. As can be seen in Fig. S3, only the elution fraction (*C*) shows luminescence.

BR in membranes

Vesicle spreading on mica is an often-used method of creating solid sBLMs (15,16,18). A trial of the lipid mixture with BR was performed on mica to investigate possible effects of BR on bilayer formation. Fig. 4 *a* shows a mica surface after incubation of the lipid alone. The surface shows a homogeneous coverage with a lipid bilayer membrane (*light gray area*) with a few defects (*dark gray areas*). The corresponding height profile shows a membrane height of 5 nm and a low roughness of the membrane surface. Compared to an sBLM without BR, the bilayer containing BR (Fig. 4 *b*) has a much higher average roughness of 709.4 pm. All in all, the surface shows a complete coverage with no membrane defects. When spreading the lipid mixture with BR onto a functionalized quartz glass surface (Fig. 4 *c*), this high average roughness not only persists but increases to 1094 pm. However, the protein-lipid layer is spread over the whole surface. It has to be noted that during the scan process (bottom to top), the structures on the surface of the

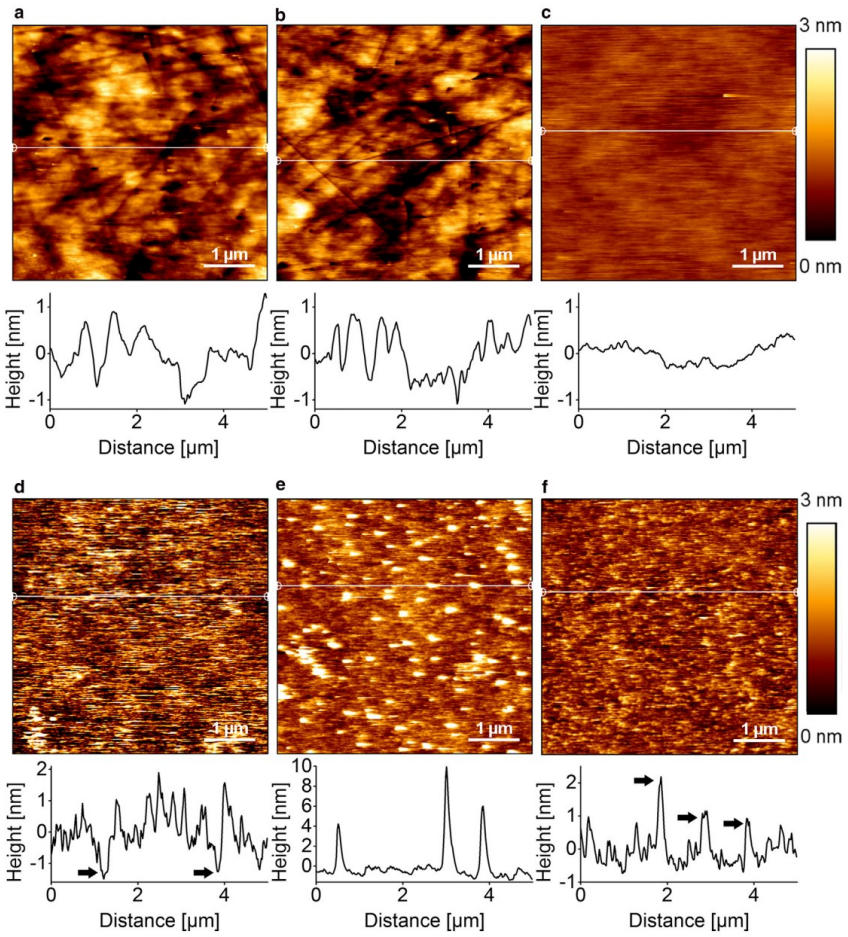

FIGURE 2 AFM scans (5 μm $\times$ 5 μm) in contact mode in buffer P1, with corresponding height profiles, represented as white horizontal lines in each image, below each scan. (*a*) The cleaned quartz glass surface shows a roughness of 511 PM. (*b*) Silanized quartz glass with APTES shows no change in surface roughness. (*c*) Binding PEG to silanized quartz reduces the roughness to 154.1 PM. (*d*) A surface functionalized only with the anchoring lipid SuccinylPE. (*e*) A surface functionalized only with the protein anchor trisNTA. (*f*) A surface functionalized with a mixture of 2:1 (mol/mol) SuccinylPE: trisNTA. To see this figure in color, go online.

protein-containing membrane appear to increase in size, which is likely due to lipid adsorption to the cantilever tip.

After scratching with the cantilever tip on a surface covered with the protein-lipid mixture (Fig. 4 *d*), a depth of 10 nm can be measured.

Force spectroscopy

Force spectroscopy measurements were performed as described in Materials and Methods on surfaces with BR bound to the protein anchor and reconstituted into the lipid/detergent membrane. Only force-distance curves showing more than two force peaks and the last force peak at a peak position of >60 nm with a measured force of >100 pN were selected, to assure that only force-distance curves on specifically oriented and complex-coupled BR were used for analysis. Fig. S4 shows three representative force-distance curves that were selected according to these criteria. Force spectroscopic data was smoothed using moving-average filtering. In Fig. 5, selected force

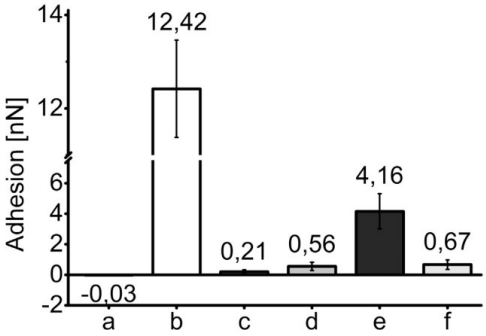

FIGURE 3 Mean adhesion measured through force-distance curves with AFM. An average of 410 ± 38 force-distance curves were analyzed per experimental condition. (*a*) Mean adhesion for cleaned quartz glass (−0.025 nN ± 0.008 nN). (*b*) Mean adhesion for silanized quartz glass (12.42 nN ± 1.04 nN). (*c*) Mean adhesion for silanized quartz glass functionalized with PEG (0.21 nN ± 0.13 nN). (*d*) Mean adhesion for SuccinylPE bound to PEG (0.56 nN ± 0.26 nN). (*e*) Mean adhesion of trisNTA bound to PEG (4.16 nN ± 1.15 nN). (*f*) Mean adhesion of a 2:1 (mol/mol) mixture of SuccinylPE:trisNTA bound to PEG (0.67 nN ± 0.30 nN).

curves were overlaid to show the four characteristic peaks for the unfolding of BR as a seven-α-helical protein (13,25,26,28). Although the first peak (Fig. 5 *a*) is inhomogeneous, the following peaks (Fig. 5 *b–d*) can be distinguished. The second and third unfolding peaks remain at forces <150 pN, whereas the last peak shows a force of ~200 pN.

DISCUSSION

Substrate characterization by XPS

To analyze the quartz glass surface and verify the first functionalization step, the surface was measured before and after silanization using XPS. A pure quartz glass surface shows the presence of a few undesired elements, namely fluorine, carbon, and sodium. As even quartz glass has some impurities, this is not surprising. However, any sign of these elements disappears after silanization with APTES. Given the structure and composition of APTES, and considering the theoretical distribution on the surface (Fig. S5 *a*), a theoretical composition of the silanized surface is shown in Fig. S5 *b*. It is also taken into account that XPS measures not only the topmost layer of a surface but can penetrate further. Thus our XPS results of the silanized surface (Fig. S5 *b*) are in accordance with a successful coverage of the surface with APTES.

Surface characterization by topography and adhesion

Surface topography

The surface functionalization steps were further characterized by AFM. AFM imaging offers the possibility of observing the changes in surface topography. A comparison of AFM imaging data of a clean quartz glass surface (Fig. 2 *a*) with a silanized quartz glass surface (Fig. 2 *b*) shows no change in average surface roughness and characteristics of the surface, in line with the small molecule size and flexibility of APTES. The short PEG linker that is coupled subsequently to the surface can have a length

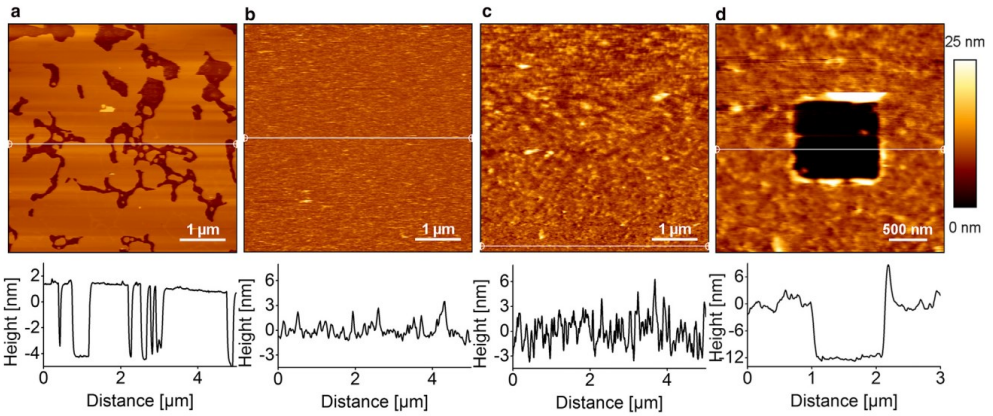

FIGURE 4 AFM scans (5 μm × 5 μm for *a–c*; 3 μm × 3 μm for *d*) in tapping mode in buffer P1, with corresponding height profiles, represented as white horizontal lines in each image, below each scan. (*a*) Membrane formation on a mica surface. (*b*) A mica surface covered with membrane containing BR. (*c*) A functionalized glass surface covered with the membrane containing BR. (*d*) Scratching was performed with the cantilever on a surface functionalized with lipid and protein anchor and incubated with the protein lipid mixture. To see this figure in color, go online.

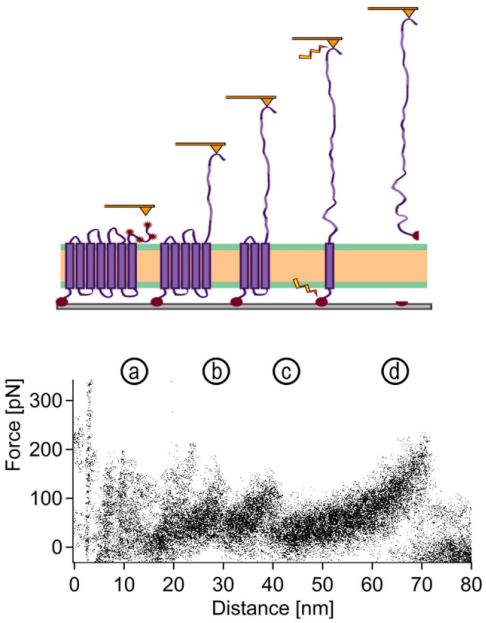

FIGURE 5 BR unfolding curves from the model tBLM. As a 7TM membrane protein, the unfolding of BR will lead to four characteristic peaks in a force-distance curve. (*a*) The first peak shows the stretching of the terminus and unfolding of the first two transmembrane helices (TMs). As the cantilever can adsorb to the terminus at different positions, the first peak is not resolved clearly. This is followed by the pairwise unfolding of the next four TMs during the next two peaks (*b* and *c*). The last peak (*d*) shows the pulling of the seventh TM until BR dissociates from the tip or from the membrane. In our case, this means the dissociation between the His10-tag and the trisNTA. To see this figure in color, go online.

of 4 nm in its stretched conformation. This linker is flexible and will either coil on the surface or stretch to accommodate for surface roughness and differences between the bilayer and protein. AFM data of this stage (Fig. 2 *c*) shows that the holes and scratches found on quartz glass disappear, suggesting that the linker can compensate for surface roughness. The homogeneity and absence of defects also indicates a complete coverage with PEG. Coupling of only the anchoring lipid SuccinylPE to PEG yields a surface with an increased average roughness (Fig. 2 *d*). Additionally, buffer repelling properties, observed during the experiments, suggest strong hydrophobic characteristics of the surface. This can be explained by the hydrophobic chains of the anchoring lipid orientating up and away from the substrate, thereby creating a hydrophobic surface. The roughness of the surface is due to the length of the anchoring lipid (2 nm). The surface is again homogeneous and shows no defects. Coupling only the protein anchor, trisNTA, to the surface leads to the appearance of round structures ~4–10 nm in height and 200 nm in diameter. This can indicate the aggregation of an excess amount of protein anchor. When the protein anchor is diluted with the lipid anchor 1:2 (mol/mol), the aggregates are no longer present. This and the uniform surface structure indicate a homogeneous mixture of lipid and protein anchor.

Adhesion

The differences in adhesion after each step are indicative of a successful functionalization process. Furthermore, a homogeneous adhesion force throughout the investigated surface implies a homogeneous surface functionalization. The strong adhesion forces for a surface functionalized only with protein anchor can relate to the presence of aggregates on the surface. Thus, even though the surface functionalized with the mixture shows only slightly higher mean adhesion forces than the surface only functionalized with the lipid anchor, a homogeneous and well distributed protein anchor is assumed due to the previously described changes in surface topography.

Specificity of protein binding

To test the specificity of protein binding to the surface and exclude unspecific adsorption, BR was coupled to a functionalized surface. The surface was then rinsed with a buffer without and with imidazole. As only imidazole-containing buffer can elute proteins with a poly-histidine-tag from NTA groups, BR will only be detected (using a dot blot system with anti-His antibodies) for the elution fraction containing imidazole. To exclude a possible binding of the antibody to the imidazole, imidazole-containing buffer was applied to the membrane as a buffer control. The results of the dot blot clearly show that the protein could only be eluted from the surface with imidazole. These data verify not only the specific binding of the protein to the surface anchor, but also the integrity of the previous coupling step leading to accessible trisNTA.

Membrane and protein reconstitution

Artificial lipid membranes have been observed to undergo phase transitions from more liquid unordered phases to ordered gel/crystalline phases at specific temperatures. The phase transition temperature depends on the membrane composition. As the integration of proteins into lipid membranes and their functionality is highly dependent on the membrane fluidity, we aimed to provide a lipid membrane system that is stable but still offers enough fluidity for the integration of membrane proteins. Future studies may benefit from the possibility of a careful selection of lipids that are compatible with the setup. We chose DPPC as the tBLM main component due to its good properties to form stable membranes on mica. DPPC has been used previously to create stable sBLMs (37,38). However, as the phase

transition occurs at a temperature of 42°C, those sBLMs are in the ordered gel-to-crystal-like phase at RT (39,40). Adding a detergent like DPC weakens lipid-lipid interactions and increases the permeability of the bilayer to proteins (41). A membrane mimetic system consisting of a lipid and detergent mixture has been described previously (42). The formation of an sBLM on mica by a mixture of DPPC and DPC was tested, and a homogeneous bilayer formation with a few defects could be detected by AFM. The bilayer height of 5 nm is in accordance with bilayer heights in previous studies (43,44). Reconstitution of BR into the lipid/detergent mixture and applying this mixture to a mica surface leads to coverage of the surface with a homogeneous layer (Fig. 4 *b*). Defects could not be observed. However, compared to an sBLM without BR (Fig. 4 *a*), the roughness of the membrane surface has increased. It is known that membrane-integrated proteins can protrude out of the membrane (45). The roughness of the membrane could thus indicate protrusions of BR out of the membrane. The protrusions persist on membranes formed on functionalized quartz glass (Fig. 4 *c*). The roughness is even more pronounced, as functionalized quartz glass in itself provides a rough substrate (Fig. 2 *f*). The increase in size of the structures observed on the surface with scan direction (bottom to top) is a broadening effect of the cantilever tip. Especially soft materials, like membranes and proteins, in our case, most likely the free lipid DPPC, can adsorb to the tip during scanning and increase the effective tip diameter. Every structure will then be broadened by the tip diameter. This is why for the first 500 nm the surface structure appears comparable to a membrane with protein on mica and becomes increasingly dissimilar during the scan process. For this reason, the height profile was measured during the first 500 nm of the scan. As a control, the membrane was also formed on a functionalized surface without BR (Fig. S6 *a*). Here, the surface was again homogeneously covered with the tBLM with only a few small defects. The surface roughness of the membrane was only influenced by the roughness of the quartz glass and the underlying functionalization, indicating that the high roughness of Fig. 4 *c* is caused by protrusions of BR. In contrast, a membrane on a surface functionalized only with trisNTA and no lipid anchor (Fig. S6 *b*) could not be formed on quartz glass under the same conditions.

Scratching of the membrane with BR on quartz glass (Fig. 4 *d*) revealed a height of 10 nm and protein clusters protruding 1–2 nm out of the membrane. When taking into account the length of the PEG linker and the height of the sBLM on mica (4 nm + 5 nm), the measured height of 10 nm is in accordance with expectations.

Force spectroscopy

Force-distance curves of force spectroscopy measurements performed on BR reconstituted into tBLMs showed the typical pattern of four peaks, consistent with a functional reconstitution of BR. In Fig. S7, a representative BR force-distance curve from BR purple membranes is compared to the measured force-distance curves of Fig. 5. The first peak of the measured force curves of BR in the tBLM was inhomogeneous, which can be attributed to the unspecific adhesion positions of the terminus to the tip (28). The second peak seems to favor lower forces and follows the shape of the intermediate peaks found in force-distance curves of purple membranes (30). Considering the average noise of the recorded force-distance curves (± 30 pN) the third peak is in accordance with unfolding forces of BR from purple membranes and nano-discs (13). During the last unfolding event, BR can either dissociate from the tip or be pulled out of the membrane completely. In the case of being pulled out completely, BR would have to also dissociate from the protein anchor. It has been shown previously on soluble proteins that the dissociation forces between triNTA and His6 can be between 100 and 400 pN (46). Our results indicate that the last peak of our force-distance curves represents these dissociation forces. Although this influence of the protein anchor on the last unfolding event should be considered during analysis, it also shows that BR reconstituted into the here-presented tBLM is coupled to the protein anchor. In addition, in the case of BR not being inserted in a defined orientation, two sets of force-distance curves are expected (one pulled from the N- and one from the C-terminus), which can be the case for reconstitution of BR into nanodiscs (13) and force spectroscopic measurements performed on BR crystals (30). As BR force-distance curves from both termini are indeed very similar, the high forces detected for the last peak indicate a complex formation between the His-tag and trisNTA, thus supporting a defined orientation of BR. Should force-distance curves be measured that do not show the dissociation forces of the complex, they can be sorted out before analysis of the data.

Apart from the influence of the trisNTA, there could also be an influence of the PEG linker on the last unfolding event. As we expect a typical stretching behavior of the PEG linker (47,48), we do not analyze the PEG-linker elasticity directly. However, it can be assumed that the influence of the PEG-linker elasticity is minimal due to its short length.

Even though higher forces for the last peak can be seen in our experimental setup, we also have to note the stronger noise. As this high noise can indicate misfolding or denaturation of BR, we cannot clearly determine whether BR is still in its functional state after reconstitution. The functional form of the protein has been checked before reconstitution into the membrane through ultraviolet-visible spectroscopy (described in the Supporting Material). An example absorbance spectrum of a 1:10 diluted solution of cell-free expressed and purified BR is shown in Fig. S8. Due to the very low protein concentration and the experimental setup,

we can, however, only assume the functional form of the protein via the measured force curves. However, we anticipate that further optimization of tBLM composition, which has to be adjusted to every new protein of interest, will allow for further stabilization of the protein conformation inside the tBLM.

CONCLUSIONS

Gaining knowledge about the structure of membrane proteins is an important endeavor to reliably study the cause of diseases and facilitate drug development. In this respect, single-molecule AFM force spectroscopy offers unique possibilities in particular for the investigation of multipass membrane proteins. We here showed that AFM force spectroscopy can be carried out in a tBLM system, and our method allows for filtering out force-distance curves specific to a defined orientation. Although the tBLM system offers a near-native environment that can be adjusted to accommodate different membrane proteins, the predefined orientation can simplify data analysis by removing a second contribution arising from different orientations and by better defining the starting conditions for each protein. In our work, we show a five-step functionalization and reconstitution process that we successfully apply to the cell-free expressed 7TM protein BR that has been frequently used as a model for GPCRs. We anticipate that the presented approach can be transferred to a broad range of target membrane proteins and surface-based techniques and may help to provide new insights into structure, function, and interactions of these important biological systems.

SUPPORTING MATERIAL

Supporting Materials and Methods and eight figures are available at http://www.biophysj.org/biophysj/supplemental/S0006-3495(16)30835-9.

AUTHOR CONTRIBUTIONS

D.H., F.O., and A.M.B. designed research; S.E. and A.M.B. performed research; F.O. and A.B contributed analytic tools; A.B. and A.M.B. analyzed data; and M.E., A.B., and A.M.B. wrote the manuscript.

ACKNOWLEDGMENTS

We thank Mario Schneider for his help in programming analysis software, as well as the groups of P.D. Dr. M. Lohrengel, Prof. Dr. Seidel, and Prof. Dr. Weinkauf of the Heinrich-Heine-Universität Düsseldorf for providing access to, and assistance with measuring X-ray photoelectron spectroscopy. We thank the group of Prof. Dr. Jacob Piehler of the University of Osnabrück for providing the trisNTA and all derivatives.

We gratefully acknowledge support (and training) from the International NRW Research School BioStruct, granted by the Ministry of Innovation, Science and Research of the State North Rhine-Westphalia, the Heinrich-Heine-University of Düsseldorf, and the Entrepreneur Foundation at the Heinrich-Heine-University of Düsseldorf, as well as from the Deutsche Forschungsgemeinschaft through Sonderforschungsbereich 974 "Communication and System Relevance in Liver Damage and Regeneration," through an Emmy Noether grant (ET 103/2-1) and through the Forschungskommission Düsseldorf.

SUPPORTING CITATIONS

Reference (49) appears in the Supporting Material.

REFERENCES

1. Liu, J., and B. Rost. 2001. Comparing function and structure between entire proteomes. *Protein Sci.* 10:1970–1979.
2. Aridor, M., and L. A. Hannan. 2000. Traffic jam: a compendium of human diseases that affect intracellular transport processes. *Traffic.* 1:836–851.
3. Aridor, M., and L. A. Hannan. 2002. Traffic jams II: an update of diseases of intracellular transport. *Traffic.* 3:781–790.
4. Cotton, R. G. H., O. Horaitis; Human Genome Organization. 2002. The HUGO Mutation Database Initiative. *Pharmacogenomics J.* 2:16–19.
5. Stenson, P. D., E. V. Ball, …, D. N. Cooper. 2003. Human Gene Mutation Database (HGMD): 2003 update. *Hum. Mutat.* 21:577–581.
6. Heyse, S., T. Stora, …, H. Vogel. 1998. Emerging techniques for investigating molecular interactions at lipid membranes. *Biochim. Biophys. Acta.* 1376:319–338.
7. Tanaka, M., and E. Sackmann. 2005. Polymer-supported membranes as models of the cell surface. *Nature.* 437:656–663.
8. Köper, I. 2007. Insulating tethered bilayer lipid membranes to study membrane proteins. *Mol. Biosyst.* 3:651–657.
9. Vockenroth, I. K., C. Ohm, …, I. Köper. 2008. Stable insulating tethered bilayer lipid membranes. *Biointerphases.* 3:FA68.
10. Deverall, M. A., E. Gindl, …, C. A. Naumann. 2005. Membrane lateral mobility obstructed by polymer-tethered lipids studied at the single molecule level. *Biophys. J.* 88:1875–1886.
11. Giess, F., M. G. Friedrich, …, W. Knoll. 2004. The protein-tethered lipid bilayer: a novel mimic of the biological membrane. *Biophys. J.* 87:3213–3220.
12. Rigaud, J.-L., and D. Lévy. 2003. Reconstitution of membrane proteins into liposomes. *Methods Enzymol.* 372:65–86.
13. Zocher, M., C. Roos, …, D. J. Müller. 2012. Single-molecule force spectroscopy from nanodiscs: an assay to quantify folding, stability, and interactions of native membrane proteins. *ACS Nano.* 6:961–971.
14. Atanasova, P. P., V. Atanasov, and I. Köper. 2007. Anchor-lipid monolayers at the air-water interface; prearranging of model membrane systems. *Langmuir.* 23:7672–7678.
15. Sinner, E. K., and W. Knoll. 2001. Functional tethered membranes. *Curr. Opin. Chem. Biol.* 5:705–711.
16. Pfeiffer, I., S. Petronis, …, M. Zäch. 2010. Vesicle adsorption and phospholipid bilayer formation on topographically and chemically nanostructured surfaces. *J. Phys. Chem. B.* 114:4623–4631.
17. Roder, F., S. Waichman, …, J. Piehler. 2011. Reconstitution of membrane proteins into polymer-supported membranes for probing diffusion and interactions by single molecule techniques. *Anal. Chem.* 83:6792–6799.
18. Coutable, A., C. Thibault, …, E. Trévisiol. 2014. Preparation of tethered-lipid bilayers on gold surfaces for the incorporation of integral membrane proteins synthesized by cell-free expression. *Langmuir.* 30:3132–3141.
19. Oberbarnscheidt, L., R. Janissen, and F. Oesterhelt. 2009. Direct and model free calculation of force-dependent dissociation rates from force spectroscopic data. *Biophys. J.* 97:L19–L21.
20. Engel, A., and H. E. Gaub. 2008. Structure and mechanics of membrane proteins. *Annu. Rev. Biochem.* 77:127–148.

21. Harris, N. C., Y. Song, and C.-H. Kiang. 2007. Experimental free energy surface reconstruction from single-molecule force spectroscopy using Jarzynski's equality. *Phys. Rev. Lett.* 99:068101.
22. Lee, G. U., D. A. Kidwell, and R. J. Colton. 1994. Sensing discrete streptavidin-biotin interactions with atomic force microscopy. *Langmuir.* 10:354–357.
23. Oberbarnscheidt, L., R. Janissen, …, F. Oesterhelt. 2009. Single-molecule force spectroscopy measures structural changes induced by light activation and transducer binding in sensory rhodopsin II. *J. Mol. Biol.* 394:383–390.
24. Pelaseyed, T., M. Zäch, …, G. C. Hansson. 2013. Unfolding dynamics of the mucin SEA domain probed by force spectroscopy suggest that it acts as a cell-protective device. *FEBS J.* 280:1491–1501.
25. Roychoudhury, A., D. Haussinger, and F. Oesterhelt. 2012. Effect of the compatible solute ectoine on the stability of the membrane proteins. *Protein Pept. Lett.* 19:791–794.
26. Roychoudhury, A., A. Bieker, …, F. Oesterhelt. 2013. Membrane protein stability depends on the concentration of compatible solutes—a single molecule force spectroscopic study. *Biol. Chem.* 394:1465–1474.
27. Wickstrand, C., R. Dods, …, R. Neutze. 2015. Bacteriorhodopsin: would the real structural intermediates please stand up? *Biochim. Biophys. Acta.* 1850:536–553.
28. Baumann, R.-P., M. Schranz, and N. Hampp. 2010. Bending of purple membranes in dependence on the pH analyzed by AFM and single molecule force spectroscopy. *Phys. Chem. Chem. Phys.* 12:4329–4335.
29. Müller, D. J., F. A. Schabert, …, A. Engel. 1995. Imaging purple membranes in aqueous solutions at sub-nanometer resolution by atomic force microscopy. *Biophys. J.* 68:1681–1686.
30. Kessler, M., and H. E. Gaub. 2006. Unfolding barriers in bacteriorhodopsin probed from the cytoplasmic and the extracellular side by AFM. *Structure.* 14:521–527.
31. Klammt, C., D. Schwarz, …, F. Bernhard. 2007. Cell-free production of G protein-coupled receptors for functional and structural studies. *J. Struct. Biol.* 158:482–493.
32. Etzkorn, M., T. Raschle, …, G. Wagner. 2013. Cell-free expressed bacteriorhodopsin in different soluble membrane mimetics: biophysical properties and NMR accessibility. *Structure.* 21:394–401.
33. Lata, S., and J. Piehler. 2005. Stable and functional immobilization of histidine-tagged proteins via multivalent chelator headgroups on a molecular poly(ethylene glycol) brush. *Anal. Chem.* 77:1096–1105.
34. Butt, H.-J., and M. Jaschke. 1995. Calculation of thermal noise in atomic I Calculation of thermal noise in atomic force microscopy. *Nanotechnology.* 6:1–7.
35. Janissen, R., L. Oberbarnscheidt, and F. Oesterhelt. 2009. Optimized straight forward procedure for covalent surface immobilization of different biomolecules for single molecule applications. *Colloids Surf. B Biointerfaces.* 71:200–207.
36. Schwarz, D., F. Junge, …, F. Bernhard. 2007. Preparative scale expression of membrane proteins in *Escherichia coli*-based continuous exchange cell-free systems. *Nat. Protoc.* 2:2945–2957.
37. Sullan, R. M. A., J. K. Li, and S. Zou. 2009. Direct correlation of structures and nanomechanical properties of multicomponent lipid bilayers. *Langmuir.* 25:7471–7477.
38. Giocondi, M.-C., D. Yamamoto, …, C. Le Grimellec. 2010. Surface topography of membrane domains. *Biochim. Biophys. Acta.* 1798:703–718.
39. Giocondi, M. C., V. Vié, …, C. Le Grimellec. 2000. In situ imaging of detergent-resistant membranes by atomic force microscopy. *J. Struct. Biol.* 131:38–43.
40. Choucair, A., M. Chakrapani, …, L. J. Johnston. 2007. Preferential accumulation of Aβ_{1-42} on gel phase domains of lipid bilayers: an AFM and fluorescence study. *Biochim. Biophys. Acta.* 1768:146–154.
41. Seddon, A. M., P. Curnow, and P. J. Booth. 2004. Membrane proteins, lipids and detergents: not just a soap opera. *Biochim. Biophys. Acta.* 1666:105–117.
42. Vasudevan, S. V., J. Schulz, …, M. J. Cocco. 2010. Protein folding at the membrane interface, the structure of Nogo-66 requires interactions with a phosphocholine surface. *Proc. Natl. Acad. Sci. USA.* 107:6847–6851.
43. Lin, H., R. Bhatia, and R. Lal. 2001. Amyloid β protein forms ion channels: implications for Alzheimer's disease pathophysiology. *FASEB J.* 15:2433–2444.
44. Redondo-Morata, L., M. I. Giannotti, and F. Sanz. 2012. Influence of cholesterol on the phase transition of lipid bilayers: a temperature-controlled force spectroscopy study. *Langmuir.* 28:12851–12860.
45. Whited, A. M., and P. S.-H. Park. 2014. Atomic force microscopy: a multifaceted tool to study membrane proteins and their interactions with ligands. *Biochim. Biophys. Acta.* 1838 (1 Pt A):56–68.
46. Tang, J., A. Ebner, …, P. Hinterdorfer. 2009. Detection of metal binding sites on functional S-layer nanoarrays using single molecule force spectroscopy. *J. Struct. Biol.* 168:217–222.
47. Heymann, B., and H. Grubmüller. 1999. Elastic properties of poly(ethylene-glycol) studied by molecular dynamics stretching simulations. *Chem. Phys. Lett.* 307:425–432.
48. Oesterhelt, F., M. Rief, and H. E. Gaub. 1999. Single molecule force spectroscopy by AFM indicates helical structure of poly(ethylene-glycol) in water. *New J. Phys.* 1:6.
49. Gruber, H. J. 2016. Amino-functionalization of AFM tips (and supports). Institute of Biophysics, Johannes Kepler University, Linz, Austria. May 6, 2016. http://www.jku.at/biophysics/content/e257042/e257048/03_AFM_tip_aminofunctionalization_2016_05_06_eng.pdf.

Biophysical Journal, Volume *111*

Supplemental Information

Oriented Membrane Protein Reconstitution into Tethered Lipid Membranes for AFM Force Spectroscopy

Anna M. Bronder, Adeline Bieker, Shantha Elter, Manuel Etzkorn, Dieter Häussinger, and Filipp Oesterhelt

1

Materials

Buffers

1) Tris-buffered saline and Tween 20 (TBT): 20 mM Tris, 150 mM NaCl, 0.1 % Tween 20, pH 7.5
2) Tris-buffered saline (TBS): 20 mM Tris, 150 mM NaCl, pH 7.5
3) phosphate buffer (P1): 46.6 mM Na_2HPO_4, 3.4 mM NaH_2PO_4, 150 mM NaCl, pH 8
4) wash buffer (DDM-W1): P1 + 0,4 mM DDM + 20 mM Imidazole
5) protein buffer (DDM-P1): P1 + 0,4 mM DDM
6) elution buffer (DDM-E): DDM-P1 + 250 mM Imidazole
7) refolding buffer (RFB): 23.1 mM Na_2HPO_4, 16.9 mM NaH_2PO_4, 1 M NaCl, 5 % DDM, 100 mM Retinal, pH 7
8) S30 buffer: 10 mM Tris-acetate, pH 8.2, 14 mM $Mg(OAc)_2$, 0.6 mM KCl, 1 mM DTT and 0.1 mM PMSF

Experimental Design and Methods

Dot Blot
A functionalized quartz surface with bound BR was first rinsed with 100 µl DDM-P1 by pipetting up and down several times. The rinsing buffer was collected as the rinsing fraction. The same surface was then rinsed the same way with 100 µl DDM-E, which was again collected as the elution fraction. A Dot blot was prepared of 100 µl DDM-E (buffer control), 100 µl rinsing fraction and 100 µl elution fraction on a membrane. The membrane was swayed in 1 % (w/v) powdered milk solution at 4 °C, overnight. After washing with water the membrane was swayed 3 x 10 min in TBT and 1 x 10 min in TBS at RT. The membrane was shortly washed with water and swayed in histidin-tag (His-tag) antibody solution (1:5000 anti-His-HRP (Miltenyi Biotec, Bergisch Gladbach, Germany) in 1 % (w/v) powdered milk solution) for 1 h, at RT. This was followed by swaying 2 x 10 min in TBT and 1 x 10 min TBS at RT and shortly rinsing with water. The membrane was covered with a 1:1 (v/v) solution of luminol enhancer solution:stable peroxide solution, (both SuperSignal West Pico, Thermo Fisher Scientific, Oberhausen, Germany) and chemoluminescence was measured with a ChemiDoc MP documentation system (Bio-Rad, Hercules, U.S.).

Protein refolding
Protein pellet from CFE was washed with S30 buffer and directly refolded or stored at -20 °C. 2 x 50 µl protein pellets were resuspended in 2 x50 µl RFB. The samples were wrapped in aluminum foil to be protected from light and let to incubate for 2 h, at RT. A Micro Bio-Spin(TM) gravity-flow column (Bio-Rad, Hercules, U.S.) was filled with 160 µl Ni-NTA-Agarose (Macherey-Nagel, Germany) for a total column volume (CV) of 80 µl. After letting the agarose settle the column was washed with 5 ml water and equilibrated with 5 ml DDM-P1. The resuspended pellets were combined and loaded onto the column. The agarose and BR sample were pipetted up and down to mix and increase binding. Covering the column from light it was let to incubate for 1 h while mixing every 20 min. The column was then washed with 6 CV DDM-W1 and 2 CV DDM-P1. BR was eluted using 4 CV DDM-E giving elution

2

fractions 1-4. Fractions 2-4 were combined for concentration. A concentrator tube (10.000 MWCO, Vivaspin 4, PES membrane, Sartorius, Göttingen, Germany) was washed with 6 x 10 ml water, 4 x 10 ml P1 and 1 x 10 ml DDM-P1 by centrifugation at 4 °C, 4000 g, 15 min each. 230 µl BR (fractions 2-4) were loaded into the concentrator and centrifuged at 4 °C, 4000 g for 20 min until the sample was concentrated to 50 µl. The sample was washed with DDM-P1 by centrifugation at 4 °C, 4000 g for 20 min until again the total volume was concentrated to 50 µl. 10 µl of the sample were used to measure the concentration in a 1:10 (v/v) dilution in DDM-P1 at the spectrophotometer (V-650, Jasco, Groß-Umstadt, Germany). An absorption spectrum was measured between 260 nm and 750 nm. The peak at 555 nm corresponds to the adsorption of successfully refolded BR and is used to calculate the concentration with an extinction coefficient of $\varepsilon = 55000\ L \bullet cm^{-1} \bullet mol^{-1}$.

Functionalization steps

Plasma activation
Quartz Slides (3" x 1" x 1 mm, TED PELLA Inc.) were placed into a plasma cleaner (Plasma, low-pressure system, Femto, Diener electronics) and 500 µl of water were distributed as drops inside the chamber and allowed to evaporate under vacuum to saturate the atmosphere inside the plasma cleaner with H_2O. The surfaces were activated for 5 min at 100 %. Further functionalization was done immediately after.

Silanization
Adapted from method B of the protocol 2 (1). A desiccator was flooded with nitrogen for 5 min. The plasma activated surfaces were placed into the desiccator together with 100 µl of APTES and 33 µl of triethylamine (Et_3N; puriss., p.a. ≥99.5 % GC, Fluka, Seelze, Germany). After 5 min of constant nitrogen flow the desiccator was closed completely and the silanization was allowed to take place for 2 h. APTES and Et_3N were removed from the desiccator and it was again flooded with nitrogen for 5 min. After closing the desiccator the surfaces were allowed to cure for at least 48 h.

Functionalization with polyethylene glycol
Mmt-NH-PEG_{12}-COO-Tfp (PEG; Iris Biotech, Marktredwitz, Germany), Et_3N and dimethylsulfoxide (DMSO; A.C.S, spectrophotometric Grade ≥99.9 %, Sigma-Aldrich, Munich, Germany) were mixed 20:1:200 (v/v/v). The silanized surfaces were taken out of the desiccator and placed into petri dishes. A small space between two silanized slides facing each other, created by clean cover slips, was filled with 10 µl/cm² of the solution followed by incubation for 2 h. After incubation the surfaces were placed into 50 ml centrifuge tubes (TPP, Gamma-sterilized, Sigma-Aldrich, Munich, Germany) and rinsed 10 x with water by filling and emptying the tube completely. After drying with nitrogen the functionalized surfaces were stored at -20 °C in fresh 50 ml falcon tubes. Figure 1 E schematically shows the surface functionalized with PEG.

Binding anchoring lipids and trisNTA to PEG
To remove the monomethoxytrityl (Mmt) protection group from PEG the surfaces were covered with 80 % acetic acid (Ultra, ≥99.5 % GC/T, Fluka, Seelze, Germany) for 1 h inside

3

50 ml falcon tubes. Meanwhile a solution was prepared depending on the targeted surface functionalization. trisNTA surface: 10:10:1 (v/v/v) of trisNTA stock:*N,N'*-Diisopropylcarbodiimide (DIC; 99 %, Sigma-Aldrich, Munich, Germany):N,N-Diisopropylethylamine (DIPEA; Reagent Plus, 99 %, Sigma-Aldrich, Munich, Germany). SuccinylPE surface: 2:10:1 (v/v/v) of SuccinylPE stock:DIC:DIPEA. Mixed surface: 1:5:10:1 (v/v/v/v) of SuccinylPE stock:trisNTA stock:DIC:DIPEA. After deprotection the slides were rinsed again ten times with water by filling and emptying the falcon tubes completely and then dried under nitrogen. A small space between two glass slides facing each other, created by clean cover slips (Microscope Cover Glasses, #1, 22 x 22 mm, Menzel Gläser, Braunschweig, Germany), was filled with 10 µl/cm² of the respective solution followed by incubation for 1 h at 75 °C. Two clean glass beakers were filled with chloroform and the functionalized surfaces were dipped and rinsed inside the beakers subsequently. The surfaces were dried with nitrogen and placed into glass petri dishes with the functionalized side facing upwards. They were covered with trifluoracetic acid (TFA; ≥99.9 % for synthesis, Carl Roth, Karlsruhe, Germany) and a few drops of water for 12 h to remove the OtBu protection groups from irisNTA.

4

Supplementary Figures

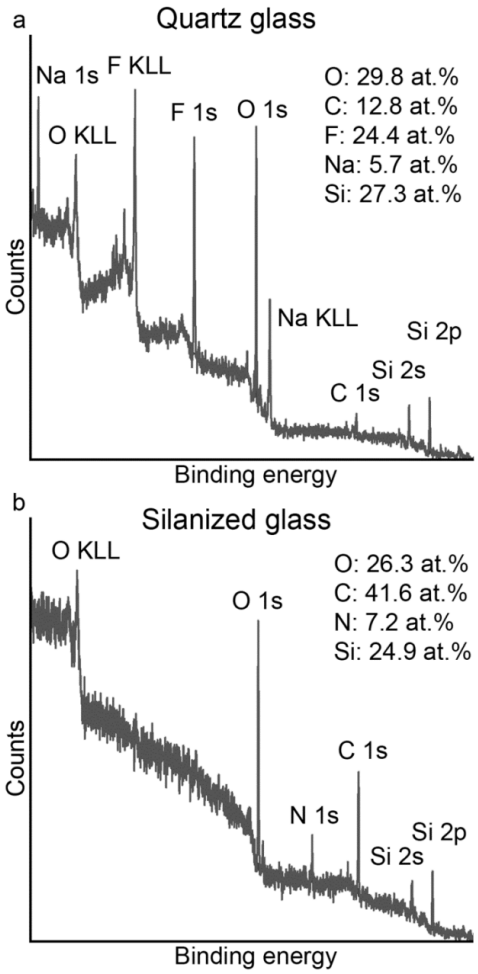

Figure S1. (a) XPS survey spectrum of cleaned quartz glass. (b) A survey spectrum after silanization with APTES only shows binding energies corresponding to levels in O, C, N and Si.

5

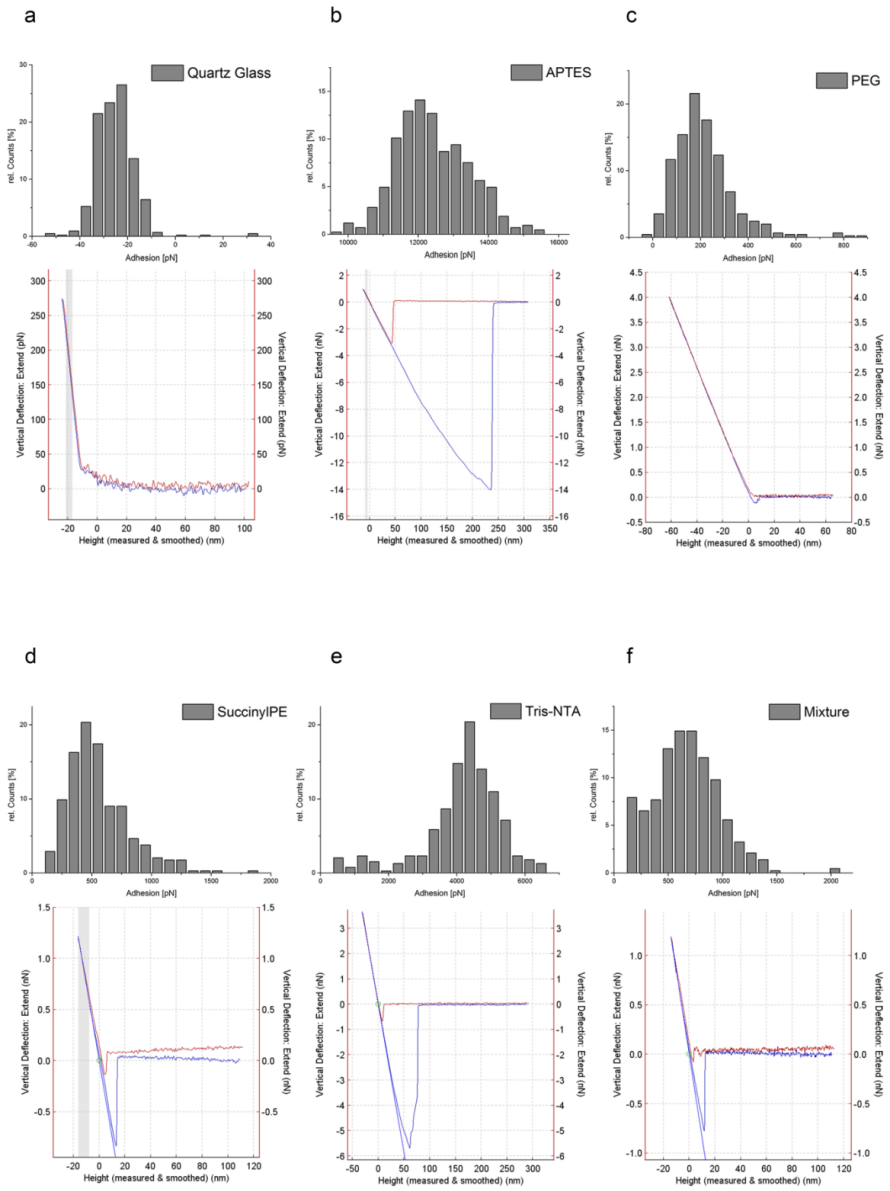

Figure S2. Histograms showing the characteristic adhesion forces for the surface functionalization steps a-f. Number of total counts: a) 419, b) 425, c) 454, d) 344, e) 392, f) 429. Bellow each histogram a typical force-distance curve is shown. The approach of the cantilever is represented by the red curve, while the retrace is shown in blue.

6

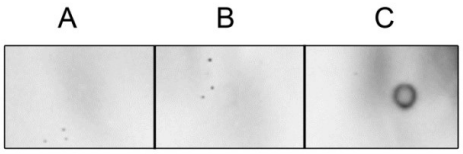

Figure S3. Dot blot of buffer control consisting of buffer DDM-E (buffer with imidazole) (A), rinsing fraction consisting of buffer P1-DDM (buffer without imidazole), which was used to rinse the surface (B) and elution fraction consisting of buffer DDM-E, which was used to rinse the surface and elute BR (C).

7

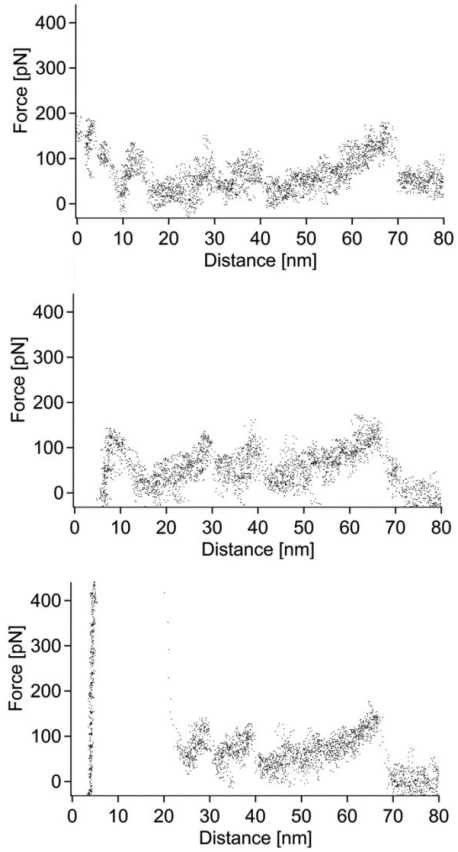

Figure S4. Single representative measured force distance curves of BR from the tBLM.

8

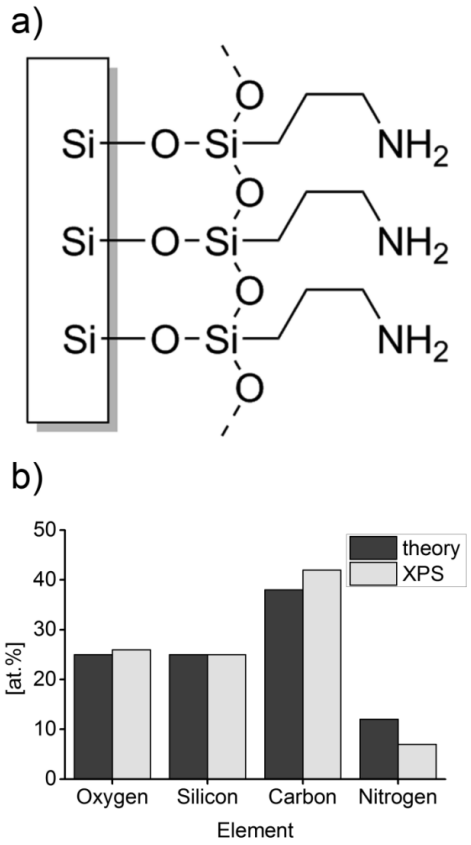

Figure S5. (a) Schematic representation of the theoretical silanization of quartz glass. (b) Theoretical composition of silanized surface (theory) compared with XPS results (XPS).

9

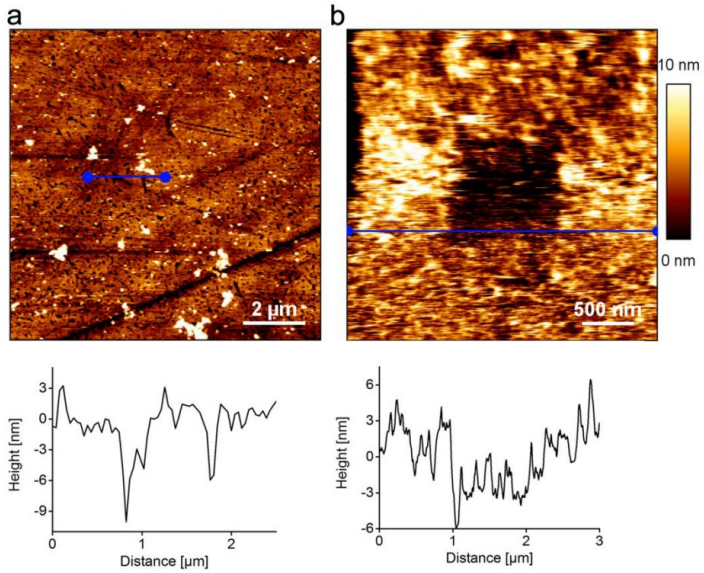

Figure S6. AFM scans (10 µm x 10 µm, contact mode for a) and 3 µm x 3 µm, tapping mode for b)) in buffer P1 with corresponding height profiles, represented as horizontal lines in each image, below each scan. (a) A membrane formed on a functionalized quartz glass surface without BR. (b) Attempted membrane formation on a quartz glass surface functionalized only with the protein anchor trisNTA and BR included in the lipid suspension. We could observe that no membrane was formed without the lipid anchor, as is indicated by the scratched area in the center.

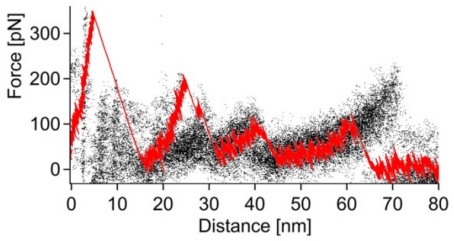

Figure S7. Representative force distance curve of BR from purple membranes pulled from the C-terminus (red force distance curve) placed over the measured force distance curves of the tBLM, also pulled from the C-terminus.

10

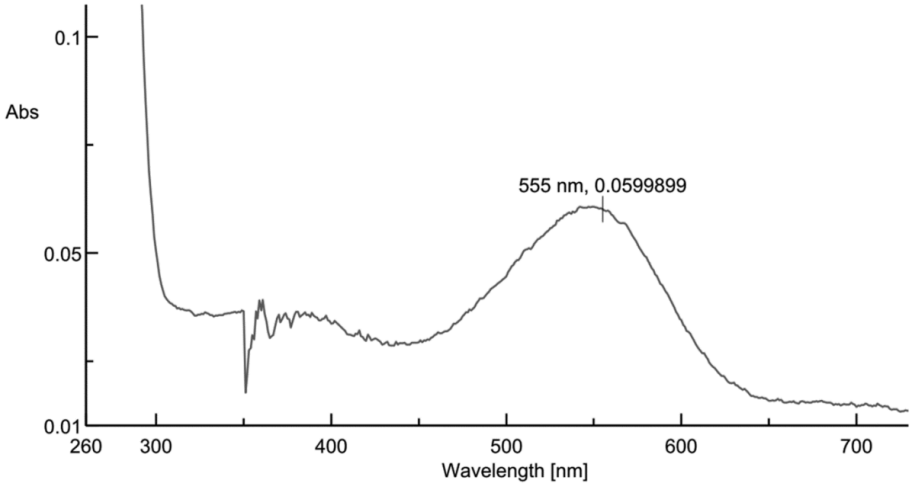

Figure S8. Example of absorbance spectrum of purified BR from CFE. 10 µl of the sample were used to measure the concentration in a 1:10 (v/v) dilution in DDM-P1 at the spectrophotometer. An absorption spectrum was measured between 260 nm and 750 nm. The peak at 555 nm corresponds to the adsorption of successfully refolded BR and is used to calculate the concentration with an extinction coefficient of ε = 55000 L • cm-1 • mol-1.

Supporting References

1. Gruber, H. J. 2016. Amino-functionalization of AFM tips (and supports). Institute of Biophysics, Johannes Kepler University, Linz, Austria. Web. 06 May 2016. http://www.jku.at/biophysics/content

2.1.3 Atomic force measurements on the specifically orientated membrane protein TGR5 reconstituted inside a tethered bilayer lipid membrane

Published in: European Journal of Medical Research

Impact Factor: 1.50

Own contribution: 80 %

Conceptualizing experimental approach, co-authoring the manuscript

Bronder et al. European Journal of Medical Research 2014, 19(Suppl 1):S11
http://www.eurjmedres.com/content/19/S1/S11

EUROPEAN JOURNAL OF MEDICAL RESEARCH

MEETING ABSTRACT Open Access

Atomic force measurements on the specifically orientated membrane protein TGR5 reconstituted inside a tethered bilayer lipid membrane

Anna Bronder[1*], Arpita Roychoudhury[1], Dieter Häussinger[2], Filipp Oesterhelt[1]

From 1st International Conference of Collaborative Research Center 974: Liver Damage and Regeneration Düsseldorf, Germany. 15-16 November 2013

Background

The G-protein coupled bile acid receptor (GPBAR1), commonly known as TGR5 is a transmembrane protein associated with diabetes, metabolic syndrome, inflammation and cancer in various organs. Together with these diseases a TGR5 deficiency, overexpression or mutation can often be observed. Due to this association of TGR5 and its mutants with different disorders, TGR5 is seen as a potential drug target. For the successful development of TGR5 agonists, it is important to have detailed information on the protein's structure and the structural changes caused by mutations. TGR5 is activated by bile acids (BAs), making BAs potential drug candidates [1]. BAs are signaling molecules with systemic endocrine functions, such as the regulation of bile acid, glucose & lipid metabolism, immune response and cell proliferation and differentiation [2]. However, BAs target several nuclear and plasma receptors, like the farnesol X receptor and TGR5, at once [3]. This makes it difficult to find TGR5 specific agonists. Knowledge about the interactions between BAs and TGR5 could help in the development of BA-derivatives and other new synthetic agonists exclusively targeting TGR5 with high efficiency. To study proteins, especially membrane proteins, different methods, e.g. atomic force microscopy and total internal reflection fluorescence microscopy can be applied. However, these methods are in need of a solid support and the protein being present in a defined orientation. In our group we have studied bacterial membrane proteins, e.g. bacteriorhodopsin, with single-molecule atomic force microscopy and spectroscopy [4,5]. The atomic force microscope (AFM) is a tool to image biological surfaces with sub-nanometer resolution. Important for biomolecules, like transmembrane proteins, is the fact that they can be studied in their natural environment, an aqueous solution. Force measurements performed with the AFM on individual molecules reveal inter- and intramolecular interaction at the pN scale [5], showing structural details, information on protein stability and the interactions between different molecules. These force measurement take advantage of the interaction between AFM tip and protein to pull the protein out of the membrane. When the terminus of the protein adsorbs to the tip, we can observe the unfolding of all protein domains as the tip moves away from the surface. Some domains of membrane proteins are embedded inside the membrane, e.g. α-helices, while other domains, e.g. loops, are outside. Using force measurements the different constitutions and chain lengths' of these domains, as well as the force required to unfold them can be identified. Due to this it was already possible to show new locations for structural changes in sensory rhodopsin 2 upon light activation. It was also demonstrated, that the conformational answer after light activation varies if another protein is bound to sensory rhodopsin 2 [4]. Further studies on the effect of compatible solutes on bacteriorhodopsin showed a general stabilization of membrane proteins by ectoine [5]. Interactions between two molecules, like TGR5 and a BA could thus also be distinguishable in a similar manner.

Although the AFM allows for us to study membrane proteins in their natural environment, an aqueous solution, membrane proteins, if removed from the cell, have to be stabilized by detergents or a lipid membrane in order to

* Correspondence: anna.bronder@hhu.de
[1]Institute of Physical Biology, AG Nanoanalytics, Heinrich Heine University, 40225 Düsseldorf, Germany
Full list of author information is available at the end of the article

Bronder et al. European Journal of Medical Research 2014, 19(Suppl 1):S11
http://www.eurjmedres.com/content/19/S1/S11

retain their native conformation. We can alternatively either use protein crystals or adsorbe the whole cell to a substrate. However, cells provide a complex system that could hinder the force measurements. Additionally, crystals are not yet available for every membrane protein. To overcome these obstacles artificial lipid bilayer membranes can be used as a suitable approach [6]. In our group we are studying the formation of artificial tethered bilayer lipid membranes (tBLMs) into which a membrane protein can be reconstituted in a defined orientation. Combining the AFM with the reconstitution of a functional membrane protein into a tBLM will allow us to gain structural information on membrane proteins.

Materials and methods

Single molecule force spectroscopy measurements are performed with the AFM MFP 3D-BIO from Asylum Research using the OMCL-TR400PSA Cantilevers from Olympus.

For the force measurements and AFM imaging the protein is reconstituted into a tBLM. To achieve this, a surface is functionalized with polyethylene glycol (PEG) linkers. To these PEG linkers anchor lipids and tris-nitrilotriacetic acid (trisNTA) are bound. A complex is formed between the surface bound trisNTA and the proteins His^6-tag. This provides the protein in a defined orientation, always with the His^6-tag containing terminus towards the surface. Detergents in the buffer solution prevent the protein from denaturing while the tBLM is incomplete. Through slow detergent-lipid exchange the tBLM is formed around the protein (Fig. 1).

The specificity of the coupling between trisNTA and His^6-tag can be studied by reflectometric interference spectroscopy (RIfS).

Conclusion

In this work we combine the advantage of concentration-controlled protein density and the knowledge about protein orientation due to specific coupling onto a solid support. The support is functionalized with trisNTA, allowing for a membrane proteins His^6-tag to couple to the surface. The protein is reconstituted into an artificial membrane, a tBLM, by slowly exchanging the detergent solution and forming a bilayer around the protein. This way we can form a tBLM on a solid surface and incorporate membrane proteins with a defined orientation. tBLMs offer a simple and reproducible approach to study membrane proteins in their natural environment. The system can be modified to meet the requirements of different membrane proteins. Protein density and orientation can be controlled by adjustments regarding the surface functionalization. We use this approach to study the membrane protein TGR5 by atomic force microscopy and spectroscopy. However, it could also be used to investigate the structure of other membrane proteins for which a protein crystal could not be obtained, yet.

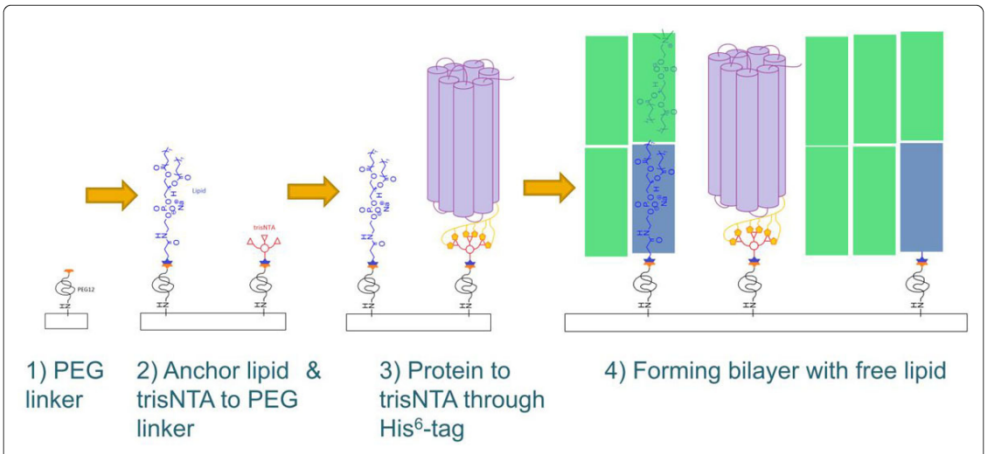

Figure 1 Coupling Steps & Incorporation of protein into artificial membrane To reconstitute a membrane protein into a tBLM in a defined orientation we use the following approach. A PEG linker is coupled to a surface functionalized with amino-groups (1). To the PEG linker's free amino-group the anchor lipid, 1,2-dipalmitoyl-sn-glycero-3-phosphoethanol-amine-N-(succinyl) sodium salt and trisNTA are bound (2). Through the proteins His^6-tag the protein is bound onto the surface with a defined orientation (3). Finally a complete membrane is formed with the free lipid 1,2-dipalmitoyl-sn-glycero-3-phosphocholine (4).

Acknowledgement
A. B. is a fellow of the NRW Research School BioStruct. This work was supported by grants from the Ministry of Innovation, Science, Research and Technology of the German Federal State North Rhine-Westphalia (NRW) and from the Entrepreneur Foundation at the Heinrich-Heine-Universität Düsseldorf. This work has also been supported by grants from the Deutsche Forschungsgemeinschaft (SFB 974).

Authors' details
[1]Institute of Physical Biology, AG Nanoanalytics, Heinrich Heine University, 40225 Düsseldorf, Germany. [2]Clinic of Gastroenterology, Hepatology and Infectious Diseases, Heinrich Heine University, 40225 Düsseldorf, Germany.

Published: 19 June 2014

References

1. Watanabe M, Morimoto K, Houten SM, Kaneko-Iwasaki N, Sugizaki T, Horai Y, Mataki C, Sato H, Murahashi K, Arita E, Schoonjans K, Suzuki T, Itoh H, Auwerx J: **Bile Acid Binding Resin Improves Metabolic Control through the Induction of Energy Expenditure.** *PLoS One* 2012, **7**:e38286.
2. Houten S, Watanabe M, Auwerx J: **Endocrine functions of bile acids.** *EMBO J* 2006, **25**:1419-1425.
3. Keitel V, Häussinger D: **Perspective: TGR5 (Gpbar-1) in liver physiology and disease.** *Clin Res Hepatol Gastroenterol* 2012, **36**:412-419.
4. Oberbarnscheidt L, Janissen R, Martell S, Engelhard M, Oesterhelt F: **Single-Molecule Force Spectroscopy Measures Structural Changes Induced by Light Activation and Transducer Binding in Sensory Rhodopsin II.** *J Mol Biol* 2009, **394**:383-390.
5. Roychoudhury A, Häussinger D, Oesterhelt F: **Effect of the Compatible Solute Ectoine on the Stability of the Membrane Proteins.** *Protein Pept Lett* 2012, **19**:791-794.
6. Köper I: **Insulating tethered bilayer lipid membranes to study membrane proteins.** *Mol Bio Syst* 2007, **3**:651-657.

doi:10.1186/2047-783X-19-S1-S11
Cite this article as: Bronder *et al.*: Atomic force measurements on the specifically orientated membrane protein TGR5 reconstituted inside a tethered bilayer lipid membrane. *European Journal of Medical Research* 2014 **19**(Suppl 1):S11.

2.2 Unpublished Results

The method to study GPCRs in a membrane mimicking system in a defined orientation has been successfully demonstrated on the IMP BR, which acts as amodel for GPCRs. A further goal of this work was to express and purify the medically relevant GPCR TGR5, to make it available to this new method.

TGR5 was first expressed in different host cells, including human embryonic kidney cells (HEK 293) and *Escherichia coli* (*E. coli*), provided by the Department of Experimental Hepatology, Heinrich-Heine-Universität Düsseldorf. While the TGR5 sequence in the HEK 293 cells has the hexahistidine-tag (His6-tag) required for immobilization in the tBLM, the construct in *E. coli* has a glutathione S-transferase (GST)-tag. However, either the addition of a His6-tag to this construct or a change in surface functionalization was feasible should expression and purification prove to be successful.

Using immobilized metal affinity chromatography (IMAC) using a nickle-nitrilotriacetic acid (Ni-NTA)-column the protein was purified from HEK 293 under denaturing conditions with the help and guidance of Stefan Klinker. Results were tested by sodium dodecyl sulfate polyacrylamide gel electrophoresis (SDS-PAGE) by coomassie staining and western blot (Figure 20). As shown by the coomassie staining (Figure 20A) and the western blot using an anti-histidine(His)-tag antibody (Gigure 20B) there are bands at around 70 kDa. As TGR5 is expected at 35 kDa this is an indication for the dimerization of the protein. However, the bands are only visible for the membrane fraction (sample after cell disruption) and both flowthrough fractions. Even though a histidine-tag (His-tag) is verified by the anti-His-tag antibody, the protein did not bind to the Ni-NTA-column.

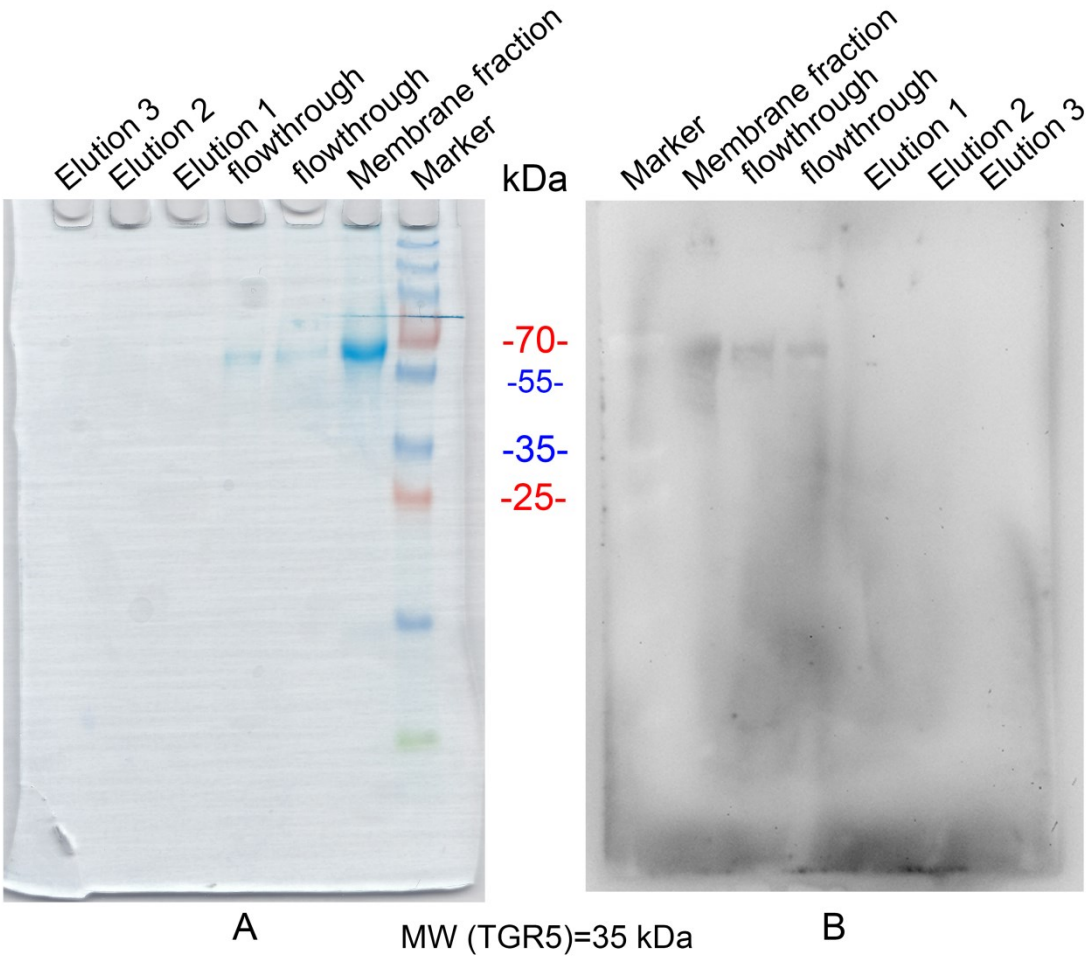

Figure 20: Purification results of TGR5 from HEK 293. (A) The coomassie stained SDS-PAGE only shows protein in the membrane flowthrough fractions. (B) The western blot also shows positive for the membrane fraction and flowthrough. In both cases the bands visible are at the 70 kDa mark.

The second host system *E. coli* was first tested for overexpression. To achieve this, samples were taken before TGR5 expression, induced by isopropyl β-D-1-thiogalactopyranoside (IPTG) and after. Results were again tested by SDS-PAGE with coomassie staining and western blot, using an anti-GST-tag antibody (Figure 21). The GST-tag alone has a molecular weight (MW) of 25 kDa. Therefore we expect a total MW for the GST-TGR5 construct of 65 kDa. While coomassie staining (Figure 21A) shows no clear overexpression for TGR5, the western blot using an anti-GST-tag antibody first of all already shows a band at around 35 kDa before induction with IPTG. After induction the band at 35 kDa becomes more pronounced and another band at 25 kDa has become visible. Since the antibody should not show an affinity against TGR5 without GST-tag both bands at 35 kDa and at 25 kDa have to be attributed to the GST-tag alone. A third, faint band at 55 kDa after induction with IPTG has also become visible. Even though this could be an indication for the GST-TGR5 construct, we have to take into considerations that either most of the GST-tag has been cleaved from TGR5 or, since the GST-tag is amino-terminal (N-terminal) and therefore translated first, the translation of the gene stops after the GST-tag.

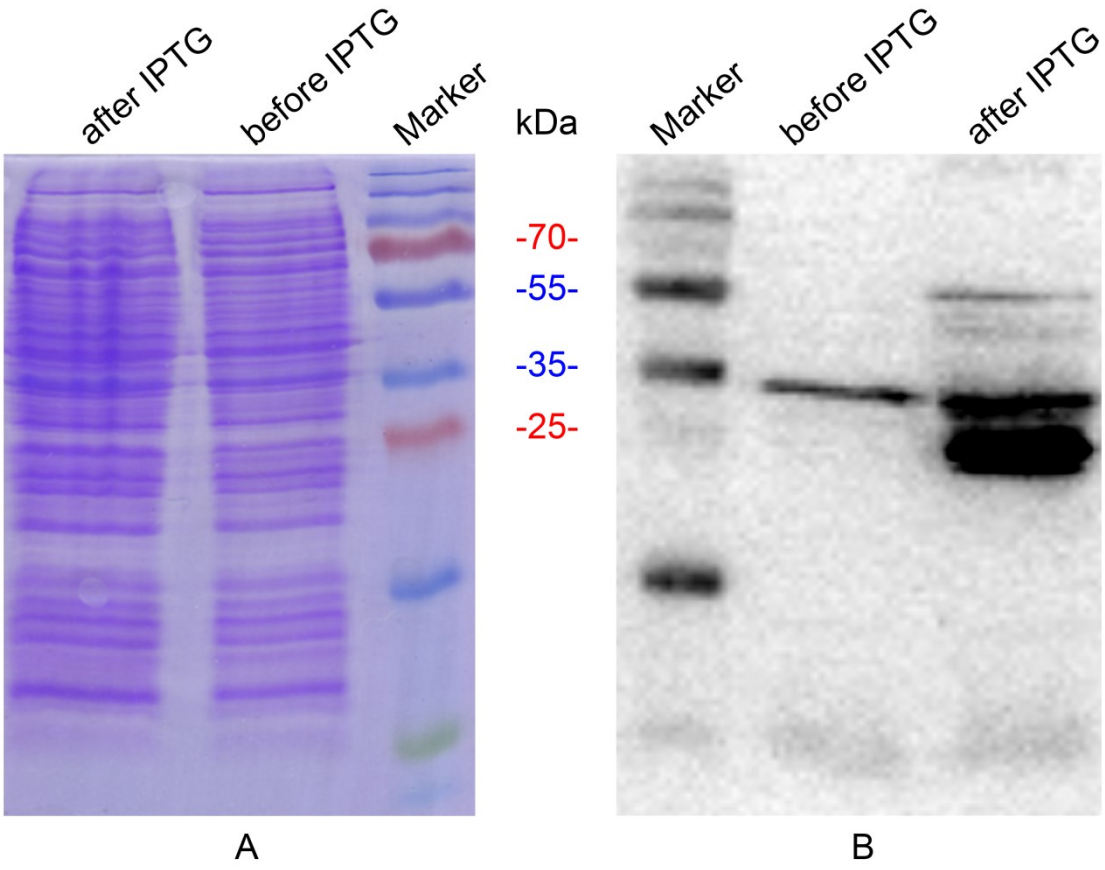

Figure 21: Results of TGR5 expression in *E. coli.* (A) The coomassie stained SDS-PAGE with samples taken before induction with IPTG and after. (B) The corresponding western blot.

As the model IMP BR was already expressed by CFE, the same approach was used to express TGR5. All following experiments have been done in cooperation with the group of Manuel Etzkorn, under the instructions of Shantha Elter. CFE experiments were conducted by Shantha Elter. Two vectors suitable for CFE were created. These vectors would yield a TGR5 construct with a carboxyl-terminal (C-terminal) His6-tag (TGR5-His6). First the pure human TGR5 sequence, codon optimized for *E. coli* was purchased from Invitrogen (Carlsbad, U.S.). This sequence was inserted into pET28a and pIVEX2.3d vectors, respectively. The pellets obtained after CFE were purified using a Ni-NTA-column and tested by SDS-PAGE with coomassie staining and western blot (Figures 22 and 23). Even though the TGR5 sequence was successfully inserted into the pET28a vector, the elution fractions of CFE yielded no visible band at 35 kDa in the coomassie stained SDS-PAGE (Figure 22A). Bands at 35 kDa in the flowthrough and wash fractions of the coomassie stained SDS-PAGE showed no corresponding bands in the western blot with anti-His-tag antibody (Figure 22B).

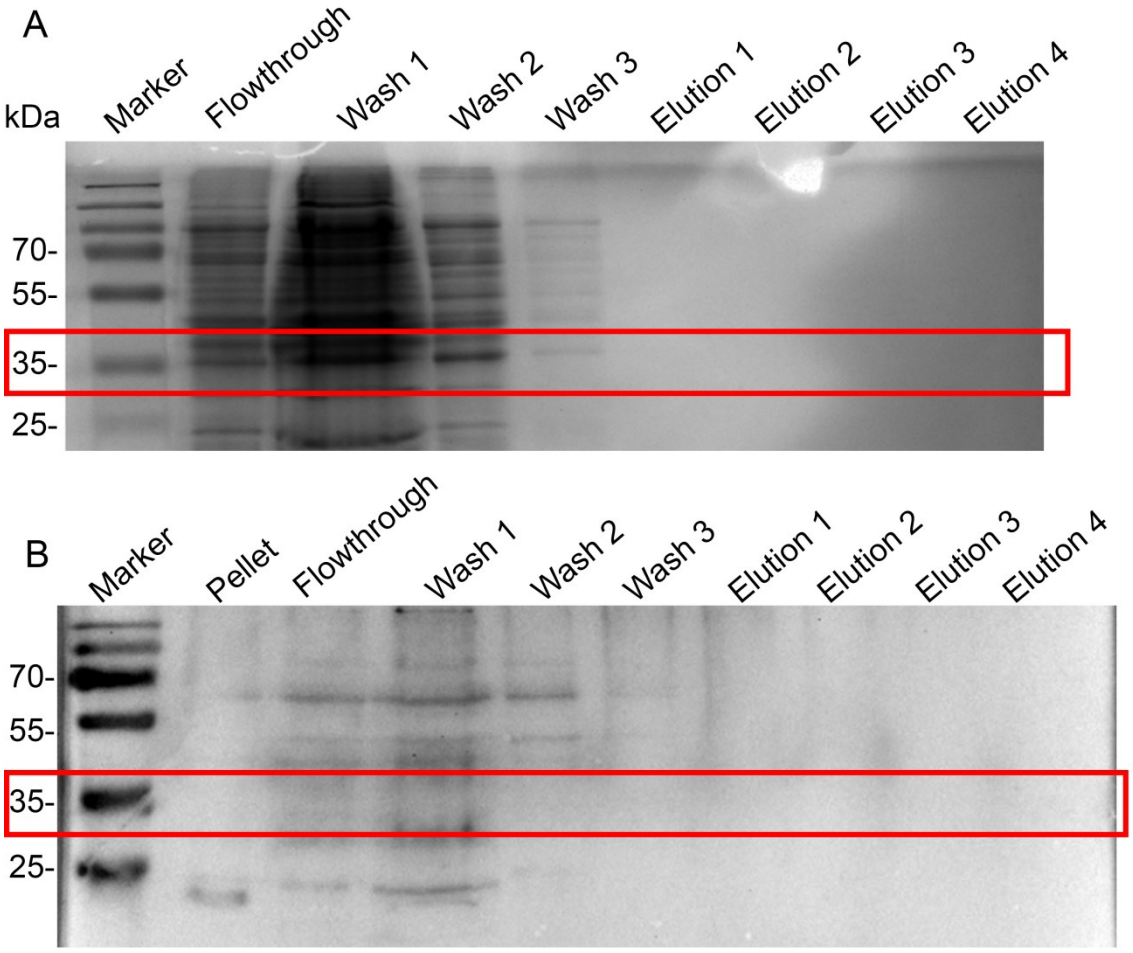

Figure 22: Results of CFE using the pET28a vector. (A) The coomassie stained SDS-PAGE only showed bands for a 35 kDa protein in the flowthrough and wash fractions. (B) The corresponding western blot indicates that these bands did not belong to TGR5.

CFE experiments using the pIVEX2.3d vector showed pronounced bands at 35 kDa and faint bands at 70 kDa in the coomassie stained gel (Figure 23A) and the western blot (Figure 23B), indicating a successful expression of TGR5.

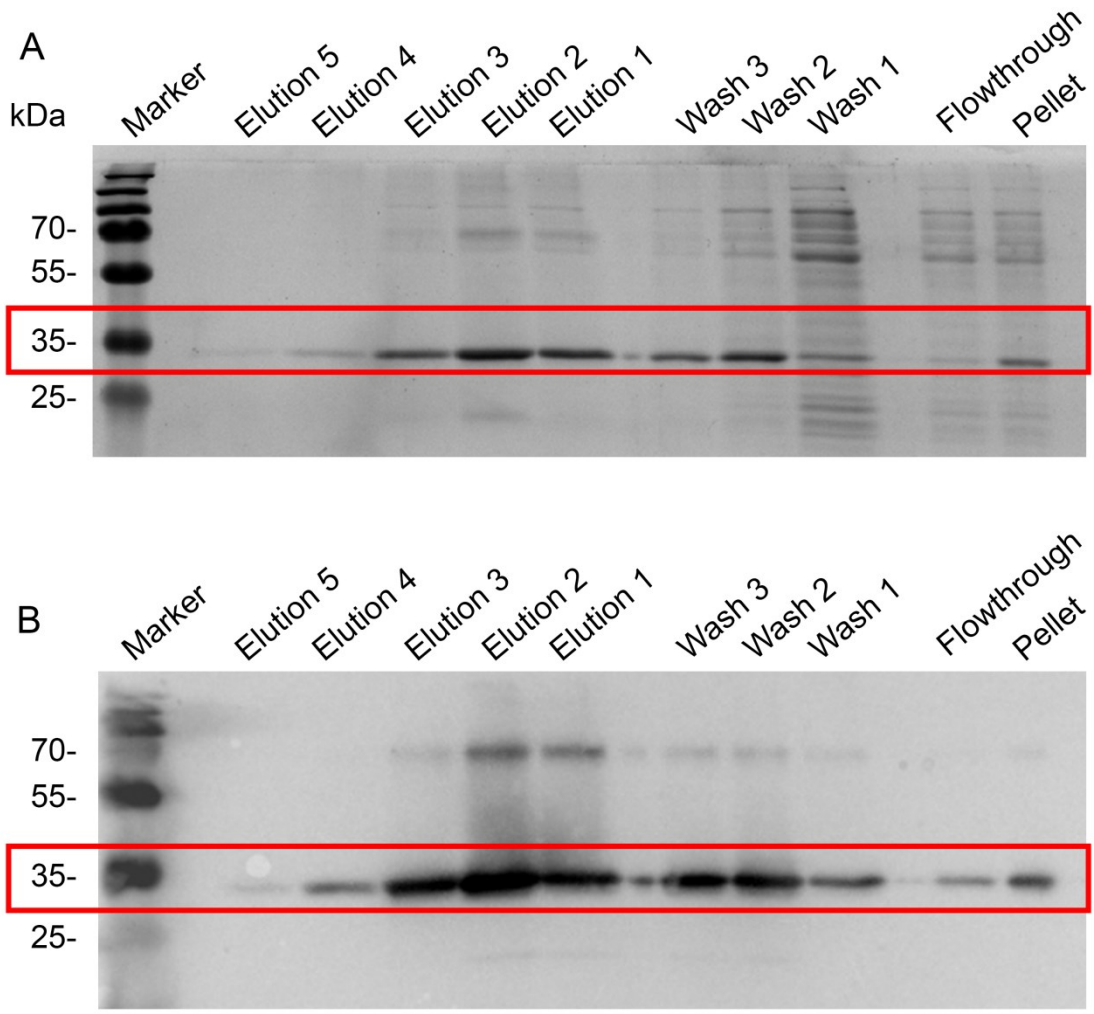

Figure 23: Results of CFE using the pIVEX2.3d vector. (A) The coomassie stained SDS-PAGE as well as the corresponding westernblot (B) showed bands at 35 kDa, indicating the expression of TGR5.

3. Discussion

The aim of this work was to study different membrane associated proteins, $A\beta_{1-42}$, BR and TGR5, with AFM using specifically designed membrane mimicking systems. Two of these proteins have been chosen due to their relevance in medical research, while one, BR, was used as a model protein. BR has been studied extensively (Roychoudhury et al. 2012; Roychoudhury et al. 2013; Wickstrand et al. 2015), can be obtained using CFE (Etzkorn et al. 2013) and stabilized in its native conformation in detergent solution for days.

$A\beta_{1-42}$, especially its oligomeric form, plays a critical role for AD development and pathogenesis (Haass, Selkoe 2007; Karran et al. 2011; Selkoe 2001). Even though the association of these oligomers with the cellular membrane has been shown in past studies (Lin et al. 2001; Quist et al. 2005; Shafrir et al. 2010), a complete understanding of the interactions that lead to pathosis has not been reached, yet. The presence of cholesterol in the cellular membrane shows an effect on Aβ insertion, accumulation and aggregation (Berthelot et al. 2013). However, there have been controversial findings on whether high cholesterol content in the cellular membrane has an inhibiting or intensifying effect on Aβ toxicity (Ali et al. 2000; Arispe, Doh 2002; Jasenosky et al. 2001).

The GPCR TGR5 plays a role in many cellular processes inside the human body (Katsuma et al. 2005; Keitel et al. 2007; Keitel et al. 2008; Knop 2010; Kumar et al. 2012). TGR5 deficiencies due to misfolding or mutation, as well as an overexpression of this bile acid receptor have been linked to diseases (Cao et al. 2013; Hov et al. 2011). As a transmembrane protein TGR5 loses its native conformation if not embedded into a bilayer lipid membrane or stabilized by detergents. Purified TGR5 was not available at the beginning of this study, thus different cellular host systems as well as CFE were implemented to express and purify TGR5.

Studying these proteins on a single molecule level in whole cells to gain knowledge about their structure and possible structural changes due to misfolding is a challenging endeavor. Consequently, the use of artificial membrane mimicking systems is preferential. Two of these membrane mimicking systems have been adjusted and implemented in this work. The first system is a sBLM, a bilayer formed on a solid substrate. This solid substrate is a mica surface, which is atomically flat, therefore especially suitable for high resolution imaging with AFM. Additionally, due to mica being a layered crystal, it offers a fresh and clean surface by removal of the top layers before each use. The second system is a tBLM, a membrane which is partially bound to its substrate through a covalently linked lipid. The substrate used here was quartz glass. Quartz glass is a readily available and easy to functionalize substrate, making it ideal for the formation of a tBLM and offering the possibility to bind the protein of interest as well. This way the protein is available already integrated into the membrane in a defined orientation. With BR as a model protein, the applicability of this system for force spectroscopic measurements was verified.

3.1 Analyzing the influence of $A\beta_{1-42}$ oligomers on cholesterol-rich sBLMs

The interaction and possible effects of $A\beta_{1-42}$ oligomers on a model sBLM containing a high ratio of cholesterol was investigated. The $A\beta_{1-42}$ oligomers used here were made available by density gradient centrifugation. This method was established previously in our group (Brener et al. 2015). As described in chapter 2.1.1, a main component of this model sBLM was the phospholipid DPPC. It has been used for formation of sBLMs previouslys (Asakawa, Fukuma 2009) and offers self-assembled sBLMs of prolonged stability. 0.8 mol % of the detergent n-dodecylphosphocholine (DPC) was added to make the membrane more permeable to proteins (Seddon et al. 2004). A phospholipid:cholesterol ratio of 1:1 (n/n), which is typically found in brain myelin (Björkhem, Meaney 2004), was investigated. This membrane composition showed successfully formed sBLMs by self-assembly, which were stable for at least 5 h. Elevated temperatures of 37 °C and a iodixanol concentration of 30 % did not decrease the membrane stability over time. $A\beta_{1-42}$ oligomers were incubated on those membranes. After 1 h small protrusions of ~3 Å were visible on the membranes, as imaged by AFM. These protrusions were not visible if incubation was performed with monomers or fibrils, as well as on membranes without cholesterol. The protrusions were interpreted as $A\beta_{1-42}$ oligomers integrated into the model sBLM. After incubation at a physiological temperature of 37 °C, membranes with incubated $A\beta_{1-42}$ oligomers dissociated from the solid support. Again this effect was not observed on sBLMs incubated with monomers or fibrils, as well as on membranes without cholesterol. The dissociated membranes were fractionated by floatation density gradient centrifugation using two different approaches. The fractions were later analyzed by ELISA. One approach was to load the sample on the bottom of the density gradient. $A\beta_{1-42}$ still associated to lipid floated into the top fractions, while lipid un-associated $A\beta_{1-42}$ stayed in the bottom fractions. Through this it was demonstrated that $A\beta_{1-42}$ still partially interacts with lipids after dissociation of the membrane. The second approach was to load the sample on the top of the gradient. Here, lipid associated $A\beta_{1-42}$ stayed in the top fractions while lipid un-associated $A\beta_{1-42}$ moved into the fractions according to its aggregation state and S-value. Using this approach it was shown that still oligomeric $A\beta_{1-42}$ stayed lipid associated, while lipid un-associated $A\beta_{1-42}$ was aggregated further. To investigate whether $A\beta_{1-42}$ oligomers lower the phase transition temperature of the model sBLM, the phase transition temperature was analyzed in fluorescence experiments of carboxyfluorecein (CF) containing vesicles (Grant, JR et al. 1992) without and with $A\beta_{1-42}$ oligomers. However, no difference in the phase transition behavior between vesicles without and with $A\beta_{1-42}$ oligomers was visible. Whether the curvature of the vesicles inhibited a successful incorporation of $A\beta_{1-42}$ oligomers or whether the effect responsible for membrane dissociation does not cause a disruption of vesicles has to be investigated further.

The here presented results demonstrate the effect of $A\beta_{1-42}$ on a model sBLM consisting mainly of phospholipids and cholesterol. Only an interaction between $A\beta_{1-42}$ oligomers and the sBLMs

has an effect on the membrane. $A\beta_{1-42}$ oligomers integrate into the sBLM at room temperature (RT) and lead to a dissociation of the sBLM from the solid support at physiological temperatures of 37 °C. While monomers and fibrils show no visible effect on the sBLM, the presence of cholesterol also plays a key role in the dissociation process. Model membranes without a cholesterol component show no incorporation of $A\beta_{1-42}$ oligomers and were stable at 37°C. $A\beta_{1-42}$ oligomers either remain associated with lipid after membrane dissociation or aggregate further into larger oligomers and fibrils. $A\beta_{1-42}$ oligomers show no effect on the stability of vesicles with the same composition as the sBLM. In conclusion the results of this study emphasize the difference between $A\beta_{1-42}$ oligomers and its monomeric and fibrillar structures and further fortify the significance of cholesterol in a membrane dissociating effect of $A\beta_{1-42}$ oligomers.

3.2 Creating a model tBLM to study integral membrane proteins in a defined orientation

tBLMs with an integrated, specifically oriented membrane protein were formed on quartz glass using several functionalization steps (chapter 2.1.2). The quartz glass surface was first silanized with (3-aminopropyl)triethoxysilane (APTES) to create a high coverage with amino groups. After this a polyethylene glycol (PEG) spacer was coupled to these amino groups, to which in turn a lipid and a protein anchor were bound. As a lipid anchor 1,2-dipalmitoyl-sn-glycero-3-phosphoethanolamine-N-(succinyl) sodium salt (SuccinylPE) was chosen, while tris-nitrilotriacetic acid (trisNTA) was the designated protein anchor. The model IMP BR, which has an N-terminal His6-tag was first mixed with a lipid/detergent solution of DPPC/DPC. This solution was then incubated on the functionalized surface to form the membrane with the integrated BR by self-assembly.

Controlling the silanization step by XPS showed a surface composition in agreement with theoretical expectations for a quartz glass surface completely covered with APTES. All surface functionalization steps were controlled through AFM spectroscopy measurements regarding surface adhesion. The measured changes in adhesion between each step indicate the success of each functionalization step. Furthermore, the surfaces after each functionalization step were analyzed by AFM imaging. Changes in the average roughness of the surface indicated a complete surface functionalization between each step.

Binding the protein to the surface through the His6-tag/trisNTA complex was first tested by a rinsing experiment controlled with dot blot. As the complex can only be broken through rinsing with buffer containing imidazole, only this type of rinsing technique, subsequently applying the rinsing solution to a dot blot, will show a detectable luminescence. To test whether the buffer containing imidazole shows an unspecific reaction with the antibody a buffer control was applied to the dot blot as well. Our results show that only the buffer containing imidazole used for rinsing the surface shows a detectable luminescence. The specific orientation of the protein inside the tBLM was also verified by force spectroscopy. Only one set of force curves, specific for a seven α-helical transmembrane protein

was obtained. If the protein were reconstituted randomly, two sets of force curves, one starting from the C-terminus and one from the N-terminus of the protein, would be expected. Furthermore the last peak in the force spectroscopic measurements is in accordance with expected forces for the dissociation of the His6-tag/trisNTA complex (Tang et al. 2009).

The detergent mediated reconstitution of a cell free expressed membrane protein into a tethered membrane mimetic system is a promising method to gain knowledge about the structure of membrane proteins. AFM based force spectroscopy and an easy to functionalize, readily available substrate has been combined in this work. The step-by-step functionalization and reconstitution process to apply this method to a model for GPCRs has been successfully demonstrated. Specific binding and thus a specific orientation of the protein on the surface is another advantage of this method.

3.3 Expression of TGR5

To make TGR5 available for force spectroscopy studies by AFM in the designed tBLM (chapter 2.1.2 and chapter 2.1.3) the protein first had to be expressed and purified (chapter 2.2). First trials using HEK 293 cells showed only a low expression of the protein, as indicated by the western blot (Figure 20B). Additionally, the protein could not be purified by IMAC, as all bands were detected either in the membrane fraction or the flowthrough. A further trial to express TGR5 with an N-terminal GST-tag showed no clear overexpression of TGR5 after induction with IPTG. Furthermore, the GST-tag alone was already being expressed before induction. This expression of the GST-tag alone increases further after induction. A faint band in the western blot (Figure 21B) at around 55 kDa can on the one hand be attributed to the GST-TGR5 construct; on the other hand it is also indicative of a GST-tag dimer.

As the model membrane protein BR used in this study has been expressed by CFE, a possible expression of TGR5 using the same system was investigated as well. For this purpose the TGR5 sequence was first inserted into two potential vectors for CFE. After successful insertion the vectors would both yield TGR5 with a C-terminal His6-tag. After sequencing results (Eurofins Genomics, Ebersberg, Germany) revealed successful insertion of the TGR5 sequence, CFE was tested with both vectors. While CFE using the vector pET28a was unsuccessful (Figure 22), the vector pIVEX2.3d showed an expression of TGR5, as can be seen in the coomassie stained SDS-PAGE and western blot with His-tag antibody (Figure 23). In conclusion the expression of the TGR5-His6-tag construct was achieved using CFE.

4. Prospects

The results presented in this work open the way for the investigation of further questions. First of all a possible long term effect of $A\beta_{1-42}$ monomers on the presented sBLMs could be studied. Even though we did not observe a dissociating effect of monomers, integration into the membrane cannot be excluded. $A\beta_{1-42}$ oligomers were shown to further aggregate over time in association with a cholesterol rich membrane. Hence it is possible that, given enough time, $A\beta_{1-42}$ monomers would show a similar dissociating effect. To further investigate the integration of $A\beta_{1-42}$ monomers indentation force spectroscopy measurements could be conducted to study the mechanical properties of the sBLM and possible changes after monomer integration. Furthermore, potential oligomer reducing drugs could be tested. A protective effect on the membrane stability could be an indication for their potency in terms of oligomer reduction or general protection against the membrane dissociating effect of $A\beta_{1-42}$ oligomers. Another question could be whether the $A\beta_{1-42}$ oligomers used here show a membrane curvature dependent dissociative effect. Generation of differently sized vesicles containing CF could be used in phase transition experiments to answer this question.

The next part of this work dealt with a second membrane mimicking system to study transmembrane proteins in a defined orientation by AFM based force spectroscopy. The tBLM was prepared together with the model membrane protein BR. The next step would be to investigate other, medically relevant proteins, like TGR5. For this purpose TGR5 has already been expressed using CFE by the group of Manuel Etzkorn. However, the method is still in need for optimization as the expression was conducted under denaturing conditions. Once a medically relevant protein is available, solubilized into detergent solution or reconstituted directly into vesicles, it can be implemented into the tBLM. Incubating the protein inside the tBLM with additives could give us insight into the structural influence of these compounds, as has been demonstrated in our group before by Arpita Roychoudhury on BR crystals. A functionalization of the cantilever tip with agonists could also pave the way to directly study the interaction forces between TGR5 and specifically designed agonists and consequently give us information on the bile acid binding pocket of TGR5. This would also give us the possibility to verify details obtained from homology modeling and molecular dynamics simulations (Gertzen, Christoph G W et al. 2015).

Further modifications to the here presented tBLM could also be performed. The tBLM presented here was built on a quartz glass substrate. Even though this substrate is easy to functionalize it presents a high surface roughness. The functionalization of an atomically flat mica surface, however more challenging to functionalize, could be a step to improve the here presented system even further. With an atomically flat surface, high resolution imaging of single proteins reconstituted in the tBLM could potentially be feasible.

5. Summary

The aim of this work was to study the different membrane associated proteins $A\beta_{1-42}$, BR and TGR5 with AFM. Two of the investigated proteins have been chosen due to their relevance in medical research, while one, BR, was used as a model protein. Studying these proteins on a single molecule level in whole cells to gain knowledge about their structure and possible structural changes due to misfolding is challenging. Therefore, the use of artificial membrane mimicking systems is needed. Two specifically designed membrane mimicking systems have been created in this work.

The first system is a sBLM, a bilayer lipid membrane formed on mica consisting mainly of phospholipids and cholesterol. The effect of $A\beta_{1-42}$ on the model sBLM has been demonstrated here. It can be concluded that only the oligomeric species of $A\beta_{1-42}$ has an observable effect on the membrane. AFM imaging showed that $A\beta_{1-42}$ oligomers integrate into the sBLM at RT and lead to a dissociation of the sBLM from the solid support at physiological temperatures of 37 °C. sBLMs without a cholesterol component show no incorporation of $A\beta_{1-42}$ oligomers and were stable at 37°C. Floatation density gradient experiments revealed that $A\beta_{1-42}$ oligomers either remain associated with lipids after membrane dissociation or aggregate further into larger oligomers and fibrils. $A\beta_{1-42}$ oligomers show no effect on the stability of vesicles with the same composition as the sBLM, as shown in phase transition experiments of CF containing vesicles.

The second system is a tBLM, which is partially bound to a quartz glass substrate through a covalently linked lipid. With BR as a model protein the applicability of this system for force spectroscopic measurements was verified. The quartz glass surface was first functionalized using silanization, binding of a PEG spacer and simultaneous binding of a protein and lipid anchor. Success of functionalization steps was verified by XPS, AFM and force spectroscopy. Binding of BR through a His6-tag/trisNTA complex was shown first through the specific elution of BR from the surface. After reconstituting BR onto the surface inside the tBLM, the specific orientation was also indicated by a single set of BR specific force curves. These curves additionally showed the dissociation forces of a His6-tag/trisNTA complex in the last peak. This peak is representative for the force needed to pull the remaining protein from the membrane. To be able to implement the here described tBLM in the study of a medically relevant protein, the sequence of the GPCR TGR5 was integrated into the pIVEX2.3d vector, which makes the protein available for CFE.

6. Zusammenfassung

Das Ziel dieser Arbeit war die Studie der verschiedenen Membran-assoziierten Proteine $A\beta_{1-42}$, BR und TGR5 mit AFM. Zwei der untersuchten Proteine wurden ausgewählt auf Grund ihrer medizinischen Relevanz, während eins, BR, als Model-Protein benutzt wurde. Die Untersuchung dieser Proteine in ganzen Zellen auf Einzel-Molekül Ebene zur Aufklärung ihrer Struktur und möglicher struktureller Änderungen auf Grund von Fehlfaltungsprozessen ist schwierig. Aus diesem Grund werden Membran-nachahmende Modelle benötigt. Zwei spezifisch entworfene Membran-nachahmende Modelle wurden in dieser Arbeit entwickelt.

Das erste Modell ist eine sBLM, eine Membran aus einer Lipid Doppelschicht, hergestellt auf Mica, welche hauptsächlich aus Phospholipiden und Cholesterin besteht. Der Effekt von $A\beta_{1-42}$ auf diese Modell-sBLM wurde hier gezeigt. Es kann geschlussfolgert werden, dass nur die Oligomer-Spezies von $A\beta_{1-42}$ einen sichtbaren Effekt auf die Membran hat. Abbildungen mit AFM haben gezeigt, dass sich $A\beta_{1-42}$ Oligomere in die sBLM bei Raumtemperatur integrieren und bei physiologischen Temperaturen von 37 °C zu einer Dissoziation der sBLM von der Oberfläche führen. sBLMs ohne Cholesterinanteil zeigten keine Integration von $A\beta_{1-42}$ Oligomeren und waren stabil bei 37 °C. Flotation Dichtegradienten Zentrifugations-Experimente ließen erkennen, dass $A\beta_{1-42}$ Oligomere entweder lipidassoziiert bleiben nach der Dissoziation der Membran, oder zu größeren Oligomeren und Fibrillen weiter aggregieren. $A\beta_{1-42}$ Phasenübergangs-Experimente mit CF befüllten Vesikeln der gleichen Komposition wie sBLMs, lassen darauf schließen, dass Oligomere keinen Effekt auf die Stabilität von diesen Vesikeln haben.

Das zweite Modell ist eine tBLM. Die hier entwickelte tBLM ist eine Membran, welche partiell durch ein kovalent gebundenes Lipid an die Quarzglas Oberfläche verankert ist. Mit BR als ein Modellprotein wurde die Anwendbarkeit dieses Systems für kraftspektroskopische Messungen bestätigt. Die Quarzglas Oberfläche wurde zunächst funktionalisiert durch Silanisierung, Anbinden eines PEG *Spacers* und das zeitgleiche Anbinden eines Protein- und Lipidankers. Der Erfolg der Funktionalisierungsschritte wurde bestätigt durch XPS, AFM und Kraftspektroskopie. Das Anbinden von BR über einen His6-tag/trisNTA Komplex wurde gezeigt durch die spezifische Elution von BR von der Oberfläche. Nach der Rekonstitution von BR auf der Oberfläche in der tBLM wurde dies ebenfalls durch einen einzigen Satz BR spezifischer Kraftkurven deutlich. Diese Kraftkurven zeigten weiterhin die zur Dissoziation eines His6-tag/trisNTA Komplexes benötigte Kraft im letzten Abriss. Dieser Abriss repräsentiert die Kraft, welche benötigt wird, um den letzten Teil des Proteins aus der Membran zu ziehen. Um die hier Beschriebene tBLM in Studien an medizinisch relevanten Proteinen einsetzen zu können, wurde die Sequenz des GPCR TGR5 in den pIVEX2.3d Vektor integriert, was das Protein für CFE zugänglich macht.

7. List of Manuscripts

Chapter 2.1.1: Disruptive effect of specific Aβ1-42 Oligomers on Cholesterol-rich Membranes…….……....26

Authors: Anna Bronder, Alexander Brener, Luitgard Nagel-Steger, Dieter Willbold
Journal: PLoS ONE
Impact Factor: 3.234
Own contribution: 50 %

Carrying out and analysis of AFM, preparation of artificial membranes, SUV preparation, ELISA, size exclusion chromatography of SUVs, co-authoring the manuscript

Changes to the manuscript: Figures have been placed at the designated places in the text.

Chapter 2.1.2: Oriented Membrane Protein Reconstitution into Tethered Lipid Membranes for AFM Force Spectroscopy….……....58

Authors: Anna Bronder, Adeline Bieker, Shantha Elter, Manuel Etzkorn, Dieter Häussinger, Filipp Oesterhelt
Journal: Biophysical Journal
Impact Factor: 3.632
Own contribution: 80 %

Carrying out and analysis of AFM imaging and force spectroscopy, surface functionalization, preparation of artificial membranes, XPS measurements and analysis, Dot Blot, refolding and purification of BR, co-authoring the manuscript, cleaning procedure

Chapter 2.1.3: Atomic force measurements on the specifically orientated membrane protein TGR5 reconstituted inside a tethered bilayer lipid membrane……80

Authors: Anna Bronder, Arpita Roychoudhury, Dieter Häussinger, Filipp Oesterhelt
Published in: European Journal of Medical Research
Impact Factor: 1.50
Own contribution: 80 %

Conceptualizing experimental approach, co-authoring the manuscript

8. References

Ali, A.; Avalos, R. T.; Ponimaskin, E.; Nayak, D. P. (2000): Influenza virus assembly: effect of influenza virus glycoproteins on the membrane association of M1 protein. In *Journal of virology* 74 (18), pp. 8709–8719.

Arispe, Nelson; Doh, Michael (2002): Plasma membrane cholesterol controls the cytotoxicity of Alzheimer's disease AbetaP (1-40) and (1-42) peptides. In *FASEB journal : official publication of the Federation of American Societies for Experimental Biology* 16 (12), pp. 1526–1536. DOI: 10.1096/fj.02-0829com.

Asakawa, Hitoshi; Fukuma, Takeshi (2009): The molecular-scale arrangement and mechanical strength of phospholipid/cholesterol mixed bilayers investigated by frequency modulation atomic force microscopy in liquid. In *Nanotechnology* 20 (26), p. 264008. DOI: 10.1088/0957-4484/20/26/264008.

Berthelot, Karine; Cullin, Christophe; Lecomte, Sophie (2013): What does make an amyloid toxic: morphology, structure or interaction with membrane? In *Biochimie* 95 (1), pp. 12–19. DOI: 10.1016/j.biochi.2012.07.011.

Binnig; Quate; Gerber (1986): Atomic force microscope. In *Physical review letters* 56 (9), pp. 930–933. DOI: 10.1103/PhysRevLett.56.930.

Björkhem, Ingemar; Meaney, Steve (2004): Brain cholesterol: long secret life behind a barrier. In *Arteriosclerosis, thrombosis, and vascular biology* 24 (5), pp. 806–815. DOI: 10.1161/01.ATV.0000120374.59826.1b.

Blennow, Kaj; Hampel, Harald; Weiner, Michael; Zetterberg, Henrik (2010): Cerebrospinal fluid and plasma biomarkers in Alzheimer disease. In *Nature reviews. Neurology* 6 (3), pp. 131–144. DOI: 10.1038/nrneurol.2010.4.

Brener, Oleksandr; Dunkelmann, Tina; Gremer, Lothar; van Groen, Thomas; Mirecka, Ewa A.; Kadish, Inga et al. (2015): QIAD assay for quantitating a compound's efficacy in elimination of toxic Aβ oligomers. In *Scientific reports* 5, p. 13222. DOI: 10.1038/srep13222.

Bustamante, Carlos; Erie, Dorothy A.; Keller, David (1994): Biochemical and structural applications of scanning force microscopy. In *Current Opinion in Structural Biology* 4 (5), pp. 750–760. DOI: 10.1016/S0959-440X(94)90175-9.

Cao, Weibiao; Tian, Wei; Hong, Jie; Li, Dan; Tavares, Rosemarie; Noble, Lelia et al. (2013): Expression of bile acid receptor TGR5 in gastric adenocarcinoma. In *American journal of physiology. Gastrointestinal and liver physiology* 304 (4), pp. G322-7. DOI: 10.1152/ajpgi.00263.2012.

Chiti, Fabrizio; Dobson, Christopher M. (2006): Protein misfolding, functional amyloid, and human disease. In *Annual review of biochemistry* 75, pp. 333–366. DOI: 10.1146/annurev.biochem.75.101304.123901.

Di Scala, Coralie; Chahinian, Henri; Yahi, Nouara; Garmy, Nicolas; Fantini, Jacques (2014): Interaction of Alzheimer's β-amyloid peptides with cholesterol: mechanistic insights into amyloid pore formation. In *Biochemistry* 53 (28), pp. 4489–4502. DOI: 10.1021/bi500373k.

Etzkorn, Manuel; Raschle, Thomas; Hagn, Franz; Gelev, Vladimir; Rice, Amanda J.; Walz, Thomas; Wagner, Gerhard (2013): Cell-free expressed bacteriorhodopsin in different soluble membrane mimetics: biophysical properties and NMR accessibility. In *Structure (London, England : 1993)* 21 (3), pp. 394–401. DOI: 10.1016/j.str.2013.01.005.

Fantini, Jacques; Yahi, Nouara; Garmy, Nicolas (2013): Cholesterol accelerates the binding of Alzheimer's β-amyloid peptide to ganglioside GM1 through a universal hydrogen-bond-dependent sterol tuning of glycolipid conformation. In *Frontiers in physiology* 4, p. 120. DOI: 10.3389/fphys.2013.00120.

Fotiadis, Dimitrios; Liang, Yan; Filipek, Slawomir; Saperstein, David A.; Engel, Andreas; Palczewski, Krzysztof (2004): The G protein-coupled receptor rhodopsin in the native membrane. In *FEBS letters* 564 (3), pp. 281–288. DOI: 10.1016/S0014-5793(04)00194-2.

Gertzen, Christoph G W; Spomer, Lina; Smits, Sander H J; Häussinger, Dieter; Keitel, Verena; Gohlke, Holger (2015): Mutational mapping of the transmembrane binding site of the G-protein coupled receptor TGR5 and binding mode prediction of TGR5 agonists. In *European journal of medicinal chemistry* 104, pp. 57–72. DOI: 10.1016/j.ejmech.2015.09.024.

Gibson Wood, W.; Eckert, Gunter P.; Igbavboa, Urule; Müller, Walter E. (2003): Amyloid beta-protein interactions with membranes and cholesterol: causes or casualties of Alzheimer's disease. In *Biochimica et Biophysica Acta (BBA) - Biomembranes* 1610 (2), pp. 281–290. DOI: 10.1016/S0005-2736(03)00025-7.

Grant, E., JR; Beeler, T. J.; Taylor, K. M.; Gable, K.; Roseman, M. A. (1992): Mechanism of magainin 2a induced permeabilization of phospholipid vesicles. In *Biochemistry* 31 (41), pp. 9912–9918.

Haass, Christian; Selkoe, Dennis J. (2007): Soluble protein oligomers in neurodegeneration: lessons from the Alzheimer's amyloid beta-peptide. In *Nature reviews. Molecular cell biology* 8 (2), pp. 101–112. DOI: 10.1038/nrm2101.

Hardy, J. A.; Higgins, G. A. (1992): Alzheimer's disease: the amyloid cascade hypothesis. In *Science (New York, N.Y.)* 256 (5054), pp. 184–185.

Hartl, F. Ulrich; Hayer-Hartl, Manajit (2009): Converging concepts of protein folding in vitro and in vivo. In *Nature structural & molecular biology* 16 (6), pp. 574–581. DOI: 10.1038/nsmb.1591.

Hov, Johannes R.; Keitel, Verena; Laerdahl, Jon K.; Spomer, Lina; Ellinghaus, Eva; ElSharawy, Abdou et al. (2010): Mutational characterization of the bile acid receptor TGR5 in primary sclerosing cholangitis. In *PloS one* 5 (8), pp. e12403. DOI: 10.1371/journal.pone.0012403.

Hov, Johannes R.; Keitel, Verena; Schrumpf, Erik; Häussinger, Dieter; Karlsen, Tom H. (2011): TGR5 sequence variation in primary sclerosing cholangitis. In *Digestive diseases (Basel, Switzerland)* 29 (1), pp. 78–84. DOI: 10.1159/000324138.

Hutter, Jeffrey L.; Bechhoefer, John (1993): Erratum: ‘‘Calibration of atomic-force microscope tips’’ [Rev. Sci. Instrum. 64, 1868 (1993)]. In *Rev. Sci. Instrum.* 64 (11), p. 3342. DOI: 10.1063/1.1144449.

Jasenosky, L. D.; Neumann, G.; Lukashevich, I.; Kawaoka, Y. (2001): Ebola virus VP40-induced particle formation and association with the lipid bilayer. In *Journal of virology* 75 (11), pp. 5205–5214. DOI: 10.1128/JVI.75.11.5205-5214.2001.

Karran, Eric; Mercken, Marc; Strooper, Bart de (2011): The amyloid cascade hypothesis for Alzheimer's disease: an appraisal for the development of therapeutics. In *Nature reviews. Drug discovery* 10 (9), pp. 698–712. DOI: 10.1038/nrd3505.

Katsuma, Susumu; Hirasawa, Akira; Tsujimoto, Gozoh (2005): Bile acids promote glucagon-like peptide-1 secretion through TGR5 in a murine enteroendocrine cell line STC-1. In *Biochemical and biophysical research communications* 329 (1), pp. 386–390. DOI: 10.1016/j.bbrc.2005.01.139.

Kawamata, Yuji; Fujii, Ryo; Hosoya, Masaki; Harada, Masataka; Yoshida, Hiromi; Miwa, Masanori et al. (2003): A G protein-coupled receptor responsive to bile acids. In *The Journal of biological chemistry* 278 (11), pp. 9435–9440. DOI: 10.1074/jbc.M209706200.

Keitel, Verena; Donner, Markus; Winandy, Stefanie; Kubitz, Ralf; Häussinger, Dieter (2008): Expression and function of the bile acid receptor TGR5 in Kupffer cells. In *Biochemical and biophysical research communications* 372 (1), pp. 78–84. DOI: 10.1016/j.bbrc.2008.04.171.

Keitel, Verena; Reinehr, Roland; Gatsios, Petros; Rupprecht, Claudia; Gorg, Boris; Selbach, Oliver et al. (2007): The G-protein coupled bile salt receptor TGR5 is expressed in liver sinusoidal endothelial cells. In *Hepatology (Baltimore, Md.)* 45 (3), pp. 695–704. DOI: 10.1002/hep.21458.

Knop, Filip K. (2010): Bile-induced secretion of glucagon-like peptide-1: pathophysiological implications in type 2 diabetes? In *American journal of physiology. Endocrinology and metabolism* 299 (1), pp. E10-3. DOI: 10.1152/ajpendo.00137.2010.

Koper, Ingo (2007): Insulating tethered bilayer lipid membranes to study membrane proteins. In *Molecular bioSystems* 3 (10), pp. 651–657. DOI: 10.1039/b707168j.

Kumar, Divya P.; Rajagopal, Senthilkumar; Mahavadi, Sunila; Mirshahi, Faridoddin; Grider, John R.; Murthy, Karnam S.; Sanyal, Arun J. (2012): Activation of transmembrane bile acid receptor TGR5 stimulates insulin secretion in pancreatic β cells. In *Biochemical and biophysical research communications* 427 (3), pp. 600–605. DOI: 10.1016/j.bbrc.2012.09.104.

Lin, H.; Bhatia, R.; Lal, R. (2001): Amyloid beta protein forms ion channels: implications for Alzheimer's disease pathophysiology. In *FASEB journal : official publication of the Federation of American Societies for Experimental Biology* 15 (13), pp. 2433–2444. DOI: 10.1096/fj.01-0377com.

Liu, J.; Rost, B. (2001): Comparing function and structure between entire proteomes. In *Protein science : a publication of the Protein Society* 10 (10), pp. 1970–1979. DOI: 10.1110/ps.10101.

Lodish, Harvey F. (2000): Molecular cell biology. 4th ed. New York: W.H. Freeman.

Los, Dmitry A.; Murata, Norio (2004): Membrane fluidity and its roles in the perception of environmental signals. In *Biochimica et biophysica acta* 1666 (1-2), pp. 142–157. DOI: 10.1016/j.bbamem.2004.08.002.

Maxfield, Frederick R.; Tabas, Ira (2005): Role of cholesterol and lipid organization in disease. In *Nature* 438 (7068), pp. 612–621. DOI: 10.1038/nature04399.

Milligan, C. E. (2000): Caspase cleavage of APP results in a cytotoxic proteolytic peptide. In *Nature medicine* 6 (4), pp. 385–386. DOI: 10.1038/74644.

Müller, Daniel J.; Engel, Andreas (2007): Atomic force microscopy and spectroscopy of native membrane proteins. In *Nature protocols* 2 (9), pp. 2191–2197. DOI: 10.1038/nprot.2007.309.

Oesterhelt, D.; Stoeckenius, W. (1971): Rhodopsin-like protein from the purple membrane of Halobacterium halobium. In *Nature: New biology* 233 (39), pp. 149–152.

Pols, Thijs W H; Noriega, Lilia G.; Nomura, Mitsunori; Auwerx, Johan; Schoonjans, Kristina (2011): The bile acid membrane receptor TGR5 as an emerging target in metabolism and inflammation. In *Journal of hepatology* 54 (6), pp. 1263–1272. DOI: 10.1016/j.jhep.2010.12.004.

Poole, D. P.; Godfrey, C.; Cattaruzza, F.; Cottrell, G. S.; Kirkland, J. G.; Pelayo, J. C. et al. (2010): Expression and function of the bile acid receptor GpBAR1 (TGR5) in the murine enteric nervous system. In *Neurogastroenterology and motility : the official journal of the European Gastrointestinal Motility Society* 22 (7), pp. 814-25, e227-8. DOI: 10.1111/j.1365-2982.2010.01487.x.

Portelius, Erik; Mattsson, Niklas; Andreasson, Ulf; Blennow, Kaj; Zetterberg, Henrik (2011): Novel abeta isoforms in Alzheimer's disease - their role in diagnosis and treatment. In *Current pharmaceutical design* 17 (25), pp. 2594–2602.

Portelius, Erik; Zetterberg, Henrik; Andreasson, Ulf; Brinkmalm, Gunnar; Andreasen, Niels; Wallin, Anders et al. (2006): An Alzheimer's disease-specific beta-amyloid fragment signature in cerebrospinal fluid. In *Neuroscience letters* 409 (3), pp. 215–219. DOI: 10.1016/j.neulet.2006.09.044.

Putman, C. A.; van der Werf, K O; de Grooth, B G; van Hulst, N F; Greve, J. (1994): Viscoelasticity of living cells allows high resolution imaging by tapping mode atomic force microscopy. In *Biophysical journal* 67 (4), pp. 1749–1753. DOI: 10.1016/S0006-3495(94)80649-6.

Quist, Arjan; Doudevski, Ivo; Lin, Hai; Azimova, Rushana; Ng, Douglas; Frangione, Blas et al. (2005): Amyloid ion channels: a common structural link for protein-misfolding disease. In *Proceedings of the National Academy of Sciences of the United States of America* 102 (30), pp. 10427–10432. DOI: 10.1073/pnas.0502066102.

Redondo-Morata, Lorena; Giannotti, Marina I.; Sanz, Fausto (2012): Influence of cholesterol on the phase transition of lipid bilayers: a temperature-controlled force spectroscopy study. In *Langmuir : the ACS journal of surfaces and colloids* 28 (35), pp. 12851–12860. DOI: 10.1021/la302620t.

Ross, Christopher A.; Poirier, Michelle A. (2004): Protein aggregation and neurodegenerative disease. In *Nature medicine* 10 Suppl, pp. S10-7. DOI: 10.1038/nm1066.

Roychoudhury, Arpita; Bieker, Adeline; Häussinger, Dieter; Oesterhelt, Filipp (2013): Membrane protein stability depends on the concentration of compatible solutes--a single molecule force spectroscopic study. In *Biological chemistry* 394 (11), pp. 1465–1474. DOI: 10.1515/hsz-2013-0173.

Roychoudhury, Arpita; Haussinger, Dieter; Oesterhelt, Filipp (2012): Effect of the compatible solute ectoine on the stability of the membrane proteins. In *Protein and peptide letters* 19 (8), pp. 791–794.

Sarid, Dror (1994): Scanning force microscopy. With applications to electric, magnetic, and atomic forces. Rev. ed. New York: Oxford University Press (Oxford series in optical and imaging sciences, 5).

Schmidt, M. L.; DiDario, A. G.; Otvos, L., JR; Hoshi, N.; Kant, J. A.; Lee, V. M.; Trojanowski, J. Q. (1994): Plaque-associated neuronal proteins: a recurrent motif in neuritic amyloid deposits throughout diverse cortical areas of the Alzheimer's disease brain. In *Experimental neurology* 130 (2), pp. 311–322. DOI: 10.1006/exnr.1994.1209.

Schneider, Birgit; Junge, Friederike; Shirokov, Vladimir A.; Durst, Florian; Schwarz, Daniel; Dötsch, Volker; Bernhard, Frank (2010): Membrane protein expression in cell-free systems. In *Methods in molecular biology (Clifton, N.J.)* 601, pp. 165–186. DOI: 10.1007/978-1-60761-344-2_11.

Seddon, Annela M.; Curnow, Paul; Booth, Paula J. (2004): Membrane proteins, lipids and detergents: not just a soap opera. In *Biochimica et biophysica acta* 1666 (1-2), pp. 105–117. DOI: 10.1016/j.bbamem.2004.04.011.

Segalat, Laurnet (2007): Loss-of-function genetic diseases and the concept of pharmaceutical targets. In *Orphanet journal of rare diseases* 2, p. 30.

Selkoe, D. J. (2001): Alzheimer's disease: genes, proteins, and therapy. In *Physiological reviews* 81 (2), pp. 741–766.

Seubert, P.; Vigo-Pelfrey, C.; Esch, F.; Lee, M.; Dovey, H.; Davis, D. et al. (1992): Isolation and quantification of soluble Alzheimer's beta-peptide from biological fluids. In *Nature* 359 (6393), pp. 325–327. DOI: 10.1038/359325a0.

Shafrir, Yinon; Durell, Stewart; Arispe, Nelson; Guy, H. Robert (2010): Models of membrane-bound Alzheimer's Abeta peptide assemblies. In *Proteins* 78 (16), pp. 3473–3487. DOI: 10.1002/prot.22853.

Singer, S. J.; Nicolson, G. L. (1972): The fluid mosaic model of the structure of cell membranes. In *Science (New York, N.Y.)* 175 (4023), pp. 720–731.

Soto, Claudio; Estrada, Lisbell D. (2008): Protein misfolding and neurodegeneration. In *Archives of neurology* 65 (2), pp. 184–189. DOI: 10.1001/archneurol.2007.56.

Tang, Jilin; Ebner, Andreas; Kraxberger, Bernhard; Leitner, Michael; Hykollari, Alba; Kepplinger, Christian et al. (2009): Detection of metal binding sites on functional S-layer nanoarrays using single molecule force spectroscopy. In *Journal of structural biology* 168 (1), pp. 217–222. DOI: 10.1016/j.jsb.2009.02.003.

Tanzi, Rudolph E.; Bertram, Lars (2005): Twenty years of the Alzheimer's disease amyloid hypothesis: a genetic perspective. In *Cell* 120 (4), pp. 545–555. DOI: 10.1016/j.cell.2005.02.008.

Tashima, Yoshihiko; Oe, Ryoko; Lee, Sannamu; Sugihara, Gohsuke; Chambers, Eric J.; Takahashi, Mitsuo; Yamada, Tatsuo (2004): The effect of cholesterol and monosialoganglioside (GM1) on the release and aggregation of amyloid beta-peptide from liposomes prepared from brain membrane-like lipids. In *The Journal of biological chemistry* 279 (17), pp. 17587–17595. DOI: 10.1074/jbc.M308622200.

Walsh, D. M.; Klyubin, I.; Fadeeva, J. V.; Rowan, M. J.; Selkoe, D. J. (2002a): Amyloid-beta oligomers: their production, toxicity and therapeutic inhibition. In *Biochemical Society transactions* 30 (4), pp. 552–557.

Walsh, D. M.; Klyubin, I.; Shankar, G. M.; Townsend, M.; Fadeeva, J. V.; Betts, V. et al. (2005): The role of cell-derived oligomers of Abeta in Alzheimer's disease and avenues for therapeutic intervention. In *Biochemical Society transactions* 33 (Pt 5), pp. 1087–1090. DOI: 10.1042/BST20051087.

Walsh, Dominic M.; Klyubin, Igor; Fadeeva, Julia V.; Cullen, William K.; Anwyl, Roger; Wolfe, Michael S. et al. (2002b): Naturally secreted oligomers of amyloid beta protein potently inhibit hippocampal long-term potentiation in vivo. In *Nature* 416 (6880), pp. 535–539. DOI: 10.1038/416535a.

Watanabe, Mitsuhiro; Morimoto, Kohkichi; Houten, Sander M.; Kaneko-Iwasaki, Nao; Sugizaki, Taichi; Horai, Yasushi et al. (2012): Bile acid binding resin improves metabolic control through the induction of energy expenditure. In *PloS one* 7 (8), pp. e38286. DOI: 10.1371/journal.pone.0038286.

Wickstrand, Cecilia; Dods, Robert; Royant, Antoine; Neutze, Richard (2015): Bacteriorhodopsin: Would the real structural intermediates please stand up? In *Biochimica et biophysica acta* 1850 (3), pp. 536–553. DOI: 10.1016/j.bbagen.2014.05.021.

Winklhofer, Konstanze F.; Tatzelt, Jörg; Haass, Christian (2008): The two faces of protein misfolding: gain- and loss-of-function in neurodegenerative diseases. In *The EMBO journal* 27 (2), pp. 336–349. DOI: 10.1038/sj.emboj.7601930.

Wolynes, P. G.; Onuchic, J. N.; Thirumalai, D. (1995): Navigating the folding routes. In *Science (New York, N.Y.)* 267 (5204), pp. 1619–1620.

Zhao, Guojun; Tan, Jianxin; Mao, Guozhang; Cui, Mei-Zhen; Xu, Xuemin (2007): The same gamma-secretase accounts for the multiple intramembrane cleavages of APP. In *Journal of neurochemistry* 100 (5), pp. 1234–1246. DOI: 10.1111/j.1471-4159.2006.04302.x.

Zhong, Q.; Inniss, D.; Kjoller, K.; Elings, V. B. (1993): Fractured polymer/silica fiber surface studied by tapping mode atomic force microscopy. In *Surface Science Letters* 290 (1-2), pp. L688. DOI: 10.1016/0167-2584(93)90906-Y.

Zwanzig, R.; Szabo, A.; Bagchi, B. (1992): Levinthal's paradox. In *Proceedings of the National Academy of Sciences of the United States of America* 89 (1), pp. 20–22.